Научном већу Института за физику
Београд,
23. април 2014.

<div align="center">

ПРЕДМЕТ:

Молба за покретање поступка за избор у звање *истраживач-сарадник*

</div>

Молим Научно веће Института за физику да покрене поступак за мој избор у звање истраживач-сарадник.

У прилогу достављам:
- Стручну биографију
- Мишљење руководиоца пројекта
- Списак и копије објављених радова
- Потврду о уписаним докторским студијама

<div align="right">

С поштовањем,

Александра Димитриевска
истраживач-приправник

</div>

Биографија кандидаткиње

Александра Димитриевска рођена је 1984. године у Бору, Република Србија. Основне студије уписала је 2003. године на Природно-математичком факултету, Универзитета у Новом Саду, на смеру дипломирани физичар, а дипломирала је 2010. са просечном оценом 9.96 и оценом 10 на дипломским радом на тему: *„Временска спектроскопија нуклеарних реакција космичких миона“*. Мастер студије завршила је на истом факултету 2011. године са просечном оценом 9.94 и мастер радом на тему: *„Расподела космичких миона по брзинама“*. Од децембра 2011. године уписана је на Докторске академске студије Физичког факултета Универзитета у Београду, смер: Физика језгара и честица, тренутно је на трећој години и положила је све испите.

У току школовања била је стипендиста Републичке фондације за развој научног и уметничког подмлатка (2002–2009), добитник школарине EFG Eurobank за најбоље студенте државних факултета у Србији (2010), као и стипендиста Фонда за младе таленте Републике Србије (2010/11).

Од 1. децембра 2011. године запослена је у Лабораторији за физику високих енергија Института за физику као истраживач-приправник, са ангажовањем на пројекту Министарства просвете, науке и технолошког развоја ОИ171004 *„АТЛАС експеримент и физика честица на ЛХЦ енергијама“*.

Учествовала је на следећим школама из физике честица:
 - Sarajevo School of High Energy Physics, May 9 – 13, 2012, Sarajevo, Bosnia and Hercegovina
 - CERN Summer Student Programme, July – August 2012, CERN, Switzerland
 - CERN – Fermilab Hadron Collider Physics Summer School, 28 August – 6 September, 2013, CERN, Switzerland

Од 2012. године учествује и ради на АТЛАС експерименту на Великом хадронском сударачу (ЛХЦ) у ЦЕРН-у. Од септембра 2012. до септембра 2013. године радила је на квалификацији за ауторство на АТЛАС експерименту. Задатак је био рад на ефективној калибрацији мионског спектрометра АТЛАС детектора помоћу распада J/ψ резонанце на два миона. Од 1. септембра 2013. године, квалификовани је аутор радова АТЛАС колаборације.

Научном већу Института за физику
Београд,
23. април 2014.

Мишљење руководиоца пројекта за избор Александре Димитриевске у звање истраживач-сарадник

Колегиница Александра Димитриевска испуњава све услове предвиђене Правилником за стицање истраживачких звања за избор у звање истраживач-сарадник и сматрам да Научно веће Института за физику треба да покрене поступак за њен избор у ово звање.

Александра Димитриевска је од 1. децембра 2011. године запослена у Лабораторији за физику високих енергија Института за физику као истраживач-приправник, и учествује на пројекту Министарства просвете, науке и технолошког развоја ОИ171004 *„АТЛАС експеримент и физика честица на ЛХЦ енергијама“*. Од 2011. године уписана на је на докторске студије на Физичком факултету, Универзитета у Београду и сада је студент треће године, положила је све испите. Учествује и ради на АТЛАС експерименту на Великом хадронском сударачу (ЛХЦ) у ЦЕРН-у и у септембру 2013. године, успешно је завршила квалификацију за аутора АТЛАС колаборације. Током 2012. и 2013. године око тридесетак пута представила је резултате свог рада на интерним састанцима радних група АТЛАС колаборације (Muon Combined Performance Working Group и W mass group у оквиру Standard Model Working group) као и на интерним скуповима АТЛАС колаборације: Muon Week и Physics and Performance Week (који се одржавају 2-3 пута годишње и на којима се даје преглед добијених резултата у оквиру радних група), као и на једном интерном Workshop-u ATLAS колаборације. Коаутор је на три интерне публикације АТЛАС колаборације, које представљају „back up“ публикације објављених у референтним часописима. Посебно признање за њен досадашњи рад био је позив да представи резулатате Muon Combined Performance Working Group-е на „LHC students poster session“ у марту 2014. године у оквиру 117th LHCC састанка (Large Hadron Collider Committee Meeting). Колегиница Димитриевска је била једна од 25 доктораната који су представљали резултате АТЛАС колаборације.

Истраживачким радом Александре Димитриевске на АТЛАС експерименту, непосредно руководи др Ненад Врањеш који се налази на постдокторском усавршавању у CEA Saclay.

За чланове Комисије за писање извештаја за избор Александре Димитриевске у звање истраживач-сарадник предлажем:

1. др Ненада Врањеша, научног сарадника Института за физику (као првог референта),
2. др Љиљану Симић, научног саветника Института за физику,
3. проф. Петра Аџића, редовног професора Физичког факултета.

Руководилац пројекта,

др Драган Поповић
научни саветник,
Институт за физику Београд

Списак научних радова и саопштења са конференција

Радови у врхунским међународним часописима (М21)
1. G. Aad, …, A. Dimitrievska *et al*. [ATLAS Collaboration], „Search for Quantum Black-Hole Production in High-Invariant-Mass Lepton+Jet Final States Using Proton-Proton Collisions at sqrt(s) = 8 TeV and the ATLAS Detector", Phys. Rev. Lett. 112 (2014) 091804, [arXiv:1311.2006[hep-ex]].
2. G. Aad, …, A. Dimitrievska *et al*. [ATLAS Collaboration], „Measurement of the electroweak production of dijets in association with a Z-boson and distributions sensitive to vector boson fusion in proton-proton collisions at sqrt(s) = 8 TeV using the ATLAS detector", J. High Energy Phys. 1404 (2014) 031, [arXiv:1401.7610[hep-ex]].
3. G. Aad, …, A. Dimitrievska *et al*. [ATLAS Collaboration], „Search for Higgs boson decays to a photon and a Z boson in pp collisions at sqrt(s)=7 and 8 TeV with the ATLAS detector*", Phys. Lett. B732 (2014) 8-27, [arXiv:1402.3051[hep-ex]]. (рад приказан у прилогу)

Остале референтне публикације АТЛАС колаборације доступне на CERN CDS серверу (cds.cern.ch)

1. T. Adye, C. Amelung, …, A. Dimitrievska, *et al*. [ATLAS Collaboration], „Supporting Document for Higgs papers: Higgs mass measurements and uncertainties in 2012", ATL-COM-PHYS-2012-1774.

2. M. Goblirsch, M. Vanadia, A. Salvucci, F. Sforza, O. Kortner, A. Dimitrievska, N. Vranjes, [ATLAS Collaboration], „Preliminary results on the muon reconstruction efficiency, momentum resolution, and momentum scale in ATLAS 2012 pp collision data", ATLAS-CONF-2013-088. (рад приказан у прилогу)

3. G. Artoni, M. Corradi, A. Dimitrievska, F. Sforza, N. Vranjes, P. Fleischmann, [ATLAS Collaboration], „Muon momentum scale and resolution corrections evaluated with Z->mumu 2 and J/psi->mumu decays on Run I ATLAS data", ATL-COM-MUON-2014-001.

Саопштења на међународним конференцијама (М34)

1. A. Dimitrievska, „Muon reconstruction efficiency, momentum scale and resolution in pp collisions at 8 TeV with ATLAS", Poster at 117th LHCC Meeting, 5 – 6 March 2014. CERN, Switzerland, ATL-COM-PHYS-2014-163. (приказан у прилогу)

Саопштења на националним конференцијама (М63)

1. А. Димитриевска, М. Димитриевска, „*Секунда – основна јединица за време у СИ систему*", Календарско знање и допринос Милутина Миланковића, 14 – 15 септембар 2011. Београд, Србија, Усмена презентација, стр. 84 – 91.

2. А. Димитриевска, Н. Врањеш, *„Карактеристике реконструкције миона ниског импулса на АТЛАС детектору*", XII Конгрес физичара Србије, Зборник радова, 28. април – 2. мај 2013. Врњачка бања, Србија, Постер у секцији: 2. Физика језгра, елементарних честица и основних интеракција, стр. 185 – 188. (рад приказан у прилогу)

Презентације на састанцима АТЛАС колаборације

1.Wmass meeting, 03.09.2012. (https://indico.cern.ch/event/205292),
L. Chevalier, A. Dimitrievska, N. Vranjes, „Effective Calibration of Muon Spectrometer using J/psi->mumu"

2. Muon Combined Performance Working Group 12.09.2012. (https://indico.cern.ch/event/207903),
L. Chevalier, A. Dimitrievska, N. Vranjes, „Muon Performance using J/psi->mumu"

3. Muon Combined Performance Working Group, 17.10.2012.(https://indico.cern.ch/event/213091),
L. Chevalier, A. Dimitrievska, N. Vranjes, „J/psi in data12"

4. Muon Week 12.11.2012. (https://indico.cern.ch/event/215927),
L. Chevalier, A. Dimitrievska, N. Vranjes, „J/psi in data11 and data12"

5. Muon Combined Performance, Working Group, 05.12.2012,
(https://indico.cern.ch/event/220934),
L. Chevalier, A. Dimitrievska, N. Vranjes, „J/psi studies"

6. Wmass meeting, 11.12.2012., (https://indico.cern.ch/event/221858),
A. Dimitrievska, „W and Z pt distributions"

7. Wmass meeting, 18.12.2012., (https://indico.cern.ch/event/223197),
A. Dimitrievska, „W and Z pt distributions"

8. Wmass meeting, 05.01.2013. (https://indico.cern.ch/event/228678),
A. Dimitrievska, „W and Z pt distributions"

9. Muon Week, 26.03.2013,. (https://indico.cern.ch/event/242777),
L. Chevalier, A. Dimitrievska, N. Vranjes, „Calorimeter energy loss corrections using J/Psi"

10. Wmass meeting, 29.03.2013. (https://indico.cern.ch/event/243992),
A. Dimitrievska, „W and Z pt distributions"

11. Wmass meeting, 19.04.2013. (https://indico.cern.ch/event/247976),
A. Dimitrievska, „Parametrization of pt W distribution"

12. Wmass meeting, 10.05.2013. (https://indico.cern.ch/event/251178),
A. Dimitrievska, „W pt distributions and recoil upper cut"

13. Muon Week, 15.05.2013. (https://indico.cern.ch/event/252338),
L. Chevalier, A. Dimitrievska, N. Vranjes, „Energy loss studies with J/psi"

14. Wmass Workshop, 14.06.2013., (https://indico.cern.ch/event/247389),
M. Boonekamp, A. Dimitrievska, N. Vranjes, „Studies towards a direct measurement of the PtW distribution"

15. Muon Combined Performance Working, 18.06.2013. (https://indico.cern.ch/event/258263),
L. Chevalier, A. Dimitrievska, N. Vranjes, „Momentum scale with J/psi"

16. Wmass meeting, 28.06.2013. (https://indico.cern.ch/event/260338),
M. Boonekamp, A. Dimitrievska, N. Vranjes, „Direct measurement of W pt"

17. Wmass meeting 23.08.2013. године (https://indico.cern.ch/event/268873),
A. Dimitrievska, „Recoil studies"

18. Wmass, 25.10.2013. (https://indico.cern.ch/event/280206),
A. Dimitrievska, „Direct measurement of W pt distribution"

19. Muon Combined Performance Working Group, 06.11.2013.
(https://indico.cern.ch/event/282091),
L. Chevalier, A. Dimitrievska, N. Vranjes, „Momentum scale validation with J/psi"

20. Physics and Performance Week, 19.11.2013. (https://indico.cern.ch/event/284010),
L. Chevalier, A. Dimitrievska, N. Vranjes, „Momentum correction validation with J/psi"

21. Muon Combined Performance Working Group, 04.12.2013.
(https://indico.cern.ch/event/286789),
L. Chevalier, A. Dimitrievska, N. Vranjes, „Update on scale correction"

22. Muon Combined Performance Working Group, 16.12.2013.
(https://indico.cern.ch/event/289036),
L. Chevalier, A. Dimitrievska, N. Vranjes, „Momentum correction validation with J/psi"

23. Muon Combined Performance Working Group, 18.12.2013.
(https://indico.cern.ch/event/289550),
L. Chevalier, A. Dimitrievska, N. Vranjes, „Momentum correction validation with J/psi"

24. Muon Combined Performance Working Group, 22.01.2014.
(https://indico.cern.ch/event/296672),
L. Chevalier, A. Dimitrievska, N. Vranjes, „Discussion on performance paper and notes"

25. Muon Combined Performance Working Group, 29.01.2014.,
(https://indico.cern.ch/event/298323),
L. Chevalier, A. Dimitrievska, N. Vranjes, „Angular distribution in J/psi"

26. Wmass meeting, 28.02.2014. (https://indico.cern.ch/event/305246),
M. Boonekamp, A. Dimitrievska, N. Vranjes, „Recoil corrections"
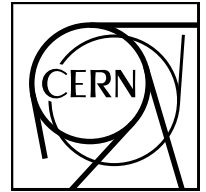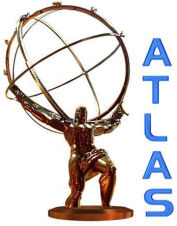
EUROPEAN ORGANISATION FOR NUCLEAR RESEARCH (CERN)

Search for Higgs boson decays to a photon and a Z boson in pp collisions at $\sqrt{s}$ = 7 and 8 TeV with the ATLAS detector

The ATLAS Collaboration

Abstract

A search is reported for a neutral Higgs boson in the decay channel $H \rightarrow Z\gamma$, $Z \rightarrow \ell^+\ell^-$ ($\ell = e, \mu$), using 4.5 fb^{-1} of pp collisions at $\sqrt{s}$ = 7 TeV and 20.3 fb^{-1} of pp collisions at $\sqrt{s}$ = 8 TeV, recorded by the ATLAS detector at the CERN Large Hadron Collider. The observed distribution of the invariant mass of the three final-state particles, $m_{\ell\ell\gamma}$, is consistent with the Standard Model hypothesis in the investigated mass range of 120–150 GeV. For a Higgs boson with a mass of 125.5 GeV, the observed upper limit at the 95% confidence level is 11 times the Standard Model expectation. Upper limits are set on the cross section times branching ratio of a neutral Higgs boson with mass in the range 120–150 GeV between 0.13 and 0.5 pb for $\sqrt{s}$ = 8 TeV at 95% confidence level.

Search for Higgs boson decays to a photon and a Z boson in pp collisions at $\sqrt{s} = 7$ and 8 TeV with the ATLAS detector

ATLAS Collaboration, G. Aad *et al.* (full author list given at the end of the article in Appendix)

Abstract

A search is reported for a neutral Higgs boson in the decay channel $H \to Z\gamma$, $Z \to \ell^+\ell^-$ ($\ell = e, \mu$), using 4.5 fb^{-1} of pp collisions at $\sqrt{s} = 7$ TeV and 20.3 fb^{-1} of pp collisions at $\sqrt{s} = 8$ TeV, recorded by the ATLAS detector at the CERN Large Hadron Collider. The observed distribution of the invariant mass of the three final-state particles, $m_{\ell\ell\gamma}$, is consistent with the Standard Model hypothesis in the investigated mass range of 120–150 GeV. For a Higgs boson with a mass of 125.5 GeV, the observed upper limit at the 95% confidence level is 11 times the Standard Model expectation. Upper limits are set on the cross section times branching ratio of a neutral Higgs boson with mass in the range 120–150 GeV between 0.13 and 0.5 pb for $\sqrt{s} = 8$ TeV at 95% confidence level.

1. Introduction

In July 2012 a new particle decaying to dibosons ($\gamma\gamma$, ZZ, WW) was discovered by the ATLAS [1] and CMS [2] experiments at the CERN Large Hadron Collider (LHC). The observed properties of this particle, such as its couplings to fermions and bosons [3, 4] and its spin and parity [5, 6], are consistent with those of a Standard Model (SM) Higgs boson with a mass near 125.5 GeV [3].

This Letter presents a search for a Higgs boson H decaying to $Z\gamma$, $Z \to \ell^+\ell^-$ ($\ell = e, \mu$),[1] using pp collisions at $\sqrt{s} = 7$ and 8 TeV recorded with the ATLAS detector at the LHC during 2011 and 2012. The Higgs boson is assumed to have SM-like spin and production properties and a mass between 120 and 150 GeV. The integrated luminosity presently available enables the exclusion of large anomalous couplings to $Z\gamma$, compared with the SM prediction. The signal is expected to yield a narrow peak in the reconstructed $\ell\ell\gamma$ invariant-mass distribution over a smooth background dominated by continuum $Z+\gamma$ production, $Z \to \ell\ell\gamma$ radiative decays and $Z+$jets events where a jet is misidentified as a photon. A similar search was recently published by the CMS Collaboration [7], which set an upper limit of 9.5 times the SM expectation, at 95% confidence level (CL), on the $pp \to H \to Z\gamma$ cross section for $m_H = 125$ GeV.

In the SM, the Higgs boson is produced mainly through five production processes: gluon fusion (ggF), vector-boson fusion (VBF), and associated production with either a W boson (WH), a Z boson (ZH) or a $t\bar{t}$ pair ($t\bar{t}H$) [8–10]. For a mass of 125.5 GeV the SM $pp \to H$ cross section is $\sigma = 22$ (17) pb at $\sqrt{s} = 8$ (7) TeV. Higgs boson decays to $Z\gamma$ in the SM proceed through loop diagrams mostly mediated by W bosons, similar to $H \to \gamma\gamma$. The $H \to Z\gamma$ branching ratio of a SM Higgs boson with a mass of 125.5 GeV is $B(H \to Z\gamma) = 1.6 \times 10^{-3}$ compared to $B(H \to \gamma\gamma) = 2.3 \times 10^{-3}$. The branching fractions of the Z to leptons leads to a $pp \to H \to \ell\ell\gamma$ cross section of 2.3 (1.8) fb at 8 (7) TeV, similar to that of $pp \to H \to ZZ^* \to 4\ell$ and only 5% of that of $pp \to H \to \gamma\gamma$.

Modifications of the $H \to Z\gamma$ coupling with respect to the SM prediction are expected if H is a neutral scalar of a different origin [11, 12] or a composite state [13], as well as in models with additional colourless charged scalars, leptons or vector bosons coupled to the Higgs boson and exchanged in the $H \to Z\gamma$ loop [14–16]. A determination of both the $H \to \gamma\gamma$ and $H \to Z\gamma$ decay rates can help to determine whether the newly discovered Higgs boson is indeed the one predicted in the SM, or provide information on the quantum numbers of the new particles exchanged in the loops or on the compositeness scale. While constraints from the observed rates in the other final states, particularly the diphoton channel, typically limit the expected $H \to Z\gamma$ decay rate in the models mentioned above to be within a factor of two of the SM expectation, larger enhancements can be obtained in some scenarios by careful parameter choices [13, 14].

2. Experimental setup and dataset

The ATLAS detector [17] is a multi-purpose particle detector with approximately forward-backward symmetric cylindrical geometry.[2] The inner tracking detector (ID) covers $|\eta| < 2.5$ and consists of a silicon pixel detector, a silicon microstrip

---

[1]In the following ℓ denotes either an electron or a muon, and the charge of the leptons is omitted for simplicity.

[2]ATLAS uses a right-handed coordinate system with its origin at the nominal interaction point (IP) in the centre of the detector and the z-axis along the beam pipe. The x-axis points from the IP to the centre of the LHC ring, and the y-axis points upward. Cylindrical coordinates (r, ϕ) are used in the transverse plane, ϕ being the azimuthal angle around the beam pipe. The pseudorapidity is defined in terms of the polar angle θ as $\eta = -\ln\tan(\theta/2)$.

detector, and a transition radiation tracker. The ID is surrounded by a thin superconducting solenoid providing a 2 T axial magnetic field and by a high-granularity lead/liquid-argon (LAr) sampling electromagnetic calorimeter. The electromagnetic calorimeter measures the energy and the position of electromagnetic showers with $|\eta| < 3.2$. It includes a presampler (for $|\eta| < 1.8$) and three sampling layers, longitudinal in shower depth, up to $|\eta| < 2.5$. LAr sampling calorimeters are also used to measure hadronic showers in the end-cap ($1.5 < |\eta| < 3.2$) and forward ($3.1 < |\eta| < 4.9$) regions, while an iron/scintillator tile calorimeter measures hadronic showers in the central region ($|\eta| < 1.7$). The muon spectrometer (MS) surrounds the calorimeters and consists of three large superconducting air-core toroid magnets, each with eight coils, a system of precision tracking chambers ($|\eta| < 2.7$), and fast tracking chambers ($|\eta| < 2.4$) for triggering. A three-level trigger system selects events to be recorded for offline analysis.

Events are collected using the lowest threshold unprescaled single-lepton or dilepton triggers [18]. For the single-muon trigger the transverse momentum, p_T, threshold is 24 (18) GeV for $\sqrt{s}$ = 8 (7) TeV, while for the single-electron trigger the transverse energy, E_T, threshold is 25 (20) GeV. For the dimuon triggers the thresholds are $p_T > 13$ (10) GeV for each muon, while for the dielectron triggers the thresholds are $E_T > 12$ GeV for each electron. At $\sqrt{s} = 8$ TeV a dimuon trigger is also used with asymmetric thresholds $p_{T1} > 18$ GeV and $p_{T2} > 8$ GeV. The trigger efficiency with respect to events satisfying the selection criteria is 99% in the $ee\gamma$ channel and 92% in the $\mu\mu\gamma$ channel due to the reduced geometric acceptance of the muon trigger system in the $|\eta| < 1.05$ and $|\eta| > 2.4$ region. Events with data quality problems are discarded. The integrated luminosity after the trigger and data quality requirements corresponds to 20.3 fb^{-1} (4.5 fb^{-1}) [19] at $\sqrt{s} = 8$ (7) TeV.

3. Simulated samples

The event generators used to model SM signal and background processes in samples of Monte Carlo (MC) simulated events are listed in Table 1.

Table 1
Event generators used to model the signal (first two rows) and background (last four rows) processes.

Process	Generator
ggF, VBF	POWHEG [20–22]+PYTHIA8 [23]
WH, ZH, $t\bar{t}H$	PYTHIA8
$Z+\gamma$ and $Z \to \ell\ell\gamma$	SHERPA [24, 25]
Z+jets	SHERPA, ALPGEN [26]+HERWIG [27]
$t\bar{t}$	MC@NLO [28, 29]+HERWIG
WZ	SHERPA, POWHEG+PYTHIA8

The $H \to Z\gamma$ signal from the dominant ggF and VBF processes, corresponding to 95% of the SM production cross section, is generated with POWHEG, interfaced to PYTHIA 8.170 for showering and hadronisation, using the CT10 parton distribution functions (PDFs) [30]. Gluon-fusion events are reweighted to match the Higgs boson p_T distribution predicted by HRES2 [31]. The signal from associated production (WH, ZH or $t\bar{t}H$) is generated with PYTHIA 8.170 using the CTEQ6L1 PDFs [32]. Signal events are generated for Higgs boson masses m_H between 120 and 150 GeV, in intervals of 5 GeV, at both $\sqrt{s} = 7$ TeV and $\sqrt{s} = 8$ TeV. For the same value of the mass, events corresponding to different Higgs boson production modes are combined according to their respective SM cross sections.

The predicted SM cross sections and branching ratios are compiled in Refs. [8–10]. The production cross sections are computed at next-to-next-to-leading order in the strong coupling constant α_s and at next-to-leading order (NLO) in the electroweak coupling constant α, except for the $t\bar{t}H$ cross section, which is calculated at NLO in α_s [33–43]. Theoretical uncertainties on the production cross section arise from the choice of renormalisation and factorisation scales in the fixed-order calculations as well as the uncertainties on the PDFs and the value of α_s used in the perturbative expansion. They depend only mildly on the centre-of-mass energy and on the Higgs boson mass in the range $120 < m_H < 150$ GeV. The scale uncertainties are uncorrelated among the five Higgs boson production modes that are considered; for $m_H = 125.5$ GeV at $\sqrt{s} = 8$ TeV, they amount to $^{+7}_{-8}$% for ggF, ±0.2% for VBF, ±1% for WH, ±3% for ZH and $^{+4}_{-9}$% for $t\bar{t}H$. PDF+α_s uncertainties are correlated among the gluon-fusion and $t\bar{t}H$ processes, which are initiated by gluons, and among the VBF and WH/ZH processes, which are initiated by quarks; for $m_H = 125.5$ GeV at $\sqrt{s} = 8$ TeV, the uncertainties are around ±8% for $gg \to H$ and $t\bar{t}H$ and around ±2.5% for the other three Higgs boson production modes. The Higgs boson branching ratios are computed using the HDECAY and Prophecy4f programs [44–46]. The relative uncertainty on the $H \to Z\gamma$ branching ratio varies between ±9% for $m_H = 120$ GeV and ±6% for $m_H = 150$ GeV. An additional ±5% [47] accounts for the effect, in the selected phase space of the $\ell\ell\gamma$ final state, of the interfering $H \to \ell\ell\gamma$ decay amplitudes that are neglected in the calculation of Refs. [8–10]. They originate from internal photon conversion in Higgs boson decays to diphotons ($H \to \gamma^*\gamma \to \ell\ell\gamma$) or from radiative Higgs boson decays to dileptons ($H \to \ell\ell^* \to \ell\ell\gamma$ in the Z mass window) [48, 49].

Various background samples are also generated: they are used to study the background parameterisation and possible systematic biases in the fit described in Section 6 and not to extract the final result. The samples produced with ALPGEN or MC@NLO are interfaced to HERWIG 6.510 [27] for parton showering, fragmentation into particles and to model the underlying event, using JIMMY 4.31 [50] to generate multiple-parton interactions. The SHERPA, MC@NLO and POWHEG samples are generated using the CT10 PDFs, while the ALPGEN samples use the CTEQ6L1 ones.

All Monte Carlo samples are processed through a complete simulation of the ATLAS detector response [51] using GEANT4 [52]. Additional pp interactions in the same and nearby bunch crossings (pile-up) are included in the simulation. The

MC samples are reweighted to reproduce the distribution of the mean number of interactions per bunch crossing (9 and 21 on average in the data taken at $\sqrt{s}$ = 7 and 8 TeV, respectively) and the length of the luminous region observed in data.

4. Event selection and backgrounds

4.1. Event selection

Events are required to contain at least one primary vertex, determined from a fit to the tracks reconstructed in the inner detector and consistent with a common origin. The primary vertex with the largest sum of the squared transverse momenta of the tracks associated with it is considered as the primary vertex of the hard interaction.

The selection of leptons and photons is similar to that used for the $H \rightarrow \gamma\gamma$ and $H \rightarrow 4\ell$ measurements [1], the main difference being the minimum transverse momentum threshold. Events are required to contain at least one photon and two opposite-sign same-flavour leptons.

Muon candidates are formed from tracks reconstructed either in the ID or in the MS [53]. They are required to have transverse momentum p_T > 10 GeV and $|\eta|$ < 2.7. In the central barrel region $|\eta|$ < 0.1, which lacks MS coverage, ID tracks are identified as muons based on the associated energy deposits in the calorimeter. These candidates must have p_T > 15 GeV. The inner detector tracks associated with muons that are identified inside the ID acceptance are required to have a minimum number of associated hits in each of the ID sub-detectors (to ensure good track reconstruction) and to have transverse (longitudinal) impact parameter d_0 (z_0), with respect to the primary vertex, smaller than 1 mm (10 mm).

Electrons and photons are reconstructed from clusters of energy deposits in the electromagnetic calorimeter [54]. Tracks matched to electron candidates (and, for 8 TeV data, from photon conversions) and having enough associated hits in the silicon detectors are fitted using a Gaussian-Sum Filter, which accounts for bremsstrahlung energy loss [55].

Electron candidates are required to have a transverse energy greater than 10 GeV, pseudorapidity $|\eta|$ < 2.47, and a well-reconstructed ID track pointing to the electromagnetic calorimeter cluster. The cluster should satisfy a set of identification criteria that require the longitudinal and transverse shower profiles to be consistent with those expected for electromagnetic showers [56]. The electron track is required to have a hit in the innermost pixel layer of the ID when passing through an active module and is also required to have a longitudinal impact parameter, with respect to the primary vertex, smaller than 10 mm.

Photon candidates are required to have a transverse energy greater than 15 GeV and pseudorapidity within the regions $|\eta|$ < 1.37 or 1.52 < $|\eta|$ < 2.37, where the first calorimeter layer has high granularity. Photons reconstructed in or near regions of the calorimeter affected by read-out or high-voltage failures are not accepted. The identification of photons is performed through a cut-based selection based on shower shapes measured in the first two longitudinal layers of the electromagnetic calorimeter and on the leakage into the hadronic calorimeter [57]. To further suppress hadronic background, the calorimeter isolation transverse energy E_T^{iso} [1] in a cone of size $\Delta R = \sqrt{(\Delta\eta)^2 + (\Delta\phi)^2}$ = 0.4 around the photon candidate is required to be lower than 4 GeV, after subtracting the contributions from the photon itself and from the underlying event and pile-up.

Removal of overlapping electrons and muons that satisfy all selection criteria and share the same inner detector track is performed: if the muon is identified by the MS, then the electron candidate is discarded; otherwise the muon candidate is rejected. Photon candidates within a ΔR = 0.3 cone of a selected electron or muon candidate are also rejected, thus suppressing background from $Z \rightarrow \ell\ell\gamma$ events and signal from radiative Higgs boson decays to dileptons.

Z boson candidates are reconstructed from pairs of same-flavour, opposite-sign leptons passing the previous selections. At least one of the two muons from $Z \rightarrow \mu\mu$ must be reconstructed both in the ID and the MS.

Higgs boson candidates are reconstructed from the combination of a Z boson and a photon candidate. In each event only the Z candidate with invariant mass closest to the Z pole mass and the photon with largest transverse energy are retained. In the selected events, the triggering leptons are required to match one (or in the case of dilepton-triggered events, both) of the Z candidate's leptons. Track and calorimeter isolation requirements, as well as additional track impact parameter selections, are also applied to the leptons forming the Z boson candidate [1]. The track isolation $\sum p_T$, inside a ΔR = 0.2 cone around the lepton, excluding the lepton track, divided by the lepton p_T, must be smaller than 0.15. The calorimeter isolation for electrons, computed similarly to E_T^{iso} for photons but with ΔR = 0.2, divided by the electron E_T, must be lower than 0.2. Muons are required to have a normalised calorimeter isolation E_T^{cone}/p_T less than 0.3 (0.15 in the case of muons without an ID track) inside a ΔR = 0.2 cone around the muon direction. For both the track- and calorimeter-based isolation any contributions due to the other lepton from the candidate Z decay are subtracted. The transverse impact parameter significance $|d_0|/\sigma_{d_0}$ of the ID track associated with a lepton within the acceptance of the inner detector is required to be less than 3.5 and 6.5 for muons and electrons, respectively. The electron impact parameter is affected by bremsstrahlung and it thus has a broader distribution.

Finally, the dilepton invariant mass ($m_{\ell\ell}$) and the invariant mass of the $\ell\ell\gamma$ final-state particles ($m_{\ell\ell\gamma}$) are required to satisfy $m_{\ell\ell}$ > m_Z − 10 GeV and 115 < $m_{\ell\ell\gamma}$ < 170 GeV, respectively. These criteria further suppress events from $Z \rightarrow \ell\ell\gamma$, as well as reducing the contribution to the signal from internal photon conversions in $H \rightarrow \gamma\gamma$ and radiation from leptons in $H \rightarrow \ell\ell$ to a negligible level [47]. The number of events satisfying all the selection criteria in $\sqrt{s}$ = 8 TeV ($\sqrt{s}$ = 7 TeV) data is 7798 (1041) in the $Z \rightarrow ee$ channel and 9530 (1400) in the $Z \rightarrow \mu\mu$ channel.

The same reconstruction algorithms and selection criteria are used for simulated events. The simulation is corrected to take into account measured data-MC differences in photon

and lepton efficiencies and energy or momentum resolution. The acceptance of the kinematic requirements for simulated $H \to Z\gamma \to \ell\ell\gamma$ signal events at $m_H = 125.5$ GeV is 54% for $\ell = e$ and 57% for $\ell = \mu$, due to the larger acceptance in muon pseudorapidity. The average photon reconstruction and selection efficiency is 68% (61%) while the $Z \to \ell\ell$ reconstruction and selection efficiency is 74% (67%) and 88% (88%) for $\ell = e$ and $\ell = \mu$, respectively, at $\sqrt{s} = 8$ (7) TeV. The larger photon and electron efficiencies in 8 TeV data are due to a re-optimisation of the photon and electron identification criteria prior to the 8 TeV data taking. Including the acceptance and the reconstruction, selection and trigger efficiencies, the overall signal efficiency for $H \to Z\gamma \to \ell\ell\gamma$ events at $m_H = 125.5$ GeV is 27% (22%) for $\ell = e$ and 33% (27%) for $\ell = \mu$ at $\sqrt{s} = 8$ (7) TeV. The relative efficiency is about 5% higher in the VBF process and 5–10% lower in the W, Z, $t\bar{t}$-associated production modes, compared to signal events produced in the dominant gluon-fusion process. For m_H increasing between 120 and 150 GeV the overall signal efficiency varies from 0.87 to 1.25 times the efficiency at $m_H = 125.5$ GeV.

4.2. Invariant-mass calculation

In order to improve the three-body invariant-mass resolution of the Higgs boson candidate events and thus improve discrimination against non-resonant background events, three corrections are applied to the three-body mass $m_{\ell\ell\gamma}$. First, the photon pseudorapidity η^γ and its transverse energy $E_T^\gamma = E^\gamma / \cosh\eta^\gamma$ are recalculated using the identified primary vertex as the photon's origin, rather than the nominal interaction point (which is used in the standard ATLAS photon reconstruction). Second, the muon momenta are corrected for collinear final-state-radiation (FSR) by including any reconstructed electromagnetic cluster with E_T above 1.5 GeV lying close (typically with $\Delta R < 0.15$) to a muon track. Third, the lepton four-momenta are recomputed by means of a Z-mass-constrained kinematic fit previously used in the ATLAS $H \to 4\ell$ search [1]. The photon direction and FSR corrections improve the invariant-mass resolution by about 1% each, while the Z-mass constraint brings an improvement of about 15–20%.

Fig. 1 illustrates the distributions of $m_{\mu\mu\gamma}$ and $m_{ee\gamma}$ for simulated signal events from $gg \to H$ at $m_H = 125$ GeV after all corrections. The $m_{ee\gamma}$ resolution is about 8% worse due to bremsstrahlung. The $m_{\ell\ell\gamma}$ distribution is modelled with the sum of a Crystal Ball function (a Gaussian with a power-law tail), representing the core of well-reconstructed events, and a small, wider Gaussian component describing the tails of the distribution. For $m_H = 125.5$ GeV the typical mass resolution σ_{CB} of the core component of the $m_{\mu\mu\gamma}$ distribution is 1.6 GeV.

4.3. Event classification

The selected events are classified into four categories, based on the pp centre-of-mass energy and the lepton flavour. To enhance the sensitivity of the analysis, each event class is further divided into categories with different signal-to-background ratios and invariant-mass resolutions, based on (i) the pseudorapidity difference $\Delta\eta_{Z\gamma}$ between the photon and the Z boson and

(ii) p_{Tt},[3] the component of the Higgs boson candidate p_T that is orthogonal to the $Z\gamma$ thrust axis in the transverse plane. Signal events are typically characterised by a larger p_{Tt} and a smaller $\Delta\eta_{Z\gamma}$ compared to background events, which are mostly due to $q\bar{q} \to Z + \gamma$ events in which the Z boson and the photon are back-to-back in the transverse plane. Signal gluon-fusion events have on average smaller p_{Tt} and larger $\Delta\eta_{Z\gamma}$ than signal events in which the Higgs boson is produced either by VBF or in association with W, Z or $t\bar{t}$ and thus is more boosted.

Higgs boson candidates are classified as *high-* (*low-*) p_{Tt} candidates if their p_{Tt} is greater (smaller) than 30 GeV. In the analysis of $\sqrt{s} = 8$ TeV data, low-p_{Tt} candidates are further split into two classes, *high-* and *low-*$\Delta\eta_{Z\gamma}$, depending on whether $|\Delta\eta_{Z\gamma}|$ is greater or less than 2.0, yielding a total of ten event categories.

As an example, the expected number of signal and background events in each category with invariant mass within a ± 5 GeV window around $m_H = 125$ GeV, the observed number of events in data in the same region, and the full-width at half-maximum (FWHM) of the signal invariant-mass distribution, are summarised in Table 2. Using this classification improves the signal sensitivity of this analysis by 33% for a Higgs boson mass of 125.5 GeV compared to a classification based only on the centre-of-mass energy and lepton flavour categories.

Table 2

Expected signal (N_S) and background (N_B) yields in a ± 5 GeV mass window around $m_H = 125$ GeV for each of the event categories under study. In addition, the observed number of events in data (N_D) and the FWHM of the signal invariant-mass distribution, modelled as described in Section 4.2, are given. The signal is assumed to have SM-like properties, including the production cross section times branching ratio. The background yield is extrapolated from the selected data event yield in the invariant-mass region outside the ± 5 GeV window around $m_H = 125$ GeV, using an analytic background model described in Section 6. The uncertainty on the FWHM from the limited size of the simulated signal samples is negligible in comparison to the systematic uncertainties described in Section 5.

$\sqrt{s}$ [TeV]	ℓ	Category	N_S	N_B	N_D	$\frac{N_S}{\sqrt{N_B}}$	FWHM [GeV]
8	μ	high p_{Tt}	2.3	310	324	0.13	3.8
8	μ	low p_{Tt}, low $\Delta\eta$	3.7	1600	1587	0.09	3.8
8	μ	low p_{Tt}, high $\Delta\eta$	0.8	600	602	0.03	4.1
8	e	high p_{Tt}	1.9	260	270	0.12	3.9
8	e	low p_{Tt}, low $\Delta\eta$	2.9	1300	1304	0.08	4.2
8	e	low p_{Tt}, high $\Delta\eta$	0.6	430	421	0.03	4.5
7	μ	high p_{Tt}	0.4	40	40	0.06	3.9
7	μ	low p_{Tt}	0.6	340	335	0.03	3.9
7	e	high p_{Tt}	0.3	25	21	0.06	3.9
7	e	low p_{Tt}	0.5	240	234	0.03	4.0

---

[3] $p_{\text{Tt}} = |(\vec{p}_T^\gamma + \vec{p}_T^Z) \times \hat{t}|$ where $\hat{t} = (\vec{p}_T^\gamma - \vec{p}_T^Z)/|\vec{p}_T^\gamma - \vec{p}_T^Z|$ denotes the thrust axis in the transverse plane, and $\vec{p}_T^\gamma$, $\vec{p}_T^Z$ are the transverse momenta of the photon and the Z boson.
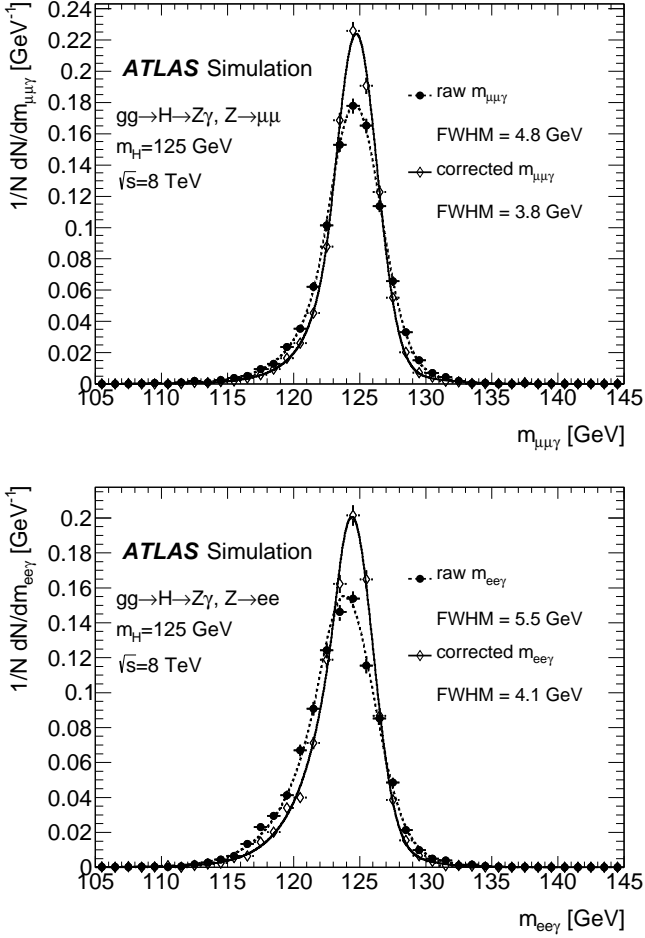
Fig. 1. Three-body invariant-mass distribution for $H \to Z\gamma$, $Z \to \mu\mu$ (top) or $Z \to ee$ (bottom) selected events in the 8 TeV, $m_H = 125$ GeV gluon-fusion signal simulation, after applying all analysis cuts, before (filled circles) and after (open diamonds) the corrections described in Section 4.2. The solid and dashed lines represent the fits of the points to the sum of a Crystal Ball and a Gaussian function.

4.4. Sample composition

The main backgrounds originate from continuum $Z+\gamma$, $Z \to \ell\ell$ production, from radiative $Z \to \ell\ell\gamma$ decays, and from Z+jet, $Z \to \ell\ell$ events in which a jet is misidentified as a photon. Small contributions arise from $t\bar{t}$ and WZ events. Continuum $Z+\gamma$ events are either produced by $q\bar{q}$ in the t- or u- channels, or from parton-to-photon fragmentation. The requirements $m_{\ell\ell} > m_Z - 10$ GeV, $m_{\ell\ell\gamma} > 115$ GeV and $\Delta R_{\ell\gamma} > 0.3$ suppress the contribution from $Z \to \ell\ell\gamma$, while the photon isolation requirement reduces the importance of the $Z+\gamma$ fragmentation component. The latter, together with the photon identification requirements, is also effective in reducing Z+jets events.

In this analysis, the estimated background composition is not used to determine the amount of expected background, which is directly fitted to the data mass spectrum, but is used to normalise the background Monte Carlo samples used for the optimisation of the selection criteria and the choice of mass spectra

background-fitting functions and the associated systematic uncertainties. Since the amplitudes for $Z+\gamma$, $Z \to \ell\ell$ and $Z \to \ell\ell\gamma$ interfere, only the total $\ell\ell\gamma$ background from the sum of the two processes is considered, and denoted with $Z\gamma$ in the following. A data-driven estimation of the background composition is performed, based on a two-dimensional sideband method [57, 58] exploiting the distribution of the photon identification and isolation variables in control regions enriched in Z+jets events, to estimate the relative $Z\gamma$ and Z+jets fractions in the selected sample. The $Z\gamma$ and Z+jets contributions are estimated *in situ* by applying this technique to the data after subtracting the 1% contribution from the $t\bar{t}$ and WZ backgrounds. Simulated events are used to estimate the small backgrounds from $t\bar{t}$ and WZ production (normalised to the data luminosity using the NLO MC cross sections), on which a conservative uncertainty of $\pm 50\%$ accounts for observed data-MC differences in the rates of fake photons and leptons from misidentified jets as well as for the uncertainties on the MC cross section due to the missing higher orders of the perturbative expansion and the PDF uncertainties. Simulated events are also used to determine the $Z\gamma$ contamination in the Z+jet background control regions and the correlation between photon identification and photon isolation for Z+jet events. The contribution to the control regions from the $H \to Z\gamma$ signal is expected to be small compared to the background and is neglected in this study. The fractions of $Z\gamma$, Z+jets and other ($t\bar{t} + WZ$) backgrounds are estimated to be around 82%, 17% and 1% at both $\sqrt{s}$ = 7 and 8 TeV. The relative uncertainty on the $Z\gamma$ purity is around 5%, dominated by the uncertainty on the correlation between the photon identification and isolation in Z+jet events, which is estimated by comparing the ALPGEN and SHERPA predictions. Good agreement between data and simulation is observed in the distributions of $m_{\ell\ell\gamma}$, as well as in the distributions of several other kinematic quantities that were also studied, including the dilepton invariant mass and the lepton and photon transverse momenta, pseudorapidity and azimuth.

5. Experimental systematic uncertainties

The following sources of experimental systematic uncertainties on the expected signal yields in each category were considered:

- The luminosity uncertainty is 1.8% for the 2011 data [19] and 2.8% for the 2012 data.[4]

- The uncertainty from the photon identification efficiency is obtained from a comparison between data-driven measurements and the simulated efficiencies in various photon and electron control samples [59] and varies between 2.6% and 3.1% depending on the category. The uncertainty from the photon reconstruction efficiency is negligible compared to that from the identification efficiency.

---

[4]The luminosity of the 2012 data is derived, following the same methodology as that detailed in Ref. [19], from a preliminary calibration of the luminosity scale derived from beam-separation scans performed in November 2012.

- The uncertainty from the electron trigger, reconstruction and identification efficiencies is estimated by varying the efficiency corrections applied to the simulation within the uncertainties of data-driven efficiency measurements. The total uncertainty, for events in which the Z boson candidate decays to electrons, varies between 2.5% and 3% depending on the category. The lepton reconstruction, identification and trigger efficiencies, as well as their energy and momentum scales and resolutions, are determined using large control samples of $Z \to \ell\ell$, $W \to \ell\nu$ and $J/\psi \to \ell\ell$ events [53, 56].

Other sources of uncertainty (muon trigger, reconstruction and identification efficiencies, lepton energy scale, resolution, and impact parameter selection efficiencies, lepton and photon isolation efficiencies) were investigated and found to have a negligible impact on the signal yield compared to the mentioned sources of uncertainty. The total relative uncertainty on the signal efficiency in each category is less than 5%, more than twice as small as the corresponding theoretical systematic uncertainty on the SM production cross section times branching ratio, described in Section 3. The uncertainty in the population of the p_{Tt} categories due to the description of the Higgs boson p_T spectrum is determined by varying the QCD scales and PDFs used in the HRES2 program. It is estimated to vary between 1.8% and 3.6% depending on the category.

The following sources of experimental systematic uncertainties on the signal $m_{\ell\ell\gamma}$ distribution were considered:

- The uncertainty on the peak position (0.2 GeV) is dominated by the photon energy scale uncertainty, which arises from the following sources: the calibration of the electron energy scale from $Z \to ee$ events, the uncertainty on its extrapolation to the energy scale of photons, dominated by the description of the detector material, and imperfect knowledge of the energy scale of the presampler detector located in front of the electromagnetic calorimeter.

- The uncertainty from the photon and electron energy resolution is estimated as the relative variation of the width of the signal $m_{\ell\ell\gamma}$ distribution after varying the corrections to the resolution of the electromagnetic particle response in the simulation within their uncertainties. It amounts to 3% for events in which the Z boson candidate decays to muons and to 10% for events in which the Z boson candidate decays to electrons.

- The uncertainty from the muon momentum resolution is estimated as the relative variation of the width of the signal $m_{\ell\ell\gamma}$ distribution after varying the muon momentum smearing corrections within their uncertainties. It is smaller than 1.5%.

To extract the signal, the background is estimated from the observed $m_{\ell\ell\gamma}$ distribution by assuming an analytical model, chosen from several alternatives to provide the best sensitivity to the signal while limiting the possible bias in the fitted signal to be within ±20% of the statistical uncertainty on the signal yield due to background fluctuations. The models are tested by performing signal+background fits of the $m_{\ell\ell\gamma}$ distribution of large simulated background-only samples scaled to the luminosity of the data and evaluating the ratio of the fitted signal yield to the statistical uncertainty on the fitted signal itself. The largest observed bias in the fitted signal for any Higgs boson mass in the range 120–150 GeV is taken as an additional systematic uncertainty; it varies between 0.5 events in poorly populated categories and 8.3 events in highly populated ones.

All systematic uncertainties, except that on the luminosity, are taken as fully correlated between the $\sqrt{s}$ = 7 TeV and the $\sqrt{s}$ = 8 TeV analyses.

6. Results

6.1. Likelihood function

The final discrimination between signal and background events is based on a likelihood fit to the $m_{\ell\ell\gamma}$ spectra in the invariant-mass region $115 < m_{\ell\ell\gamma} < 170$ GeV. The likelihood function depends on a single parameter of interest, the Higgs boson production signal strength μ, defined as the signal yield normalised to the SM expectation, as well as on several nuisance parameters that describe the shape and normalisation of the background distribution in each event category and the systematic uncertainties. Results for the inclusive cross section times branching ratio are also provided. In that case, the likelihood function depends on two parameters of interest, the signal cross sections times branching ratios at $\sqrt{s}$ = 7 TeV and $\sqrt{s}$ = 8 TeV, and the systematic uncertainties on the SM cross sections and branching ratios.

The background model in each event category is chosen based on the studies of sensitivity versus bias described in the previous section. For 2012 data, fifth- and fourth-order polynomials are chosen to model the background in the low-p_{Tt} categories while an exponentiated second-order polynomial is chosen for the high-p_{Tt} categories. For 2011 data, a fourth-order polynomial is used for the low-p_{Tt} categories and an exponential function is chosen for the high-p_{Tt} ones. The signal resolution functions in each category are described by the model illustrated in Section 4.2, fixing the fraction of events in each category to the MC predictions. For each fixed value of the Higgs boson mass between 120 and 150 GeV, in steps of 0.5 GeV, the parameters of the signal model are obtained, separately for each event category, through interpolation of the fully simulated MC samples.

For each of the nuisance parameters describing systematic uncertainties the likelihood is multiplied by a constraint term for each of the experimental systematic uncertainties evaluated as described in Section 5. For systematic uncertainties affecting the expected total signal yields for different centre-of-mass or lepton flavour, a log-normal constraint is used while for the uncertainties on the fractions of signal events in different $p_{Tt} - \Delta\eta_{Z\gamma}$ categories and on the signal $m_{\ell\ell\gamma}$ resolution a Gaussian constraint is used [60].

6.2. Statistical analysis

The data are compared to background and signal-plus-background hypotheses using a profile likelihood test statis-

tic [60]. Higgs boson decays to final states other than $\ell\ell\gamma$ are expected to contribute negligibly to the background in the selected sample. For each fixed value of the Higgs boson mass between 120 and 150 GeV fits are performed in steps of 0.5 GeV to determine the best value of μ ($\hat{\mu}$) or to maximise the likelihood with respect to all the nuisance parameters for alternative values of μ, including $\mu = 0$ (background-only hypothesis) and $\mu = 1$ (background plus Higgs boson of that mass, with SM-like production cross section times branching ratio). The compatibility between the data and the background-only hypothesis is quantified by the p-value of the $\mu = 0$ hypothesis, p_0, which provides an estimate of the significance of a possible observation. Upper limits on the signal strength at 95% CL are set using a modified frequentist (CL_s) method [61], by identifying the value μ_{up} for which the CL_s is equal to 0.05. Closed-form asymptotic formulae [62] are used to derive the results. Fits to the data are performed to obtain observed results. Fits to Asimov pseudo-data [62], generated either according to the $\mu = 1$ or $\mu = 0$ hypotheses, are performed to compute expected p_0 and CL_s upper limits, respectively.
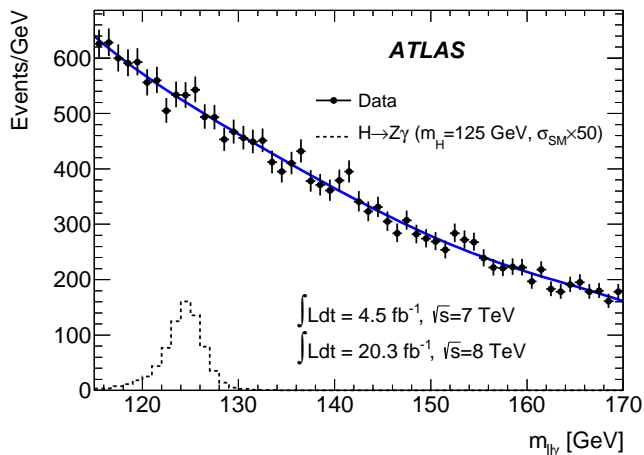
Fig. 2. Distribution of the reconstructed $\ell\ell\gamma$ invariant mass in data, after combining all the event categories (points with error bars). The solid blue line shows the sum of background-only fits to the data performed in each category. The dashed histogram corresponds to the signal expectation for a Higgs boson mass of 125 GeV decaying to $Z\gamma$ at 50 times the SM-predicted rate.

Figure 2 shows the $m_{\ell\ell\gamma}$ distribution of all events selected in data, compared to the sum of the background-only fits to the data in each of the ten event categories. No significant excess with respect to the background is visible, and the observed p_0 is compatible with the data being composed of background only. The smallest p_0 (0.05), corresponding to a significance of 1.6 σ, occurs for a mass of 141 GeV. The expected p_0 ranges between 0.34 and 0.44 for a Higgs boson with a mass $120 < m_H < 150$ GeV and SM-like cross section and branching ratio, corresponding to significances around 0.2 σ. The expected p_0 at $m_H = 125.5$ GeV is 0.42, corresponding to a significance of 0.2 σ, while the observed p_0 at the same mass is 0.27 (0.6 σ).

Observed and expected 95% CL upper limits on the value of the signal strength μ are derived and shown in Fig. 3. The expected limit ranges between 5 and 15 and the observed limit varies between 3.5 and 18 for a Higgs boson mass between 120 and 150 GeV. In particular, for a mass of 125.5 GeV, the observed and expected limits are equal to 11 and 9 times the Standard Model prediction, respectively. At the same mass the expected limit on μ assuming the existence of a SM ($\mu = 1$) Higgs boson with $m_H = 125.5$ GeV is 10. The results are dominated by the statistical uncertainties: neglecting all systematic uncertainties, the observed and expected 95% CL limits on the cross section at 125.5 GeV decrease by about 5%.
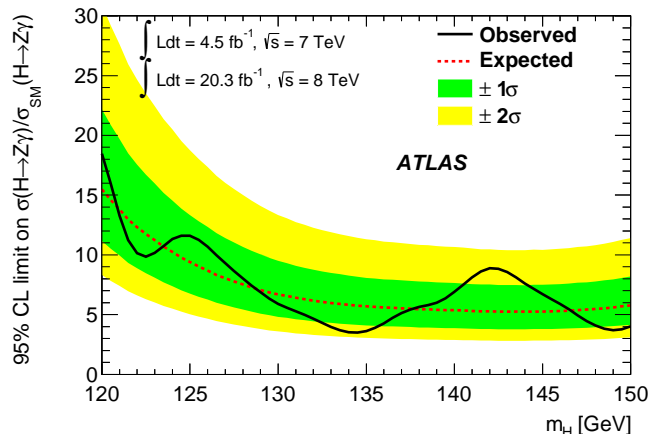
Fig. 3. Observed 95% CL limits (solid black line) on the production cross section of a SM Higgs boson decaying to $Z\gamma$ divided by the SM expectation. The limits are computed as a function of the Higgs boson mass. The median expected 95% CL exclusion limits (dashed red line), in the case of no expected signal, are also shown. The green and yellow bands correspond to the $\pm 1\sigma$ and $\pm 2\sigma$ intervals.

Upper limits on the $pp \to H \to Z\gamma$ cross section times branching ratio are also derived at 95% CL, for $\sqrt{s} = 7$ and 8 TeV. For $\sqrt{s} = 8$ TeV, the limit ranges between 0.13 and 0.5 pb; for $\sqrt{s} = 7$ TeV, it ranges between 0.20 and 0.8 pb.

7. Conclusions

A search for a Higgs boson in the decay channel $H \to Z\gamma$, $Z \to \ell\ell$ ($\ell = e, \mu$), in the mass range 120-150 GeV, was performed using 4.5 fb^{-1} of proton–proton collisions at $\sqrt{s} = 7$ TeV and 20.3 fb^{-1} of proton–proton collisions at $\sqrt{s} = 8$ TeV recorded with the ATLAS detector at the LHC. No excess with respect to the background is found in the $\ell\ell\gamma$ invariant-mass distribution and 95% CL upper limits on the cross section times branching ratio are derived. For $\sqrt{s} = 8$ TeV, the limit ranges between 0.13 and 0.5 pb. Combining $\sqrt{s} = 7$ and 8 TeV data and dividing the cross section by the Standard Model expectation, for a mass of 125.5 GeV, the observed 95% confidence limit is 11 times the SM prediction.

References

References

[1] ATLAS Collaboration, Observation of a new particle in the search for the Standard Model Higgs boson with the ATLAS detector at the LHC, Phys. Lett. B 716 (2012) 1. arXiv:1207.7214, doi:10.1016/j.physletb.2012.08.020.

[2] CMS Collaboration, Observation of a new boson at a mass of 125 GeV with the CMS experiment at the LHC, Phys. Lett. B 716 (2012) 30. arXiv:1207.7235, doi:10.1016/j.physletb.2012.08.021.

[3] ATLAS Collaboration, Measurements of Higgs boson production and couplings in diboson final states with the ATLAS detector at the LHC, Phys. Lett. B 726 (2013) 88–119. arXiv:1307.1427, doi:10.1016/j.physletb.2013.08.010.

[4] CMS Collaboration, Observation of a new boson with mass near 125 GeV in pp collisions at $\sqrt{s}$ = 7 and 8 TeV, JHEP 1306 (2013) 081. arXiv:1303.4571, doi:10.1007/JHEP06(2013)081.

[5] ATLAS Collaboration, Evidence for the spin-0 nature of the Higgs boson using ATLAS data, Phys. Lett. B 726 (2013) 120–144. arXiv:1307.1432, doi:10.1016/j.physletb.2013.08.026.

[6] CMS Collaboration, Study of the mass and spin-parity of the Higgs boson candidate via its decays to Z boson pairs, Phys. Rev. Lett. 110 (2013) 081803. arXiv:1212.6639.

[7] CMS Collaboration, Search for a Higgs boson decaying into a Z and a photon in pp collisions at $\sqrt{s}$ = 7 and 8 TeV, Phys. Lett. B 726 (2013) 587–609. arXiv:1307.5515, doi:10.1016/j.physletb.2013.09.057.

[8] LHC Higgs Cross Section Working Group, S. Dittmaier, C. Mariotti, G. Passarino, R. Tanaka (Eds.), Handbook of LHC Higgs cross sections: 1. Inclusive observables, CERN-2011-002. arXiv:1101.0593.

[9] LHC Higgs Cross Section Working Group, S. Dittmaier, C. Mariotti, G. Passarino, R. Tanaka (Eds.), Handbook of LHC Higgs cross sections: 2. Differential distributions, CERN-2012-002. arXiv:1201.3084.

[10] LHC Higgs Cross Section Working Group, S. Heinemeyer, C. Mariotti, G. Passarino, R. Tanaka (Eds.), Handbook of LHC Higgs Cross Sections: 3. Higgs Properties, CERN-2013-004. arXiv:1307.1347.

[11] I. Low, J. Lykken, G. Shaughnessy, Singlet scalars as Higgs imposters at the Large Hadron Collider, Phys. Rev. D 84 (2011) 035027. arXiv:1105.4587, doi:10.1103/PhysRevD.84.035027.

[12] I. Low, J. Lykken, G. Shaughnessy, Have we observed the Higgs (imposter)?, Phys. Rev. D 86 (2012) 093012. arXiv:1207.1093, doi:10.1103/PhysRevD.86.093012.

[13] A. Azatov, R. Contino, A. Di Iura, J. Galloway, New Prospects for Higgs Compositeness in $h \to Z\gamma$, Phys. Rev. D 88 (2013) 075019. arXiv:1308.2676, doi:10.1103/PhysRevD.88.075019.

[14] C.-W. Chiang, K. Yagyu, Higgs boson decays to $\gamma\gamma$ and $Z\gamma$ in models with Higgs extensions, Phys. Rev. D 87 (2013) 033003. arXiv:1207.1065, doi:10.1103/PhysRevD.87.033003.

[15] C.-S. Chen, C.-Q. Geng, D. Huang, L.-H. Tsai, New Scalar Contributions to $h \to Z\gamma$, Phys. Rev. D 87 (2013) 075019. arXiv:1301.4694, doi:10.1103/PhysRevD.87.075019.

[16] M. Carena, I. Low, C. E. Wagner, Implications of a Modified Higgs to Diphoton Decay Width, JHEP 1208 (2012) 060. arXiv:1206.1082, doi:10.1007/JHEP08(2012)060.

[17] ATLAS Collaboration, The ATLAS experiment at the CERN Large Hadron Collider, JINST 3 (2008) S08003. doi:10.1088/1748-0221/3/08/S08003.

[18] ATLAS Collaboration, Performance of the ATLAS trigger system in 2010, Eur. Phys. J. C 72 (2012) 1849. arXiv:1110.1530, doi:10.1140/epjc/s10052-011-1849-1.

[19] ATLAS Collaboration, Improved luminosity determination in pp collisions at $\sqrt{s}$ = 7 TeV using the ATLAS detector at the LHC, Eur. Phys. J. C 73 (2013) 2518. arXiv:1302.4393, doi:10.1140/epjc/s10052-013-2518-3.

[20] S. Alioli, P. Nason, C. Oleari and E. Re, NLO Higgs boson production via gluon fusion matched with shower in POWHEG, JHEP 0904 (2009) 002. arXiv:0812.0578, doi:10.1088/1126-6708/2009/04/002.

[21] P. Nason and C. Oleari, NLO Higgs boson production via vector-boson fusion matched with shower in POWHEG, JHEP 1002 (2010) 037. arXiv:0911.5299, doi:10.1007/JHEP02(2010)037.

[22] E. Bagnaschi, G. Degrassi, P. Slavich, A. Vicini, Higgs production via gluon fusion in the POWHEG approach in the SM and in the MSSM, JHEP 1202 (2012) 088. arXiv:1111.2854, doi:10.1007/JHEP02(2012)088.

[23] T. Sjöstrand, S. Mrenna, P. Skands, A brief introduction to PYTHIA 8.1, Comput. Phys. Commun. 178 (2008) 852–867. arXiv:0710.3820, doi:10.1016/j.cpc.2008.01.036.

[24] T. Gleisberg, et al., Event generation with SHERPA 1.1, JHEP 0902 (2009) 007. arXiv:0811.4622, doi:10.1088/1126-6708/2009/02/007.

[25] S. Hoeche, S. Schumann, F. Siegert, Hard photon production and matrix-element parton-shower merging, Phys. Rev. D 81 (2010) 034026. arXiv:0912.3501, doi:10.1103/PhysRevD.81.034026.

[26] M. L. Mangano, et al., ALPGEN, a generator for hard multi-parton processes in hadronic collisions, JHEP 0307 (2003) 001. arXiv:hep-ph/0206293, doi:10.1088/1126-6708/2003/07/001.

[27] G. Corcella, et al., HERWIG 6: an event generator for hadron emission reactions with interfering gluons (including super-symmetric processes) , JHEP 0101 (2001) 010. doi:10.1088/1126-6708/2001/01/010.

[28] S. Frixione, B. R. Webber, Matching NLO QCD computations and parton shower simulations, JHEP 0206 (2002) 029. arXiv:hep-ph/0204244.

[29] S. Frixione, P. Nason, B. R. Webber, Matching NLO QCD and parton showers in heavy flavour production, JHEP 0308 (2003) 007. arXiv:hep-ph/0305252, doi:10.1088/1126-6708/2003/08/007.

[30] H.-L. Lai, M. Guzzi, J. Huston, Z. Li, P. M. Nadolsky, et al., New parton distributions for collider physics, Phys. Rev. D 82 (2010) 074024. arXiv:1007.2241, doi:10.1103/PhysRevD.82.074024.

[31] M. Grazzini, H. Sargsyan, Heavy-quark mass effects in Higgs boson

8

production at the LHC, JHEP 1309 (2013) 129. arXiv:1306.4581, doi:10.1007/JHEP09(2013)129.

[32] J. Pumplin, et al., New generation of parton distributions with uncertainties from global qcd analysis, JHEP 0207 (2002) 012. doi:10.1088/1126-6708/2002/07/012.

[33] R. V. Harlander, W. B. Kilgore, Next-to-next-to-leading order Higgs production at hadron colliders, Phys. Rev. Lett. 88 (2002) 201801. arXiv:hep-ph/0201206, doi:10.1103/PhysRevLett.88.201801.

[34] C. Anastasiou, K. Melnikov, Higgs boson production at hadron colliders in NNLO QCD, Nucl. Phys. B 646 (2002) 220–256. arXiv:hep-ph/0207004, doi:10.1016/S0550-3213(02)00837-4.

[35] V. Ravindran, J. Smith, W. L. van Neerven, NNLO corrections to the total cross section for Higgs boson production in hadron hadron collisions, Nucl. Phys. B 665 (2003) 325–366. arXiv:hep-ph/0302135, doi:10.1016/S0550-3213(03)00457-7.

[36] C. Anastasiou, S. Buehler, F. Herzog, A. Lazopoulos, Inclusive Higgs boson cross-section for the LHC at 8 TeV, JHEP 1204 (2012) 004. arXiv:1202.3638, doi:10.1007/JHEP04(2012)004.

[37] D. de Florian, M. Grazzini, Higgs production at the LHC: updated cross sections at $\sqrt{s}$ = 8 TeV, Phys. Lett. B 718 (2012) 117–120. arXiv:1206.4133, doi:10.1016/j.physletb.2012.10.019.

[38] U. Aglietti, R. Bonciani, G. Degrassi, A. Vicini, Two-loop light fermion contribution to Higgs production and decays, Phys. Lett. B 595 (2004) 432–441. arXiv:hep-ph/0404071, doi:10.1016/j.physletb.2004.06.063.

[39] S. Actis, G. Passarino, C. Sturm, S. Uccirati, NLO electroweak corrections to Higgs boson production at hadron colliders, Phys. Lett. B 670 (2008) 12–17. arXiv:0809.1301, doi:10.1016/j.physletb.2008.10.018.

[40] O. Brein, A. Djouadi, R. Harlander, NNLO QCD corrections to the Higgs-strahlung processes at hadron colliders, Phys. Lett. B 579 (2004) 149. arXiv:hep-ph/0307206, doi:10.1016/j.physletb.2003.10.112.

[41] M. L. Ciccolini, S. Dittmaier, M. Kramer, Electroweak radiative corrections to associated *WH* and *ZH* production at hadron colliders, Phys. Rev. D 68 (2003) 073003. arXiv:hep-ph/0306234, doi:10.1103/PhysRevD.68.073003.

[42] W. Beenakker, et al., NLO QCD corrections to $t\bar{t}H$ production in hadron collisions., Nucl. Phys. B 653 (2003) 151–203. arXiv:hep-ph/0211352, doi:10.1016/S0550-3213(03)00044-0.

[43] S. Dawson, C. Jackson, L. H. Orr, L. Reina, D. Wackeroth, Associated Higgs production with top quarks at the Large Hadron Collider: NLO QCD corrections, Phys. Rev. D 68 (2003) 034022. arXiv:hep-ph/0305087, doi:10.1103/PhysRevD.68.034022.

[44] A. Djouadi, J. Kalinowski, M. Spira, HDECAY: A program for Higgs boson decays in the standard model and its supersymmetric extension, Comput. Phys. Commun. 108 (1998) 56–74. arXiv:hep-ph/9704448, doi:10.1016/S0010-4655(97)00123-9.

[45] A. Bredenstein, A. Denner, S. Dittmaier, M. M. Weber, Precise predictions for the Higgs-boson decay $H \rightarrow WW/ZZ \rightarrow$ 4leptons, Phys. Rev. D 74 (2006) 013004. arXiv:hep-ph/0604011, doi:10.1103/PhysRevD.74.013004.

[46] S. Actis, G. Passarino, C. Sturm, S. Uccirati, NNLO computational techniques: the cases $H \rightarrow \gamma\gamma$ and $H \rightarrow gg$, Nucl. Phys. B 811 (2009) 182–273. arXiv:0809.3667, doi:10.1016/j.nuclphysb.2008.11.024.

[47] D. A. Dicus, C. Kao, W. W. Repko, Comparison of $H \rightarrow \ell\bar{\ell}\gamma$ and $H \rightarrow \gamma Z, Z \rightarrow \ell\bar{\ell}$ including the ATLAS cuts. arXiv:1310.4380.

[48] L.-B. Chen, C.-F. Qiao, R.-L. Zhu, Reconstructing the 125 GeV SM Higgs boson through $\ell\bar{\ell}\gamma$. arXiv:1211.6058.

[49] A. Firan, R. Stroynowski, Internal conversions in Higgs decays to two photons, Phys. Rev. D 76 (2007) 057301. arXiv:0704.3987, doi:10.1103/PhysRevD.76.057301.

[50] J. M. Butterworth, J. R. Forshaw, M. H. Seymour, Multiparton interactions in photoproduction at HERA, Z. Phys. C 72 (1996) 637–646. arXiv:hep-ph/9601371, doi:10.1007/s002880050286.

[51] ATLAS Collaboration, The ATLAS simulation infrastructure, Eur. Phys. J. C 70 (2010) 823–874. arXiv:1005.4568, doi:10.1140/epjc/s10052-010-1429-9.

[52] S. Agostinelli, et al., Geant4 - a simulation toolkit, Nucl. Instrum. Methods A 506 (2003) 250. doi:10.1016/S0168-9002(03)01368-8.

[53] ATLAS Collaboration, Muon reconstruction efficiency in reprocessed 2010 LHC proton-proton collision data recorded with the ATLAS detector, ATLAS-CONF-2011-063 (2010) http://cds.cern.ch/record/1345743.

[54] ATLAS Collaboration, Expected photon performance in the ATLAS experiment, ATLAS-PHYS-PUB-2011-007 (2011), http://cds.cern.ch/record/1345329.

[55] ATLAS Collaboration, Improved electron reconstruction in ATLAS using the Gaussian Sum Filter-based model for bremsstrahlung, ATLAS-CONF-2012-047 (2012), http://cds.cern.ch/record/1449796.

[56] ATLAS Collaboration, Electron performance measurements with the ATLAS detector using the 2010 LHC proton-proton collision data, Eur. Phys. J. C 72 (2012) 1909. arXiv:1110.3174, doi:10.1140/epjc/s10052-012-1909-1.

[57] ATLAS Collaboration, Measurement of the inclusive isolated photon cross section in pp collisions at $\sqrt{s}$ = 7 TeV with the ATLAS detector, Phys. Rev. D 83 (2011) 052005. arXiv:1012.4389, doi:10.1103/PhysRevD.83.052005.

[58] ATLAS Collaboration, Measurements of $W\gamma$ and $Z\gamma$ production in pp collisions at $\sqrt{s}$= 7 TeV with the ATLAS detector at the LHC, Phys. Rev. D 87 (2013) 112003. arXiv:1302.1283, doi:10.1103/PhysRevD.87.112003.

[59] ATLAS Collaboration, Measurements of the photon identification efficiency with the ATLAS detector using 4.9 fb^{-1} of pp collision data collected in 2011, ATLAS-CONF-2012-123.
URL http://cds.cern.ch/record/1473426/

[60] ATLAS and CMS Collaborations, Procedure for the LHC Higgs boson search combination in Summer 2011, ATLAS-PHYS-PUB-2011-011, CMS NOTE-2011/005.

[61] A. L. Read, Presentation of search results: The CL(s) technique, J. Phys. G: Nucl. Part. Phys 28 (2002) 2693. doi:10.1088/0954-3899/28/10/313.

[62] G. Cowan, K. Cranmer, E. Gross, O. Vitells, Asymptotic formulae for likelihood-based tests of new physics, Eur. Phys. J. C 71 (2011) 1554. arXiv:1007.1727, doi:10.1140/epjc/s10052-011-1554-0.

9

The ATLAS Collaboration

G. Aad[84], T. Abajyan[21], B. Abbott[112], J. Abdallah[152], S. Abdel Khalek[116], O. Abdinov[11], R. Aben[106], B. Abi[113], M. Abolins[89], O.S. AbouZeid[159], H. Abramowicz[154], H. Abreu[137], Y. Abulaiti[147a,147b], B.S. Acharya[165a,165b,a], L. Adamczyk[38a], D.L. Adams[25], T.N. Addy[56], J. Adelman[177], S. Adomeit[99], T. Adye[130], T. Agatonovic-Jovin[13b], J.A. Aguilar-Saavedra[125f,125a], M. Agustoni[17], S.P. Ahlen[22], A. Ahmad[149], F. Ahmadov[64,b], G. Aielli[134a,134b], T.P.A. Åkesson[80], G. Akimoto[156], A.V. Akimov[95], J. Albert[170], S. Albrand[55], M.J. Alconada Verzini[70], M. Aleksa[30], I.N. Aleksandrov[64], C. Alexa[26a], G. Alexander[154], G. Alexandre[49], T. Alexopoulos[10], M. Alhroob[165a,165c], G. Alimonti[90a], L. Alio[84], J. Alison[31], B.M.M. Allbrooke[18], L.J. Allison[71], P.P. Allport[73], S.E. Allwood-Spiers[53], J. Almond[83], A. Aloisio[103a,103b], R. Alon[173], A. Alonso[36], F. Alonso[70], C. Alpigiani[75], A. Altheimer[35], B. Alvarez Gonzalez[89], M.G. Alviggi[103a,103b], K. Amako[65], Y. Amaral Coutinho[24a], C. Amelung[23], D. Amidei[88], V.V. Ammosov[129,*], S.P. Amor Dos Santos[125a,125c], A. Amorim[125a,125b], S. Amoroso[48], N. Amram[154], G. Amundsen[23], C. Anastopoulos[140], L.S. Ancu[17], N. Andari[30], T. Andeen[35], C.F. Anders[58b], G. Anders[30], K.J. Anderson[31], A. Andreazza[90a,90b], V. Andrei[58a], X.S. Anduaga[70], S. Angelidakis[9], P. Anger[44], A. Angerami[35], F. Anghinolfi[30], A.V. Anisenkov[108], N. Anjos[125a], A. Annovi[47], A. Antonaki[9], M. Antonelli[47], A. Antonov[97], J. Antos[145b], F. Anulli[133a], M. Aoki[65], L. Aperio Bella[18], R. Apolle[119,c], G. Arabidze[89], I. Aracena[144], Y. Arai[65], J.P. Araque[125a], A.T.H. Arce[45], J-F. Arguin[94], S. Argyropoulos[42], M. Arik[19a], A.J. Armbruster[88], O. Arnaez[82], V. Arnal[81], O. Arslan[21], A. Artamonov[96], G. Artoni[23], S. Asai[156], N. Asbah[94], A. Ashkenazi[154], S. Ask[28], B. Åsman[147a,147b], L. Asquith[6], K. Assamagan[25], R. Astalos[145a], M. Atkinson[166], N.B. Atlay[142], B. Auerbach[6], E. Auge[116], K. Augsten[127], M. Aurousseau[146b], G. Avolio[30], G. Azuelos[94,d], Y. Azuma[156], M.A. Baak[30], C. Bacci[135a,135b], A.M. Bach[15], H. Bachacou[137], K. Bachas[155], M. Backes[30], M. Backhaus[30], J. Backus Mayes[144], E. Badescu[26a], P. Bagiacchi[133a,133b], P. Bagnaia[133a,133b], Y. Bai[33a], D.C. Bailey[159], T. Bain[35], J.T. Baines[130], O.K. Baker[177], S. Baker[77], P. Balek[128], F. Balli[137], E. Banas[39], Sw. Banerjee[174], D. Banfi[30], A. Bangert[151], A.A.E. Bannoura[176], V. Bansal[170], H.S. Bansil[18], L. Barak[173], S.P. Baranov[95], T. Barber[48], E.L. Barberio[87], D. Barberis[50a,50b], M. Barbero[84], T. Barillari[100], M. Barisonzi[176], T. Barklow[144], N. Barlow[28], B.M. Barnett[130], R.M. Barnett[15], Z. Barnovska[5], A. Baroncelli[135a], G. Barone[49], A.J. Barr[119], F. Barreiro[81], J. Barreiro Guimarães da Costa[57], R. Bartoldus[144], A.E. Barton[71], P. Bartos[145a], V. Bartsch[150], A. Bassalat[116], A. Basye[166], R.L. Bates[53], L. Batkova[145a], J.R. Batley[28], M. Battistin[30], F. Bauer[137], H.S. Bawa[144,e], T. Beau[79], P.H. Beauchemin[162], R. Beccherle[123a,123b], P. Bechtle[21], H.P. Beck[17], K. Becker[176], S. Becker[99], M. Beckingham[139], C. Becot[116], A.J. Beddall[19c], A. Beddall[19c], S. Bedikian[177], V.A. Bednyakov[64], C.P. Bee[149], L.J. Beemster[106], T.A. Beermann[176], M. Begel[25], K. Behr[119], C. Belanger-Champagne[86], P.J. Bell[49], W.H. Bell[49], G. Bella[154], L. Bellagamba[20a], A. Bellerive[29], M. Bellomo[85], A. Belloni[57], O.L. Beloborodova[108,f], K. Belotskiy[97], O. Beltramello[30], O. Benary[154], D. Benchekroun[136a], K. Bendtz[147a,147b], N. Benekos[166], Y. Benhammou[154], E. Benhar Noccioli[49], J.A. Benitez Garcia[160b], D.P. Benjamin[45], J.R. Bensinger[23], K. Benslama[131], S. Bentvelsen[106], D. Berge[106], E. Bergeaas Kuutmann[16], N. Berger[5], F. Berghaus[170], E. Berglund[106], J. Beringer[15], C. Bernard[22], P. Bernat[77], C. Bernius[78], F.U. Bernlochner[170], T. Berry[76], P. Berta[128], C. Bertella[84], F. Bertolucci[123a,123b], M.I. Besana[90a], G.J. Besjes[105], O. Bessidskaia[147a,147b], N. Besson[137], C. Betancourt[48], S. Bethke[100], W. Bhimji[46], R.M. Bianchi[124], L. Bianchini[23], M. Bianco[30], O. Biebel[99], S.P. Bieniek[77], K. Bierwagen[54], J. Biesiada[15], M. Biglietti[135a], J. Bilbao De Mendizabal[49], H. Bilokon[47], M. Bindi[54], S. Binet[116], A. Bingul[19c], C. Bini[133a,133b], C.W. Black[151], J.E. Black[144], K.M. Black[22], D. Blackburn[139], R.E. Blair[6], J.-B. Blanchard[137], T. Blazek[145a], I. Bloch[42], C. Blocker[23], W. Blum[82,*], U. Blumenschein[54], G.J. Bobbink[106], V.S. Bobrovnikov[108], S.S. Bocchetta[80], A. Bocci[45], C.R. Boddy[119], M. Boehler[48], J. Boek[176], T.T. Boek[176], J.A. Bogaerts[30], A.G. Bogdanchikov[108], A. Bogouch[91,*], C. Bohm[147a], J. Bohm[126], V. Boisvert[76], T. Bold[38a], V. Boldea[26a], A.S. Boldyrev[98], N.M. Bolnet[137], M. Bomben[79], M. Bona[75], M. Boonekamp[137], A. Borisov[129], G. Borissov[71], M. Borri[83], S. Borroni[42], J. Bortfeldt[99], V. Bortolotto[135a,135b], K. Bos[106], D. Boscherini[20a], M. Bosman[12], H. Boterenbrood[106], J. Boudreau[124], J. Bouffard[2], E.V. Bouhova-Thacker[71], D. Boumediene[34], C. Bourdarios[116], N. Bousson[113], S. Boutouil[136d], A. Boveia[31], J. Boyd[30], I.R. Boyko[64], I. Bozovic-Jelisavcic[13b], J. Bracinik[18], P. Branchini[135a], A. Brandt[8], G. Brandt[15], O. Brandt[58a], U. Bratzler[157], B. Brau[85], J.E. Brau[115], H.M. Braun[176,*], S.F. Brazzale[165a,165c], B. Brelier[159], K. Brendlinger[121], A.J. Brennan[87], R. Brenner[167], S. Bressler[173], K. Bristow[146c], T.M. Bristow[46], D. Britton[53], F.M. Brochu[28], I. Brock[21], R. Brock[89], C. Bromberg[89], J. Bronner[100], G. Brooijmans[35], T. Brooks[76], W.K. Brooks[32b], J. Brosamer[15], E. Brost[115], G. Brown[83], J. Brown[55], P.A. Bruckman de Renstrom[39], D. Bruncko[145b], R. Bruneliere[48], S. Brunet[60], A. Bruni[20a], G. Bruni[20a], M. Bruschi[20a], L. Bryngemark[80], T. Buanes[14], Q. Buat[143], F. Bucci[49], P. Buchholz[142], R.M. Buckingham[119], A.G. Buckley[53], S.I. Buda[26a], I.A. Budagov[64], F. Buehrer[48], L. Bugge[118], M.K. Bugge[118], O. Bulekov[97], A.C. Bundock[73], H. Burckhart[30], S. Burdin[73], B. Burghgrave[107], S. Burke[130], I. Burmeister[43], E. Busato[34], V. Büscher[82], P. Bussey[53], C.P. Buszello[167], B. Butler[57], J.M. Butler[22], A.I. Butt[3], C.M. Buttar[53], J.M. Butterworth[77], P. Butti[106], W. Buttinger[28], A. Buzatu[53], M. Byszewski[10], S. Cabrera Urbán[168], D. Caforio[20a,20b], O. Cakir[4a], P. Calafiura[15], G. Calderini[79], P. Calfayan[99], R. Calkins[107], L.P. Caloba[24a], D. Calvet[34], S. Calvet[34], R. Camacho Toro[49], S. Camarda[42], P. Camarri[134a,134b], D. Cameron[118], L.M. Caminada[15], R. Caminal Armadans[12], S. Campana[30], M. Campanelli[77], A. Campoverde[149], V. Canale[103a,103b], A. Canepa[160a], J. Cantero[81], R. Cantrill[76], T. Cao[40], M.D.M. Capeans Garrido[30], I. Caprini[26a], M. Caprini[26a], M. Capua[37a,37b], R. Caputo[82], R. Cardarelli[134a], T. Carli[30], G. Carlino[103a], L. Carminati[90a,90b], S. Caron[105], E. Carquin[32a], G.D. Carrillo-Montoya[146c], A.A. Carter[75], J.R. Carter[28], J. Carvalho[125a,125c], D. Casadei[77], M.P. Casado[12], E. Castaneda-Miranda[146b], A. Castelli[106], V. Castillo Gimenez[168], N.F. Castro[125a], P. Catastini[57], A. Catinaccio[30], J.R. Catmore[71], A. Cattai[30], G. Cattani[134a,134b], S. Caughron[89], V. Cavaliere[166], D. Cavalli[90a], M. Cavalli-Sforza[12],

V. Cavasinni[123a,123b], F. Ceradini[135a,135b], B. Cerio[45], K. Cerny[128], A.S. Cerqueira[24b], A. Cerri[150], L. Cerrito[75], F. Cerutti[15], M. Cerv[30], A. Cervelli[17], S.A. Cetin[19b], A. Chafaq[136a], D. Chakraborty[107], I. Chalupkova[128], K. Chan[3], P. Chang[166], B. Chapleau[86], J.D. Chapman[28], D. Charfeddine[116], D.G. Charlton[18], C.C. Chau[159], C.A. Chavez Barajas[150], S. Cheatham[86], A. Chegwidden[89], S. Chekanov[6], S.V. Chekulaev[160a], G.A. Chelkov[64], M.A. Chelstowska[88], C. Chen[63], H. Chen[25], K. Chen[149], L. Chen[33d,g], S. Chen[33c], X. Chen[146c], Y. Chen[35], H.C. Cheng[88], Y. Cheng[31], A. Cheplakov[64], R. Cherkaoui El Moursli[136e], V. Chernyatin[25,*], E. Cheu[7], L. Chevalier[137], V. Chiarella[47], G. Chiefari[103a,103b], J.T. Childers[6], A. Chilingarov[71], G. Chiodini[72a], A.S. Chisholm[18], R.T. Chislett[77], A. Chitan[26a], M.V. Chizhov[64], S. Chouridou[9], B.K.B. Chow[99], I.A. Christidi[77], D. Chromek-Burckhart[30], M.L. Chu[152], J. Chudoba[126], L. Chytka[114], G. Ciapetti[133a,133b], A.K. Ciftci[4a], R. Ciftci[4a], D. Cinca[62], V. Cindro[74], A. Ciocio[15], P. Cirkovic[13b], Z.H. Citron[173], M. Citterio[90a], M. Ciubancan[26a], A. Clark[49], P.J. Clark[46], R.N. Clarke[15], W. Cleland[124], J.C. Clemens[84], B. Clement[55], C. Clement[147a,147b], Y. Coadou[84], M. Cobal[165a,165c], A. Coccaro[139], J. Cochran[63], L. Coffey[23], J.G. Cogan[144], J. Coggeshall[166], B. Cole[35], S. Cole[107], A.P. Colijn[106], C. Collins-Tooth[53], J. Collot[55], T. Colombo[58c], G. Colon[85], G. Compostella[100], P. Conde Muiño[125a,125b], E. Coniavitis[167], M.C. Conidi[12], S.H. Connell[146b], I.A. Connelly[76], S.M. Consonni[90a,90b], V. Consorti[48], S. Constantinescu[26a], C. Conta[120a,120b], G. Conti[57], F. Conventi[103a,h], M. Cooke[15], B.D. Cooper[77], A.M. Cooper-Sarkar[119], N.J. Cooper-Smith[76], K. Copic[15], T. Cornelissen[176], M. Corradi[20a], F. Corriveau[86,i], A. Corso-Radu[164], A. Cortes-Gonzalez[12], G. Cortiana[100], G. Costa[90a], M.J. Costa[168], D. Costanzo[140], D. Côté[8], G. Cottin[28], G. Cowan[76], B.E. Cox[83], K. Cranmer[109], G. Cree[29], S. Crépé-Renaudin[55], F. Crescioli[79], M. Crispin Ortuzar[119], M. Cristinziani[21], G. Crosetti[37a,37b], C.-M. Cuciuc[26a], C. Cuenca Almenar[177], T. Cuhadar Donszelmann[140], J. Cummings[177], M. Curatolo[47], C. Cuthbert[151], H. Czirr[142], P. Czodrowski[3], Z. Czyczula[177], S. D'Auria[53], M. D'Onofrio[73], M.J. Da Cunha Sargedas De Sousa[125a,125b], C. Da Via[83], W. Dabrowski[38a], A. Dafinca[119], T. Dai[88], O. Dale[14], F. Dallaire[94], C. Dallapiccola[85], M. Dam[36], A.C. Daniells[18], M. Dano Hoffmann[137], V. Dao[105], G. Darbo[50a], G.L. Darlea[26c], S. Darmora[8], J.A. Dassoulas[42], W. Davey[21], C. David[170], T. Davidek[128], E. Davies[119,c], M. Davies[94], O. Davignon[79], A.R. Davison[77], P. Davison[77], Y. Davygora[58a], E. Dawe[143], I. Dawson[140], R.K. Daya-Ishmukhametova[23], K. De[8], R. de Asmundis[103a], S. De Castro[20a,20b], S. De Cecco[79], J. de Graat[99], N. De Groot[105], P. de Jong[106], C. De La Taille[116], H. De la Torre[81], F. De Lorenzi[63], L. De Nooij[106], D. De Pedis[133a], A. De Salvo[133a], U. De Sanctis[165a,165c], A. De Santo[150], J.B. De Vivie De Regie[116], G. De Zorzi[133a,133b], W.J. Dearnaley[71], R. Debbe[25], C. Debenedetti[46], B. Dechenaux[55], D.V. Dedovich[64], J. Degenhardt[121], I. Deigaard[106], J. Del Peso[81], T. Del Prete[123a,123b], F. Deliot[137], M. Deliyergiyev[74], A. Dell'Acqua[30], L. Dell'Asta[22], M. Dell'Orso[123a,123b], M. Della Pietra[103a,h], D. della Volpe[49], M. Delmastro[5], P.A. Delsart[55], C. Deluca[106], S. Demers[177], M. Demichev[64], A. Demilly[79], S.P. Denisov[129], D. Derendarz[39], J.E. Derkaoui[136d], F. Derue[79], P. Dervan[73], K. Desch[21], C. Deterre[42], P.O. Deviveiros[106], A. Dewhurst[130], S. Dhaliwal[106], A. Di Ciaccio[134a,134b], L. Di Ciaccio[5], A. Di Domenico[133a,133b], C. Di Donato[103a,103b], A. Di Girolamo[30], B. Di Girolamo[30], A. Di Mattia[153], B. Di Micco[135a,135b], R. Di Nardo[47], A. Di Simone[48], R. Di Sipio[20a,20b], D. Di Valentino[29], M.A. Diaz[32a], E.B. Diehl[88], J. Dietrich[42], T.A. Dietzsch[58a], S. Diglio[87], A. Dimitrievska[13a], J. Dingfelder[21], C. Dionisi[133a,133b], P. Dita[26a], S. Dita[26a], F. Dittus[30], F. Djama[84], T. Djobava[51b], M.A.B. do Vale[24c], A. Do Valle Wemans[125a,125g], T.K.O. Doan[5], D. Dobos[30], E. Dobson[77], C. Doglioni[49], T. Doherty[53], T. Dohmae[156], J. Dolejsi[128], Z. Dolezal[128], B.A. Dolgoshein[97,*], S. Donati[123a,123b], P. Dondero[120a,120b], J. Donini[34], J. Dopke[30], A. Doria[103a], A. Dos Anjos[174], A. Dotti[123a,123b], M.T. Dova[70], A.T. Doyle[53], M. Dris[10], J. Dubbert[88], S. Dube[15], E. Dubreuil[34], E. Duchovni[173], G. Duckeck[99], O.A. Ducu[26a], D. Duda[176], A. Dudarev[30], F. Dudziak[63], L. Duflot[116], L. Duguid[76], M. Dührssen[30], M. Dunford[58a], H. Duran Yildiz[4a], M. Düren[52], A. Durglishvili[51b], M. Dwuznik[38a], M. Dyndal[38a], J. Ebke[99], W. Edson[2], N.C. Edwards[46], W. Ehrenfeld[21], T. Eifert[144], G. Eigen[14], K. Einsweiler[15], T. Ekelof[167], M. El Kacimi[136c], M. Ellert[167], S. Elles[5], F. Ellinghaus[82], K. Ellis[75], N. Ellis[30], J. Elmsheuser[99], M. Elsing[30], D. Emeliyanov[130], Y. Enari[156], O.C. Endner[82], M. Endo[117], R. Engelmann[149], J. Erdmann[177], A. Ereditato[17], D. Eriksson[147a], G. Ernis[176], J. Ernst[2], M. Ernst[25], J. Ernwein[137], D. Errede[166], S. Errede[166], E. Ertel[82], M. Escalier[116], H. Esch[43], C. Escobar[124], B. Esposito[47], A.I. Etienvre[137], E. Etzion[154], H. Evans[60], L. Fabbri[20a,20b], G. Facini[30], R.M. Fakhrutdinov[129], S. Falciano[133a], Y. Fang[33a], M. Fanti[90a,90b], A. Farbin[8], A. Farilla[135a], T. Farooque[12], S. Farrell[164], S.M. Farrington[171], P. Farthouat[30], F. Fassi[168], P. Fassnacht[30], D. Fassouliotis[9], A. Favareto[50a,50b], L. Fayard[116], P. Federic[145a], O.L. Fedin[122], W. Fedorko[169], M. Fehling-Kaschek[48], S. Feigl[30], L. Feligioni[84], C. Feng[33d], E.J. Feng[6], H. Feng[88], A.B. Fenyuk[129], S. Fernandez Perez[30], W. Fernando[6], S. Ferrag[53], J. Ferrando[53], V. Ferrara[42], A. Ferrari[167], P. Ferrari[106], R. Ferrari[120a], D.E. Ferreira de Lima[53], A. Ferrer[168], D. Ferrere[49], C. Ferretti[88], A. Ferretto Parodi[50a,50b], M. Fiascaris[31], F. Fiedler[82], A. Filipčič[74], M. Filipuzzi[42], F. Filthaut[105], M. Fincke-Keeler[170], K.D. Finelli[151], M.C.N. Fiolhais[125a,125c], L. Fiorini[168], A. Firan[40], J. Fischer[176], M.J. Fisher[110], W.C. Fisher[89], E.A. Fitzgerald[23], M. Flechl[48], I. Fleck[142], P. Fleischmann[175], S. Fleischmann[176], G.T. Fletcher[140], G. Fletcher[75], T. Flick[176], A. Floderus[80], L.R. Flores Castillo[174], A.C. Florez Bustos[160b], M.J. Flowerdew[100], A. Formica[137], A. Forti[83], D. Fortin[160a], D. Fournier[116], H. Fox[71], S. Fracchia[12], P. Francavilla[12], M. Franchini[20a,20b], S. Franchino[30], D. Francis[30], M. Franklin[57], S. Franz[61], M. Fraternali[120a,120b], S.T. French[28], C. Friedrich[42], F. Friedrich[44], D. Froidevaux[30], J.A. Frost[28], C. Fukunaga[157], E. Fullana Torregrosa[82], B.G. Fulsom[144], J. Fuster[168], C. Gabaldon[55], O. Gabizon[173], A. Gabrielli[20a,20b], A. Gabrielli[133a,133b], S. Gadatsch[106], S. Gadomski[49], G. Gagliardi[50a,50b], P. Gagnon[60], C. Galea[105], B. Galhardo[125a,125c], E.J. Gallas[119], V. Gallo[17], B.J. Gallop[130], P. Gallus[127], G. Galster[36], K.K. Gan[110], R.P. Gandrajula[62], J. Gao[33b,g], Y.S. Gao[144,e], F.M. Garay Walls[46], F. Garberson[177], C. García[168], J.E. García Navarro[168], M. Garcia-Sciveres[15], R.W. Gardner[31], N. Garelli[144], V. Garonne[30], C. Gatti[47], G. Gaudio[120a], B. Gaur[142], L. Gauthier[94], P. Gauzzi[133a,133b], I.L. Gavrilenko[95], C. Gay[169], G. Gaycken[21], E.N. Gazis[10],

11

P. Ge[33d,j], Z. Gecse[169], C.N.P. Gee[130], D.A.A. Geerts[106], Ch. Geich-Gimbel[21], K. Gellerstedt[147a,147b], C. Gemme[50a],
A. Gemmell[53], M.H. Genest[55], S. Gentile[133a,133b], M. George[54], S. George[76], D. Gerbaudo[164], A. Gershon[154], H. Ghazlane[136b],
N. Ghodbane[34], B. Giacobbe[20a], S. Giagu[133a,133b], V. Giangiobbe[12], P. Giannetti[123a,123b], F. Gianotti[30], B. Gibbard[25],
S.M. Gibson[76], M. Gilchriese[15], T.P.S. Gillam[28], D. Gillberg[30], D.M. Gingrich[3,d], N. Giokaris[9], M.P. Giordani[165a,165c],
R. Giordano[103a,103b], F.M. Giorgi[16], P.F. Giraud[137], D. Giugni[90a], C. Giuliani[48], M. Giulini[58b], B.K. Gjelsten[118], I. Gkialas[155,k],
L.K. Gladilin[98], C. Glasman[81], J. Glatzer[30], P.C.F. Glaysher[46], A. Glazov[42], G.L. Glonti[64], M. Goblirsch-Kolb[100], J.R. Goddard[75],
J. Godfrey[143], J. Godlewski[30], C. Goeringer[82], S. Goldfarb[88], T. Golling[177], D. Golubkov[129], A. Gomes[125a,125b,125d],
L.S. Gomez Fajardo[42], R. Gonçalo[125a], J. Goncalves Pinto Firmino Da Costa[42], L. Gonella[21], S. González de la Hoz[168],
G. Gonzalez Parra[12], M.L. Gonzalez Silva[27], S. Gonzalez-Sevilla[49], L. Goossens[30], P.A. Gorbounov[96], H.A. Gordon[25],
I. Gorelov[104], G. Gorfine[176], B. Gorini[30], E. Gorini[72a,72b], A. Gorišek[74], E. Gornicki[39], A.T. Goshaw[6], C. Gössling[43],
M.I. Gostkin[64], M. Gouighri[136a], D. Goujdami[136c], M.P. Goulette[49], A.G. Goussiou[139], C. Goy[5], S. Gozpinar[23], H.M.X. Grabas[137],
L. Graber[54], I. Grabowska-Bold[38a], P. Grafström[20a,20b], K-J. Grahn[42], J. Gramling[49], E. Gramstad[118], F. Grancagnolo[72a],
S. Grancagnolo[16], V. Grassi[149], V. Gratchev[122], H.M. Gray[30], E. Graziani[135a], O.G. Grebenyuk[122], Z.D. Greenwood[78,l],
K. Gregersen[36], I.M. Gregor[42], P. Grenier[144], J. Griffiths[8], N. Grigalashvili[64], A.A. Grillo[138], K. Grimm[71], S. Grinstein[12,m],
Ph. Gris[34], Y.V. Grishkevich[98], J.-F. Grivaz[116], J.P. Grohs[44], A. Grohsjean[42], E. Gross[173], J. Grosse-Knetter[54], G.C. Grossi[134a,134b],
J. Groth-Jensen[173], Z.J. Grout[150], K. Grybel[142], L. Guan[33b], F. Guescini[49], D. Guest[177], O. Gueta[154], C. Guicheney[34],
E. Guido[50a,50b], T. Guillemin[116], S. Guindon[2], U. Gul[53], C. Gumpert[44], J. Gunther[127], J. Guo[35], S. Gupta[119], P. Gutierrez[112],
N.G. Gutierrez Ortiz[53], C. Gutschow[77], N. Guttman[154], C. Guyot[137], C. Gwenlan[119], C.B. Gwilliam[73], A. Haas[109], C. Haber[15],
H.K. Hadavand[8], N. Haddad[136e], P. Haefner[21], S. Hageboeck[21], Z. Hajduk[39], H. Hakobyan[178], M. Haleem[42], D. Hall[119],
G. Halladjian[89], K. Hamacher[176], P. Hamal[114], K. Hamano[87], M. Hamer[54], A. Hamilton[146a], S. Hamilton[162], P.G. Hamnett[42],
L. Han[33b], K. Hanagaki[117], K. Hanawa[156], M. Hance[15], P. Hanke[58a], J.R. Hansen[36], J.B. Hansen[36], J.D. Hansen[36], P.H. Hansen[36],
K. Hara[161], A.S. Hard[174], T. Harenberg[176], S. Harkusha[91], D. Harper[88], R.D. Harrington[46], O.M. Harris[139], P.F. Harrison[171],
F. Hartjes[106], A. Harvey[56], S. Hasegawa[102], Y. Hasegawa[141], A Hasib[112], S. Hassani[137], S. Haug[17], M. Hauschild[30], R. Hauser[89],
M. Havranek[126], C.M. Hawkes[18], R.J. Hawkings[30], A.D. Hawkins[80], T. Hayashi[161], D. Hayden[89], C.P. Hays[119], H.S. Hayward[73],
S.J. Haywood[130], S.J. Head[18], T. Heck[82], V. Hedberg[80], L. Heelan[8], S. Heim[121], T. Heim[176], B. Heinemann[15], L. Heinrich[109],
S. Heisterkamp[36], J. Hejbal[126], L. Helary[22], C. Heller[99], M. Heller[30], S. Hellman[147a,147b], D. Hellmich[21], C. Helsens[30],
J. Henderson[119], R.C.W. Henderson[71], C. Hengler[42], A. Henrichs[177], A.M. Henriques Correia[30], S. Henrot-Versille[116],
C. Hensel[54], G.H. Herbert[16], Y. Hernández Jiménez[168], R. Herrberg-Schubert[16], G. Herten[48], R. Hertenberger[99], L. Hervas[30],
G.G. Hesketh[77], N.P. Hessey[106], R. Hickling[75], E. Higón-Rodriguez[168], J.C. Hill[28], K.H. Hiller[42], S. Hillert[21], S.J. Hillier[18],
I. Hinchliffe[15], E. Hines[121], M. Hirose[117], D. Hirschbuehl[176], J. Hobbs[149], N. Hod[106], M.C. Hodgkinson[140], P. Hodgson[140],
A. Hoecker[30], M.R. Hoeferkamp[104], J. Hoffman[40], D. Hoffmann[84], J.I. Hofmann[58a], M. Hohlfeld[82], T.R. Holmes[15], T.M. Hong[121],
L. Hooft van Huysduynen[109], J-Y. Hostachy[55], S. Hou[152], A. Hoummada[136a], J. Howard[119], J. Howarth[42], M. Hrabovsky[114],
I. Hristova[16], J. Hrivnac[116], T. Hryn'ova[5], P.J. Hsu[82], S.-C. Hsu[139], D. Hu[35], X. Hu[25], Y. Huang[146c], Z. Hubacek[30], F. Hubaut[84],
F. Huegging[21], T.B. Huffman[119], E.W. Hughes[35], G. Hughes[71], M. Huhtinen[30], T.A. Hülsing[82], M. Hurwitz[15], N. Huseynov[64,b],
J. Huston[89], J. Huth[57], G. Iacobucci[49], G. Iakovidis[10], I. Ibragimov[142], L. Iconomidou-Fayard[116], J. Idarraga[116], E. Ideal[177],
P. Iengo[103a], O. Igonkina[106], T. Iizawa[172], Y. Ikegami[65], K. Ikematsu[142], M. Ikeno[65], D. Iliadis[155], N. Ilic[159], Y. Inamaru[66],
T. Ince[100], P. Ioannou[9], M. Iodice[135a], K. Iordanidou[9], V. Ippolito[57], A. Irles Quiles[168], C. Isaksson[167], M. Ishino[67], M. Ishitsuka[158],
R. Ishmukhametov[110], C. Issever[119], S. Istin[19a], J.M. Iturbe Ponce[83], A.V. Ivashin[129], W. Iwanski[39], H. Iwasaki[65], J.M. Izen[41],
V. Izzo[103a], B. Jackson[121], J.N. Jackson[73], M. Jackson[73], P. Jackson[1], M.R. Jaekel[30], V. Jain[2], K. Jakobs[48], S. Jakobsen[36],
T. Jakoubek[126], J. Jakubek[127], D.O. Jamin[152], D.K. Jana[78], E. Jansen[77], H. Jansen[30], J. Janssen[21], M. Janus[171], G. Jarlskog[80],
T. Javůrek[48], L. Jeanty[15], G.-Y. Jeng[151], D. Jennens[87], P. Jenni[48,n], J. Jentzsch[43], C. Jeske[171], S. Jézéquel[5], H. Ji[174], W. Ji[82],
J. Jia[149], Y. Jiang[33b], M. Jimenez Belenguer[42], S. Jin[33a], A. Jinaru[26a], O. Jinnouchi[158], M.D. Joergensen[36], K.E. Johansson[147a],
P. Johansson[140], K.A. Johns[7], K. Jon-And[147a,147b], G. Jones[171], R.W.L. Jones[71], T.J. Jones[73], J. Jongmanns[58a], P.M. Jorge[125a,125b],
K.D. Joshi[83], J. Jovicevic[148], X. Ju[174], C.A. Jung[43], R.M. Jungst[30], P. Jussel[61], A. Juste Rozas[12,m], M. Kaci[168], A. Kaczmarska[39],
M. Kado[116], H. Kagan[110], M. Kagan[144], E. Kajomovitz[45], S. Kama[40], N. Kanaya[156], M. Kaneda[30], S. Kaneti[28], T. Kanno[158],
V.A. Kantserov[97], J. Kanzaki[65], B. Kaplan[109], A. Kapliy[31], D. Kar[53], K. Karakostas[10], N. Karastathis[10], M. Karnevskiy[82],
S.N. Karpov[64], K. Karthik[109], V. Kartvelishvili[71], A.N. Karyukhin[129], L. Kashif[174], G. Kasieczka[58b], R.D. Kass[110], A. Kastanas[14],
Y. Kataoka[156], A. Katre[49], J. Katzy[42], V. Kaushik[7], K. Kawagoe[69], T. Kawamoto[156], G. Kawamura[54], S. Kazama[156],
V.F. Kazanin[108], M.Y. Kazarinov[64], R. Keeler[170], P.T. Keener[121], R. Kehoe[40], M. Keil[54], J.S. Keller[42], H. Keoshkerian[5],
O. Kepka[126], B.P. Kerševan[74], S. Kersten[176], K. Kessoku[156], J. Keung[159], F. Khalil-zada[11], H. Khandanyan[147a,147b], A. Khanov[113],
A. Khodinov[97], A. Khomich[58a], T.J. Khoo[28], G. Khoriauli[21], A. Khoroshilov[176], V. Khovanskiy[96], E. Khramov[64], J. Khubua[51b],
H.Y. Kim[8], H. Kim[147a,147b], S.H. Kim[161], N. Kimura[172], O. Kind[16], B.T. King[73], M. King[168], R.S.B. King[119], S.B. King[169],
J. Kirk[130], A.E. Kiryunin[100], T. Kishimoto[66], D. Kisielewska[38a], F. Kiss[48], T. Kitamura[66], T. Kittelmann[124], K. Kiuchi[161],
E. Kladiva[145b], M. Klein[73], U. Klein[73], K. Kleinknecht[82], P. Klimek[147a,147b], A. Klimentov[25], R. Klingenberg[43], J.A. Klinger[83],
E.B. Klinkby[36], T. Klioutchnikova[30], P.F. Klok[105], E.-E. Kluge[58a], P. Kluit[106], S. Kluth[100], E. Kneringer[61], E.B.F.G. Knoops[84],
A. Knue[53], T. Kobayashi[156], M. Kobel[44], M. Kocian[144], P. Kodys[128], P. Koevesarki[21], T. Koffas[29], E. Koffeman[106], L.A. Kogan[119],
S. Kohlmann[176], Z. Kohout[127], T. Kohriki[65], T. Koi[144], H. Kolanoski[16], I. Koletsou[5], J. Koll[89], A.A. Komar[95,*], Y. Komori[156],

T. Kondo[65], K. Köneke[48], A.C. König[105], S. König[82], T. Kono[65,o], R. Konoplich[109,p], N. Konstantinidis[77], R. Kopeliansky[153], S. Koperny[38a], L. Köpke[82], A.K. Kopp[48], K. Korcyl[39], K. Kordas[155], A. Korn[77], A.A. Korol[108], I. Korolkov[12], E.V. Korolkova[140], V.A. Korotkov[129], O. Kortner[100], S. Kortner[100], V.V. Kostyukhin[21], S. Kotov[100], V.M. Kotov[64], A. Kotwal[45], C. Kourkoumelis[9], V. Kouskoura[155], A. Koutsman[160a], R. Kowalewski[170], T.Z. Kowalski[38a], W. Kozanecki[137], A.S. Kozhin[129], V. Kral[127], V.A. Kramarenko[98], G. Kramberger[74], D. Krasnopevtsev[97], M.W. Krasny[79], A. Krasznahorkay[30], J.K. Kraus[21], A. Kravchenko[25], S. Kreiss[109], M. Kretz[58c], J. Kretzschmar[73], K. Kreutzfeldt[52], P. Krieger[159], K. Kroeninger[54], H. Kroha[100], J. Kroll[121], J. Kroseberg[21], J. Krstic[13a], U. Kruchonak[64], H. Krüger[21], T. Kruker[17], N. Krumnack[63], Z.V. Krumshteyn[64], A. Kruse[174], M.C. Kruse[45], M. Kruskal[22], T. Kubota[87], S. Kuday[4a], S. Kuehn[48], A. Kugel[58c], A. Kuhl[138], T. Kuhl[42], V. Kukhtin[64], Y. Kulchitsky[91], S. Kuleshov[32b], M. Kuna[133a,133b], J. Kunkle[121], A. Kupco[126], H. Kurashige[66], Y.A. Kurochkin[91], R. Kurumida[66], V. Kus[126], E.S. Kuwertz[148], M. Kuze[158], J. Kvita[143], A. La Rosa[49], L. La Rotonda[37a,37b], L. Labarga[81], C. Lacasta[168], F. Lacava[133a,133b], J. Lacey[29], H. Lacker[16], D. Lacour[79], V.R. Lacuesta[168], E. Ladygin[64], R. Lafaye[5], B. Laforge[79], T. Lagouri[177], S. Lai[48], H. Laier[58a], L. Lambourne[77], S. Lammers[60], C.L. Lampen[7], W. Lampl[7], E. Lançon[137], U. Landgraf[48], M.P.J. Landon[75], V.S. Lang[58a], C. Lange[42], A.J. Lankford[164], F. Lanni[25], K. Lantzsch[30], A. Lanza[120a], S. Laplace[79], C. Lapoire[21], J.F. Laporte[137], T. Lari[90a], M. Lassnig[30], P. Laurelli[47], V. Lavorini[37a,37b], W. Lavrijsen[15], A.T. Law[138], P. Laycock[73], B.T. Le[55], O. Le Dortz[79], E. Le Guirriec[84], E. Le Menedeu[12], T. LeCompte[6], F. Ledroit-Guillon[55], C.A. Lee[152], H. Lee[106], J.S.H. Lee[117], S.C. Lee[152], L. Lee[177], G. Lefebvre[79], M. Lefebvre[170], F. Legger[99], C. Leggett[15], A. Lehan[73], M. Lehmacher[21], G. Lehmann Miotto[30], X. Lei[7], A.G. Leister[177], M.A.L. Leite[24d], R. Leitner[128], D. Lellouch[173], B. Lemmer[54], K.J.C. Leney[77], T. Lenz[106], G. Lenzen[176], B. Lenzi[30], R. Leone[7], K. Leonhardt[44], S. Leontsinis[10], C. Leroy[94], C.G. Lester[28], C.M. Lester[121], J. Levêque[5], D. Levin[88], L.J. Levinson[173], M. Levy[18], A. Lewis[119], G.H. Lewis[109], A.M. Leyko[21], M. Leyton[41], B. Li[33b,q], B. Li[84], H. Li[149], H.L. Li[31], S. Li[45], X. Li[88], Y. Li[116,r], Z. Liang[119,s], H. Liao[34], B. Liberti[134a], P. Lichard[30], K. Lie[166], J. Liebal[21], W. Liebig[14], C. Limbach[21], A. Limosani[87], M. Limper[62], S.C. Lin[152,t], F. Linde[106], B.E. Lindquist[149], J.T. Linnemann[89], E. Lipeles[121], A. Lipniacka[14], M. Lisovyi[42], T.M. Liss[166], D. Lissauer[25], A. Lister[169], A.M. Litke[138], B. Liu[152], D. Liu[152], J.B. Liu[33b], K. Liu[33b,u], L. Liu[88], M. Liu[45], M. Liu[33b], Y. Liu[33b], M. Livan[120a,120b], S.S.A. Livermore[119], A. Lleres[55], J. Llorente Merino[81], S.L. Lloyd[75], F. Lo Sterzo[152], E. Lobodzinska[42], P. Loch[7], W.S. Lockman[138], T. Loddenkoetter[21], F.K. Loebinger[83], A.E. Loevschall-Jensen[36], A. Loginov[177], C.W. Loh[169], T. Lohse[16], K. Lohwasser[48], M. Lokajicek[126], V.P. Lombardo[5], J.D. Long[88], R.E. Long[71], L. Lopes[125a], D. Lopez Mateos[57], B. Lopez Paredes[140], J. Lorenz[99], N. Lorenzo Martinez[60], M. Losada[163], P. Loscutoff[15], M.J. Losty[160a,*], X. Lou[41], A. Lounis[116], J. Love[6], P.A. Love[71], A.J. Lowe[144,e], F. Lu[33a], H.J. Lubatti[139], C. Luci[133a,133b], A. Lucotte[55], F. Luehring[60], W. Lukas[61], L. Luminari[133a], O. Lundberg[147a,147b], B. Lund-Jensen[148], M. Lungwitz[82], D. Lynn[25], R. Lysak[126], E. Lytken[80], H. Ma[25], L.L. Ma[33d], G. Maccarrone[47], A. Macchiolo[100], B. Maček[74], J. Machado Miguens[125a,125b], D. Macina[30], D. Madaffari[84], R. Madar[48], H.J. Maddocks[71], W.F. Mader[44], A. Madsen[167], M. Maeno[8], T. Maeno[25], E. Magradze[54], K. Mahboubi[48], J. Mahlstedt[106], S. Mahmoud[73], C. Maiani[137], C. Maidantchik[24a], A. Maio[125a,125b,125d], S. Majewski[115], Y. Makida[65], N. Makovec[116], P. Mal[137,v], B. Malaescu[79], Pa. Malecki[39], V.P. Maleev[122], F. Malek[55], U. Mallik[62], D. Malon[6], C. Malone[144], S. Maltezos[10], V.M. Malyshev[108], S. Malyukov[30], J. Mamuzic[13b], B. Mandelli[30], L. Mandelli[90a], I. Mandić[74], R. Mandrysch[62], J. Maneira[125a,125b], A. Manfredini[100], L. Manhaes de Andrade Filho[24b], J.A. Manjarres Ramos[160b], A. Mann[99], P.M. Manning[138], A. Manousakis-Katsikakis[9], B. Mansoulie[137], R. Mantifel[86], S. Manzoni[90a,90b], L. Mapelli[30], L. March[168], J.F. Marchand[29], F. Marchese[134a,134b], G. Marchiori[79], M. Marcisovsky[126], C.P. Marino[170], C.N. Marques[125a], F. Marroquim[24a], S.P. Marsden[83], Z. Marshall[15], L.F. Marti[17], S. Marti-Garcia[168], B. Martin[30], B. Martin[89], J.P. Martin[94], T.A. Martin[171], V.J. Martin[46], B. Martin dit Latour[49], H. Martinez[137], M. Martinez[12,m], S. Martin-Haugh[130], A.C. Martyniuk[77], M. Marx[139], F. Marzano[133a], A. Marzin[30], L. Masetti[82], T. Mashimo[156], R. Mashinistov[95], J. Masik[83], A.L. Maslennikov[108], I. Massa[20a,20b], N. Massol[5], P. Mastrandrea[149], A. Mastroberardino[37a,37b], T. Masubuchi[156], P. Matricon[116], H. Matsunaga[156], T. Matsushita[66], P. Mättig[176], S. Mättig[42], J. Mattmann[82], J. Maurer[26a], S.J. Maxfield[73], D.A. Maximov[108,f], R. Mazini[152], L. Mazzaferro[134a,134b], G. Mc Goldrick[159], S.P. Mc Kee[88], A. McCarn[88], R.L. McCarthy[149], T.G. McCarthy[29], N.A. McCubbin[130], K.W. McFarlane[56,*], J.A. Mcfayden[77], G. Mchedlidze[54], T. Mclaughlan[18], S.J. McMahon[130], R.A. McPherson[170,i], A. Meade[85], J. Mechnich[106], M. Medinnis[42], S. Meehan[31], R. Meera-Lebbai[112], S. Mehlhase[36], A. Mehta[73], K. Meier[58a], C. Meineck[99], B. Meirose[80], C. Melachrinos[31], B.R. Mellado Garcia[146c], F. Meloni[90a,90b], L. Mendoza Navas[163], A. Mengarelli[20a,20b], S. Menke[100], E. Meoni[162], K.M. Mercurio[57], S. Mergelmeyer[21], N. Meric[137], P. Mermod[49], L. Merola[103a,103b], C. Meroni[90a], F.S. Merritt[31], H. Merritt[110], A. Messina[30,w], J. Metcalfe[25], A.S. Mete[164], C. Meyer[82], C. Meyer[31], J-P. Meyer[137], J. Meyer[30], R.P. Middleton[130], S. Migas[73], L. Mijović[137], G. Mikenberg[173], M. Mikestikova[126], M. Mikuž[74], D.W. Miller[31], C. Mills[46], A. Milov[173], D.A. Milstead[147a,147b], D. Milstein[173], A.A. Minaenko[129], M. Miñano Moya[168], I.A. Minashvili[64], A.I. Mincer[109], B. Mindur[38a], M. Mineev[64], Y. Ming[174], L.M. Mir[12], G. Mirabelli[133a], T. Mitani[172], J. Mitrevski[99], V.A. Mitsou[168], S. Mitsui[65], A. Miucci[49], P.S. Miyagawa[140], J.U. Mjörnmark[80], T. Moa[147a,147b], K. Mochizuki[84], V. Moeller[28], S. Mohapatra[35], W. Mohr[48], S. Molander[147a,147b], R. Moles-Valls[168], K. Mönig[42], C. Monini[55], J. Monk[36], E. Monnier[84], J. Montejo Berlingen[12], F. Monticelli[70], S. Monzani[133a,133b], R.W. Moore[3], C. Mora Herrera[49], A. Moraes[53], N. Morange[62], J. Morel[54], D. Moreno[82], M. Moreno Llácer[54], P. Morettini[50a], M. Morgenstern[44], M. Morii[57], S. Moritz[82], A.K. Morley[148], G. Mornacchi[30], J.D. Morris[75], L. Morvaj[102], H.G. Moser[100], M. Mosidze[51b], J. Moss[110], R. Mount[144], E. Mountricha[25], S.V. Mouraviev[95,*], E.J.W. Moyse[85], S.G. Muanza[84], R.D. Mudd[18], F. Mueller[58a], J. Mueller[124], K. Mueller[21], T. Mueller[28], T. Mueller[82], D. Muenstermann[49], Y. Munwes[154], J.A. Murillo Quijada[18], W.J. Murray[171,c], E. Musto[153], A.G. Myagkov[129,x], M. Myska[126], O. Nackenhorst[54], J. Nadal[54],

13

K. Nagai[61], R. Nagai[158], Y. Nagai[84], K. Nagano[65], A. Nagarkar[110], Y. Nagasaka[59], M. Nagel[100], A.M. Nairz[30], Y. Nakahama[30], K. Nakamura[65], T. Nakamura[156], I. Nakano[111], H. Namasivayam[41], G. Nanava[21], R. Narayan[58b], T. Nattermann[21], T. Naumann[42], G. Navarro[163], R. Nayyar[7], H.A. Neal[88], P.Yu. Nechaeva[95], T.J. Neep[83], A. Negri[120a,120b], G. Negri[30], M. Negrini[20a], S. Nektarijevic[49], A. Nelson[164], T.K. Nelson[144], S. Nemecek[126], P. Nemethy[109], A.A. Nepomuceno[24a], M. Nessi[30,y], M.S. Neubauer[166], M. Neumann[176], R.M. Neves[109], P. Nevski[25], F.M. Newcomer[121], P.R. Newman[18], D.H. Nguyen[6], R.B. Nickerson[119], R. Nicolaidou[137], B. Nicquevert[30], J. Nielsen[138], N. Nikiforou[35], A. Nikiforov[16], V. Nikolaenko[129,x], I. Nikolic-Audit[79], K. Nikolics[49], K. Nikolopoulos[18], P. Nilsson[8], Y. Ninomiya[156], A. Nisati[133a], R. Nisius[100], T. Nobe[158], L. Nodulman[6], M. Nomachi[117], I. Nomidis[155], S. Norberg[112], M. Nordberg[30], J. Novakova[128], S. Nowak[100], M. Nozaki[65], L. Nozka[114], K. Ntekas[10], G. Nunes Hanninger[87], T. Nunnemann[99], E. Nurse[77], F. Nuti[87], B.J. O'Brien[46], F. O'grady[7], D.C. O'Neil[143], V. O'Shea[53], F.G. Oakham[29,d], H. Oberlack[100], T. Obermann[21], J. Ocariz[79], A. Ochi[66], M.I. Ochoa[77], S. Oda[69], S. Odaka[65], H. Ogren[60], A. Oh[83], S.H. Oh[45], C.C. Ohm[30], H. Ohman[167], T. Ohshima[102], W. Okamura[117], H. Okawa[25], Y. Okumura[31], T. Okuyama[156], A. Olariu[26a], A.G. Olchevski[64], S.A. Olivares Pino[46], D. Oliveira Damazio[25], E. Oliver Garcia[168], D. Olivito[121], A. Olszewski[39], J. Olszowska[39], A. Onofre[125a,125e], P.U.E. Onyisi[31,z], C.J. Oram[160a], M.J. Oreglia[31], Y. Oren[154], D. Orestano[135a,135b], N. Orlando[72a,72b], C. Oropeza Barrera[53], R.S. Orr[159], B. Osculati[50a,50b], R. Ospanov[121], G. Otero y Garzon[27], H. Otono[69], M. Ouchrif[136d], E.A. Ouellette[170], F. Ould-Saada[118], A. Ouraou[137], K.P. Oussoren[106], Q. Ouyang[33a], A. Ovcharova[15], M. Owen[83], V.E. Ozcan[19a], N. Ozturk[8], K. Pachal[119], A. Pacheco Pages[12], C. Padilla Aranda[12], M. Pagáčová[48], S. Pagan Griso[15], E. Paganis[140], C. Pahl[100], F. Paige[25], P. Pais[85], K. Pajchel[118], G. Palacino[160b], S. Palestini[30], D. Pallin[34], A. Palma[125a,125b], J.D. Palmer[18], Y.B. Pan[174], E. Panagiotopoulou[10], J.G. Panduro Vazquez[76], P. Pani[106], N. Panikashvili[88], S. Panitkin[25], D. Pantea[26a], L. Paolozzi[134a,134b], Th.D. Papadopoulou[10], K. Papageorgiou[155,k], A. Paramonov[6], D. Paredes Hernandez[34], M.A. Parker[28], F. Parodi[50a,50b], J.A. Parsons[35], U. Parzefall[48], E. Pasqualucci[133a], S. Passaggio[50a], A. Passeri[135a], F. Pastore[135a,135b,*], Fr. Pastore[76], G. Pásztor[49,aa], S. Pataraia[176], N.D. Patel[151], J.R. Pater[83], S. Patricelli[103a,103b], T. Pauly[30], J. Pearce[170], M. Pedersen[118], S. Pedraza Lopez[168], R. Pedro[125a,125b], S.V. Peleganchuk[108], D. Pelikan[167], H. Peng[33b], B. Penning[31], J. Penwell[60], D.V. Perepelitsa[25], E. Perez Codina[160a], M.T. Pérez García-Estañ[168], V. Perez Reale[35], L. Perini[90a,90b], H. Pernegger[30], R. Perrino[72a], R. Peschke[42], V.D. Peshekhonov[64], K. Peters[30], R.F.Y. Peters[83], B.A. Petersen[87], J. Petersen[30], T.C. Petersen[36], E. Petit[42], A. Petridis[147a,147b], C. Petridou[155], E. Petrolo[133a], F. Petrucci[135a,135b], M. Petteni[143], N.E. Pettersson[158], R. Pezoa[32b], P.W. Phillips[130], G. Piacquadio[144], E. Pianori[171], A. Picazio[49], E. Piccaro[75], M. Piccinini[20a,20b], S.M. Piec[42], R. Piegaia[27], D.T. Pignotti[110], J.E. Pilcher[31], A.D. Pilkington[77], J. Pina[125a,125b,125d], M. Pinamonti[165a,165c,ab], A. Pinder[119], J.L. Pinfold[3], A. Pingel[36], B. Pinto[125a], S. Pires[79], C. Pizio[90a,90b], M.-A. Pleier[25], V. Pleskot[128], E. Plotnikova[64], P. Plucinski[147a,147b], S. Poddar[58a], F. Podlyski[34], R. Poettgen[82], L. Poggioli[116], D. Pohl[21], M. Pohl[49], G. Polesello[120a], A. Policicchio[37a,37b], R. Polifka[159], A. Polini[20a], C.S. Pollard[45], V. Polychronakos[25], K. Pommès[30], L. Pontecorvo[133a], B.G. Pope[89], G.A. Popeneciu[26b], D.S. Popovic[13a], A. Poppleton[30], X. Portell Bueso[12], G.E. Pospelov[100], S. Pospisil[127], K. Potamianos[15], I.N. Potrap[64], C.J. Potter[150], C.T. Potter[115], G. Poulard[30], J. Poveda[60], V. Pozdnyakov[64], R. Prabhu[77], P. Pralavorio[84], A. Pranko[15], S. Prasad[30], R. Pravahan[8], S. Prell[63], D. Price[83], J. Price[73], L.E. Price[6], D. Prieur[124], M. Primavera[72a], M. Proissl[46], K. Prokofiev[109], F. Prokoshin[32b], E. Protopapadaki[137], S. Protopopescu[25], J. Proudfoot[6], M. Przybycien[38a], H. Przysiezniak[5], E. Ptacek[115], E. Pueschel[85], D. Puldon[149], M. Purohit[25,ac], P. Puzo[116], Y. Pylypchenko[62], J. Qian[88], G. Qin[53], A. Quadt[54], D.R. Quarrie[15], W.B. Quayle[165a,165b], D. Quilty[53], A. Qureshi[160b], V. Radeka[25], V. Radescu[42], S.K. Radhakrishnan[149], P. Radloff[115], P. Rados[87], F. Ragusa[90a,90b], G. Rahal[179], S. Rajagopalan[25], M. Rammensee[30], M. Rammes[142], A.S. Randle-Conde[40], C. Rangel-Smith[79], K. Rao[164], F. Rauscher[99], T.C. Rave[48], T. Ravenscroft[53], M. Raymond[30], A.L. Read[118], N.P. Readioff[73], D.M. Rebuzzi[120a,120b], A. Redelbach[175], G. Redlinger[25], R. Reece[138], K. Reeves[41], L. Rehnisch[16], A. Reinsch[115], H. Reisin[27], M. Relich[164], C. Rembser[30], Z.L. Ren[152], A. Renaud[116], M. Rescigno[133a], S. Resconi[90a], B. Resende[137], P. Reznicek[128], R. Rezvani[94], R. Richter[100], M. Ridel[79], P. Rieck[16], M. Rijssenbeek[149], A. Rimoldi[120a,120b], L. Rinaldi[20a], E. Ritsch[61], I. Riu[12], F. Rizatdinova[113], E. Rizvi[75], S.H. Robertson[86,i], A. Robichaud-Veronneau[119], D. Robinson[28], J.E.M. Robinson[83], A. Robson[53], C. Roda[123a,123b], L. Rodrigues[30], S. Roe[30], O. Røhne[118], S. Rolli[162], A. Romaniouk[97], M. Romano[20a,20b], G. Romeo[27], E. Romero Adam[168], N. Rompotis[139], L. Roos[79], E. Ros[168], S. Rosati[133a], K. Rosbach[49], A. Rose[150], M. Rose[76], P.L. Rosendahl[14], O. Rosenthal[142], V. Rossetti[147a,147b], E. Rossi[103a,103b], L.P. Rossi[50a], R. Rosten[139], M. Rotaru[26a], I. Roth[173], J. Rothberg[139], D. Rousseau[116], C.R. Royon[137], A. Rozanov[84], Y. Rozen[153], X. Ruan[146c], F. Rubbo[12], I. Rubinskiy[42], V.I. Rud[98], C. Rudolph[44], M.S. Rudolph[159], F. Rühr[48], A. Ruiz-Martinez[63], Z. Rurikova[48], N.A. Rusakovich[64], A. Ruschke[99], J.P. Rutherfoord[7], N. Ruthmann[48], Y.F. Ryabov[122], M. Rybar[128], G. Rybkin[116], N.C. Ryder[119], A.F. Saavedra[151], S. Sacerdoti[27], A. Saddique[3], I. Sadeh[154], H.F-W. Sadrozinski[138], R. Sadykov[64], F. Safai Tehrani[133a], H. Sakamoto[156], Y. Sakurai[172], G. Salamanna[75], A. Salamon[134a], M. Saleem[112], D. Salek[106], P.H. Sales De Bruin[139], D. Salihagic[100], A. Salnikov[144], J. Salt[168], B.M. Salvachua Ferrando[6], D. Salvatore[37a,37b], F. Salvatore[150], A. Salvucci[105], A. Salzburger[30], D. Sampsonidis[155], A. Sanchez[103a,103b], J. Sánchez[168], V. Sanchez Martinez[168], H. Sandaker[14], H.G. Sander[82], M.P. Sanders[99], M. Sandhoff[176], T. Sandoval[28], C. Sandoval[163], R. Sandstroem[100], D.P.C. Sankey[130], A. Sansoni[47], C. Santoni[34], R. Santonico[134a,134b], H. Santos[125a], I. Santoyo Castillo[150], K. Sapp[124], A. Sapronov[64], J.G. Saraiva[125a,125d], B. Sarrazin[21], G. Sartisohn[176], O. Sasaki[65], Y. Sasaki[156], I. Satsounkevitch[91], G. Sauvage[5,*], E. Sauvan[5], P. Savard[159,d], D.O. Savu[30], C. Sawyer[119], L. Sawyer[78,l], D.H. Saxon[53], J. Saxon[121], C. Sbarra[20a], A. Sbrizzi[3], T. Scanlon[30], D.A. Scannicchio[164], M. Scarcella[151], J. Schaarschmidt[173], P. Schacht[100], D. Schaefer[121], R. Schaefer[42], A. Schaelicke[46], S. Schaepe[21], S. Schaetzel[58b], U. Schäfer[82], A.C. Schaffer[116],

14

D. Schaile[99], R.D. Schamberger[149], V. Scharf[58a], V.A. Schegelsky[122], D. Scheirich[128], M. Schernau[164], M.I. Scherzer[35], C. Schiavi[50a,50b], J. Schieck[99], C. Schillo[48], M. Schioppa[37a,37b], S. Schlenker[30], E. Schmidt[48], K. Schmieden[30], C. Schmitt[82], C. Schmitt[99], S. Schmitt[58b], B. Schneider[17], Y.J. Schnellbach[73], U. Schnoor[44], L. Schoeffel[137], A. Schoening[58b], B.D. Schoenrock[89], A.L.S. Schorlemmer[54], M. Schott[82], D. Schouten[160a], J. Schovancova[25], M. Schram[86], S. Schramm[159], M. Schreyer[175], C. Schroeder[82], N. Schuh[82], M.J. Schultens[21], H.-C. Schultz-Coulon[58a], H. Schulz[16], M. Schumacher[48], B.A. Schumm[138], Ph. Schune[137], A. Schwartzman[144], Ph. Schwegler[100], Ph. Schwemling[137], R. Schwienhorst[89], J. Schwindling[137], T. Schwindt[21], M. Schwoerer[5], F.G. Sciacca[17], E. Scifo[116], G. Sciolla[23], W.G. Scott[130], F. Scuri[123a,123b], F. Scutti[21], J. Searcy[88], G. Sedov[42], E. Sedykh[122], S.C. Seidel[104], A. Seiden[138], F. Seifert[127], J.M. Seixas[24a], G. Sekhniaidze[103a], S.J. Sekula[40], K.E. Selbach[46], D.M. Seliverstov[122,*], G. Sellers[73], N. Semprini-Cesari[20a,20b], C. Serfon[30], L. Serin[116], L. Serkin[54], T. Serre[84], R. Seuster[160a], H. Severini[112], F. Sforza[100], A. Sfyrla[30], E. Shabalina[54], M. Shamim[115], L.Y. Shan[33a], J.T. Shank[22], Q.T. Shao[87], M. Shapiro[15], P.B. Shatalov[96], K. Shaw[165a,165c], P. Sherwood[77], S. Shimizu[66], C.O. Shimmin[164], M. Shimojima[101], T. Shin[56], M. Shiyakova[64], A. Shmeleva[95], M.J. Shochet[31], D. Short[119], S. Shrestha[63], E. Shulga[97], M.A. Shupe[7], S. Shushkevich[42], P. Sicho[126], D. Sidorov[113], A. Sidoti[133a], F. Siegert[44], Dj. Sijacki[13a], O. Silbert[173], J. Silva[125a,125d], Y. Silver[154], D. Silverstein[144], S.B. Silverstein[147a], V. Simak[127], O. Simard[5], Lj. Simic[13a], S. Simion[116], E. Simioni[82], B. Simmons[77], R. Simoniello[90a,90b], M. Simonyan[36], P. Sinervo[159], N.B. Sinev[115], V. Sipica[142], G. Siragusa[175], A. Sircar[78], A.N. Sisakyan[64,*], S.Yu. Sivoklokov[98], J. Sjölin[147a,147b], T.B. Sjursen[14], L.A. Skinnari[15], H.P. Skottowe[57], K.Yu. Skovpen[108], P. Skubic[112], M. Slater[18], T. Slavicek[127], K. Sliwa[162], V. Smakhtin[173], B.H. Smart[46], L. Smestad[118], S.Yu. Smirnov[97], Y. Smirnov[97], L.N. Smirnova[98,ad], O. Smirnova[80], K.M. Smith[53], M. Smizanska[71], K. Smolek[127], A.A. Snesarev[95], G. Snidero[75], J. Snow[112], S. Snyder[25], R. Sobie[170,i], F. Socher[44], J. Sodomka[127], A. Soffer[154], D.A. Soh[152,s], C.A. Solans[30], M. Solar[127], J. Solc[127], E.Yu. Soldatov[97], U. Soldevila[168], E. Solfaroli Camillocci[133a,133b], A.A. Solodkov[129], O.V. Solovyanov[129], V. Solovyev[122], P. Sommer[48], H.Y. Song[33b], N. Soni[1], A. Sood[15], V. Sopko[127], B. Sopko[127], V. Sorin[12], M. Sosebee[8], R. Soualah[165a,165c], P. Soueid[94], A.M. Soukharev[108], D. South[42], S. Spagnolo[72a,72b], F. Spanò[76], W.R. Spearman[57], R. Spighi[20a], G. Spigo[30], M. Spousta[128], T. Spreitzer[159], B. Spurlock[8], R.D. St. Denis[53], S. Staerz[44], J. Stahlman[121], R. Stamen[58a], E. Stanecka[39], R.W. Stanek[6], C. Stanescu[135a], M. Stanescu-Bellu[42], M.M. Stanitzki[42], S. Stapnes[118], E.A. Starchenko[129], J. Stark[55], P. Staroba[126], P. Starovoitov[42], R. Staszewski[39], P. Stavina[145a,*], G. Steele[53], P. Steinberg[25], I. Stekl[127], B. Stelzer[143], H.J. Stelzer[30], O. Stelzer-Chilton[160a], H. Stenzel[52], S. Stern[100], G.A. Stewart[53], J.A. Stillings[21], M.C. Stockton[86], M. Stoebe[86], K. Stoerig[48], G. Stoicea[26a], P. Stolte[54], S. Stonjek[100], A.R. Stradling[8], A. Straessner[44], J. Strandberg[148], S. Strandberg[147a,147b], A. Strandlie[118], E. Strauss[144], M. Strauss[112], P. Strizenec[145b], R. Ströhmer[175], D.M. Strom[115], R. Stroynowski[40], S.A. Stucci[17], B. Stugu[14], N.A. Styles[42], D. Su[144], J. Su[124], HS. Subramania[3], R. Subramaniam[78], A. Succurro[12], Y. Sugaya[117], C. Suhr[107], M. Suk[127], V.V. Sulin[95], S. Sultansoy[4c], T. Sumida[67], X. Sun[33a], J.E. Sundermann[48], K. Suruliz[140], G. Susinno[37a,37b], M.R. Sutton[150], Y. Suzuki[65], M. Svatos[126], S. Swedish[169], M. Swiatlowski[144], I. Sykora[145a], T. Sykora[128], D. Ta[89], K. Tackmann[42], J. Taenzer[159], A. Taffard[164], R. Tafirout[160a], N. Taiblum[154], Y. Takahashi[102], H. Takai[25], R. Takashima[68], H. Takeda[66], T. Takeshita[141], Y. Takubo[65], M. Talby[84], A.A. Talyshev[108,f], J.Y.C. Tam[175], M.C. Tamsett[78,ae], K.G. Tan[87], J. Tanaka[156], R. Tanaka[116], S. Tanaka[132], S. Tanaka[65], A.J. Tanasijczuk[143], K. Tani[66], B.B. Tannenwald[110], N. Tannoury[84], S. Tapprogge[82], S. Tarem[153], F. Tarrade[29], G.F. Tartarelli[90a], P. Tas[128], M. Tasevsky[126], T. Tashiro[67], E. Tassi[37a,37b], A. Tavares Delgado[125a,125b], Y. Tayalati[136d], C. Taylor[77], F.E. Taylor[93], G.N. Taylor[87], W. Taylor[160b], F.A. Teischinger[30], M. Teixeira Dias Castanheira[75], P. Teixeira-Dias[76], K.K. Temming[48], H. Ten Kate[30], P.K. Teng[152], S. Terada[65], K. Terashi[156], J. Terron[81], S. Terzo[100], M. Testa[47], R.J. Teuscher[159,i], J. Therhaag[21], T. Theveneaux-Pelzer[34], S. Thoma[48], J.P. Thomas[18], J. Thomas-wilsker[76], E.N. Thompson[35], P.D. Thompson[18], P.D. Thompson[159], A.S. Thompson[53], L.A. Thomsen[36], E. Thomson[121], M. Thomson[28], W.M. Thong[87], R.P. Thun[88,*], F. Tian[35], M.J. Tibbetts[15], V.O. Tikhomirov[95,af], Yu.A. Tikhonov[108,f], S. Timoshenko[97], E. Tiouchichine[84], P. Tipton[177], S. Tisserant[84], T. Todorov[5], S. Todorova-Nova[128], B. Toggerson[164], J. Tojo[69], S. Tokár[145a], K. Tokushuku[65], K. Tollefson[89], L. Tomlinson[83], M. Tomoto[102], L. Tompkins[31], K. Toms[104], N.D. Topilin[64], E. Torrence[115], H. Torres[143], E. Torró Pastor[168], J. Toth[84,aa], F. Touchard[84], D.R. Tovey[140], H.L. Tran[116], T. Trefzger[175], L. Tremblet[30], A. Tricoli[30], I.M. Trigger[160a], S. Trincaz-Duvoid[79], M.F. Tripiana[70], N. Triplett[25], W. Trischuk[159], B. Trocmé[55], C. Troncon[90a], M. Trottier-McDonald[143], M. Trovatelli[135a,135b], P. True[89], M. Trzebinski[39], A. Trzupek[39], C. Tsarouchas[30], J.C-L. Tseng[119], P.V. Tsiareshka[91], D. Tsionou[137], G. Tsipolitis[10], N. Tsirintanis[9], S. Tsiskaridze[12], V. Tsiskaridze[48], E.G. Tskhadadze[51a], I.I. Tsukerman[96], V. Tsulaia[15], S. Tsuno[65], D. Tsybychev[149], A. Tua[140], A. Tudorache[26a], V. Tudorache[26a], A.N. Tuna[121], S.A. Tupputi[20a,20b], S. Turchikhin[98,ad], D. Turecek[127], I. Turk Cakir[4d], R. Turra[90a,90b], P.M. Tuts[35], A. Tykhonov[74], M. Tylmad[147a,147b], M. Tyndel[130], K. Uchida[21], I. Ueda[156], R. Ueno[29], M. Ughetto[84], M. Ugland[14], M. Uhlenbrock[21], F. Ukegawa[161], G. Unal[30], A. Undrus[25], G. Unel[164], F.C. Ungaro[48], Y. Unno[65], D. Urbaniec[35], P. Urquijo[21], G. Usai[8], A. Usanova[61], L. Vacavant[84], V. Vacek[127], B. Vachon[86], N. Valencic[106], S. Valentinetti[20a,20b], A. Valero[168], L. Valery[34], S. Valkar[128], E. Valladolid Gallego[168], S. Vallecorsa[49], J.A. Valls Ferrer[168], R. Van Berg[121], P.C. Van Der Deijl[106], R. van der Geer[106], H. van der Graaf[106], R. Van Der Leeuw[106], D. van der Ster[30], N. van Eldik[30], P. van Gemmeren[6], J. Van Nieuwkoop[143], I. van Vulpen[106], M.C. van Woerden[30], M. Vanadia[133a,133b], W. Vandelli[30], A. Vaniachine[6], P. Vankov[42], F. Vannucci[79], G. Vardanyan[178], R. Vari[133a], E.W. Varnes[7], T. Varol[85], D. Varouchas[79], A. Vartapetian[8], K.E. Varvell[151], V.I. Vassilakopoulos[56], F. Vazeille[34], T. Vazquez Schroeder[54], J. Veatch[7], F. Veloso[125a,125c], S. Veneziano[133a], A. Ventura[72a,72b], D. Ventura[85], M. Venturi[48], N. Venturi[159], A. Venturini[23], V. Vercesi[120a], M. Verducci[139], W. Verkerke[106], J.C. Vermeulen[106], A. Vest[44], M.C. Vetterli[143,d], O. Viazlo[80], I. Vichou[166],

15

T. Vickey[146c,ag], O.E. Vickey Boeriu[146c], G.H.A. Viehhauser[119], S. Viel[169], R. Vigne[30], M. Villa[20a,20b], M. Villaplana Perez[168],
E. Vilucchi[47], M.G. Vincter[29], V.B. Vinogradov[64], J. Virzi[15], O. Vitells[173], I. Vivarelli[150], F. Vives Vaque[3], S. Vlachos[10],
D. Vladoiu[99], M. Vlasak[127], A. Vogel[21], P. Vokac[127], G. Volpi[47], M. Volpi[87], H. von der Schmitt[100], H. von Radziewski[48],
E. von Toerne[21], V. Vorobel[128], M. Vos[168], R. Voss[30], J.H. Vossebeld[73], N. Vranjes[137], M. Vranjes Milosavljevic[106], V. Vrba[126],
M. Vreeswijk[106], T. Vu Anh[48], R. Vuillermet[30], I. Vukotic[31], Z. Vykydal[127], W. Wagner[176], P. Wagner[21], S. Wahrmund[44],
J. Wakabayashi[102], J. Walder[71], R. Walker[99], W. Walkowiak[142], R. Wall[177], P. Waller[73], B. Walsh[177], C. Wang[152], C. Wang[45],
F. Wang[174], H. Wang[15], H. Wang[40], J. Wang[42], J. Wang[33a], K. Wang[86], R. Wang[104], S.M. Wang[152], T. Wang[21], X. Wang[177],
A. Warburton[86], C.P. Ward[28], D.R. Wardrope[77], M. Warsinsky[48], A. Washbrook[46], C. Wasicki[42], I. Watanabe[66], P.M. Watkins[18],
A.T. Watson[18], I.J. Watson[151], M.F. Watson[18], G. Watts[139], S. Watts[83], B.M. Waugh[77], S. Webb[83], M.S. Weber[17], S.W. Weber[175],
J.S. Webster[31], A.R. Weidberg[119], P. Weigell[100], B. Weinert[60], J. Weingarten[54], C. Weiser[48], H. Weits[106], P.S. Wells[30],
T. Wenaus[25], D. Wendland[16], Z. Weng[152,s], T. Wengler[30], S. Wenig[30], N. Wermes[21], M. Werner[48], P. Werner[30], M. Wessels[58a],
J. Wetter[162], K. Whalen[29], A. White[8], M.J. White[1], R. White[32b], S. White[123a,123b], D. Whiteson[164], D. Wicke[176], F.J. Wickens[130],
W. Wiedenmann[174], M. Wielers[130], P. Wienemann[21], C. Wiglesworth[36], L.A.M. Wiik-Fuchs[21], P.A. Wijeratne[77], A. Wildauer[100],
M.A. Wildt[42,ah], H.G. Wilkens[30], J.Z. Will[99], H.H. Williams[121], S. Williams[28], C. Willis[89], S. Willocq[85], J.A. Wilson[18],
A. Wilson[88], I. Wingerter-Seez[5], S. Winkelmann[48], F. Winklmeier[115], M. Wittgen[144], T. Wittig[43], J. Wittkowski[99], S.J. Wollstadt[82],
M.W. Wolter[39], H. Wolters[125a,125c], B.K. Wosiek[39], J. Wotschack[30], M.J. Woudstra[83], K.W. Wozniak[39], M. Wright[53], S.L. Wu[174],
X. Wu[49], Y. Wu[88], E. Wulf[35], T.R. Wyatt[83], B.M. Wynne[46], S. Xella[36], M. Xiao[137], D. Xu[33a], L. Xu[33b,ai], B. Yabsley[151],
S. Yacoob[146b,aj], M. Yamada[65], H. Yamaguchi[156], Y. Yamaguchi[156], A. Yamamoto[65], K. Yamamoto[63], S. Yamamoto[156],
T. Yamamura[156], T. Yamanaka[156], K. Yamauchi[102], Y. Yamazaki[66], Z. Yan[22], H. Yang[33e], H. Yang[174], U.K. Yang[83], Y. Yang[110],
S. Yanush[92], L. Yao[33a], W-M. Yao[15], Y. Yasu[65], E. Yatsenko[42], K.H. Yau Wong[21], J. Ye[40], S. Ye[25], A.L. Yen[57], E. Yildirim[42],
M. Yilmaz[4b], R. Yoosoofmiya[124], K. Yorita[172], R. Yoshida[6], K. Yoshihara[156], C. Young[144], C.J.S. Young[30], S. Youssef[22],
D.R. Yu[15], J. Yu[8], J.M. Yu[88], J. Yu[113], L. Yuan[66], A. Yurkewicz[107], B. Zabinski[39], R. Zaidan[62], A.M. Zaitsev[129,x], A. Zaman[149],
S. Zambito[23], L. Zanello[133a,133b], D. Zanzi[100], A. Zaytsev[25], C. Zeitnitz[176], M. Zeman[127], A. Zemla[38a], K. Zengel[23], O. Zenin[129],
T. Ženiš[145a], D. Zerwas[116], G. Zevi della Porta[57], D. Zhang[88], F. Zhang[174], H. Zhang[89], J. Zhang[6], L. Zhang[152], X. Zhang[33d],
Z. Zhang[116], Z. Zhao[33b], A. Zhemchugov[64], J. Zhong[119], B. Zhou[88], L. Zhou[35], N. Zhou[164], C.G. Zhu[33d], H. Zhu[33a], J. Zhu[88],
Y. Zhu[33b], X. Zhuang[33a], A. Zibell[99], D. Zieminska[60], N.I. Zimine[64], C. Zimmermann[82], R. Zimmermann[21], S. Zimmermann[21],
S. Zimmermann[48], Z. Zinonos[54], M. Ziolkowski[142], R. Zitoun[5], G. Zobernig[174], A. Zoccoli[20a,20b], M. zur Nedden[16],
G. Zurzolo[103a,103b], V. Zutshi[107], L. Zwalinski[30].

[1] Department of Physics, University of Adelaide, Adelaide, Australia

[2] Physics Department, SUNY Albany, Albany NY, United States of America

[3] Department of Physics, University of Alberta, Edmonton AB, Canada

[4] [a] Department of Physics, Ankara University, Ankara; [b] Department of Physics, Gazi University, Ankara; [c] Division of Physics, TOBB University of Economics and Technology, Ankara; [d] Turkish Atomic Energy Authority, Ankara, Turkey

[5] LAPP, CNRS/IN2P3 and Université de Savoie, Annecy-le-Vieux, France

[6] High Energy Physics Division, Argonne National Laboratory, Argonne IL, United States of America

[7] Department of Physics, University of Arizona, Tucson AZ, United States of America

[8] Department of Physics, The University of Texas at Arlington, Arlington TX, United States of America

[9] Physics Department, University of Athens, Athens, Greece

[10] Physics Department, National Technical University of Athens, Zografou, Greece

[11] Institute of Physics, Azerbaijan Academy of Sciences, Baku, Azerbaijan

[12] Institut de Física d'Altes Energies and Departament de Física de la Universitat Autònoma de Barcelona, Barcelona, Spain

[13] [a] Institute of Physics, University of Belgrade, Belgrade; [b] Vinca Institute of Nuclear Sciences, University of Belgrade, Belgrade, Serbia

[14] Department for Physics and Technology, University of Bergen, Bergen, Norway

[15] Physics Division, Lawrence Berkeley National Laboratory and University of California, Berkeley CA, United States of America

[16] Department of Physics, Humboldt University, Berlin, Germany

[17] Albert Einstein Center for Fundamental Physics and Laboratory for High Energy Physics, University of Bern, Bern, Switzerland

[18] School of Physics and Astronomy, University of Birmingham, Birmingham, United Kingdom

[19] [a] Department of Physics, Bogazici University, Istanbul; [b] Department of Physics, Dogus University, Istanbul; [c] Department of Physics Engineering, Gaziantep University, Gaziantep, Turkey

[20] [a] INFN Sezione di Bologna; [b] Dipartimento di Fisica e Astronomia, Università di Bologna, Bologna, Italy

[21] Physikalisches Institut, University of Bonn, Bonn, Germany

[22] Department of Physics, Boston University, Boston MA, United States of America

[23] Department of Physics, Brandeis University, Waltham MA, United States of America

[24] [a] Universidade Federal do Rio De Janeiro COPPE/EE/IF, Rio de Janeiro; [b] Federal University of Juiz de Fora (UFJF), Juiz de Fora; [c] Federal University of Sao Joao del Rei (UFSJ), Sao Joao del Rei; [d] Instituto de Fisica, Universidade de Sao Paulo, Sao

Paulo, Brazil

[25] Physics Department, Brookhaven National Laboratory, Upton NY, United States of America

[26] (a) National Institute of Physics and Nuclear Engineering, Bucharest; (b) National Institute for Research and Development of Isotopic and Molecular Technologies, Physics Department, Cluj Napoca; (c) University Politehnica Bucharest, Bucharest; (d) West University in Timisoara, Timisoara, Romania

[27] Departamento de Física, Universidad de Buenos Aires, Buenos Aires, Argentina

[28] Cavendish Laboratory, University of Cambridge, Cambridge, United Kingdom

[29] Department of Physics, Carleton University, Ottawa ON, Canada

[30] CERN, Geneva, Switzerland

[31] Enrico Fermi Institute, University of Chicago, Chicago IL, United States of America

[32] (a) Departamento de Física, Pontificia Universidad Católica de Chile, Santiago; (b) Departamento de Física, Universidad Técnica Federico Santa María, Valparaíso, Chile

[33] (a) Institute of High Energy Physics, Chinese Academy of Sciences, Beijing; (b) Department of Modern Physics, University of Science and Technology of China, Anhui; (c) Department of Physics, Nanjing University, Jiangsu; (d) School of Physics, Shandong University, Shandong; (e) Physics Department, Shanghai Jiao Tong University, Shanghai, China

[34] Laboratoire de Physique Corpusculaire, Clermont Université and Université Blaise Pascal and CNRS/IN2P3, Clermont-Ferrand, France

[35] Nevis Laboratory, Columbia University, Irvington NY, United States of America

[36] Niels Bohr Institute, University of Copenhagen, Kobenhavn, Denmark

[37] (a) INFN Gruppo Collegato di Cosenza, Laboratori Nazionali di Frascati; (b) Dipartimento di Fisica, Università della Calabria, Rende, Italy

[38] (a) AGH University of Science and Technology, Faculty of Physics and Applied Computer Science, Krakow; (b) Marian Smoluchowski Institute of Physics, Jagiellonian University, Krakow, Poland

[39] The Henryk Niewodniczanski Institute of Nuclear Physics, Polish Academy of Sciences, Krakow, Poland

[40] Physics Department, Southern Methodist University, Dallas TX, United States of America

[41] Physics Department, University of Texas at Dallas, Richardson TX, United States of America

[42] DESY, Hamburg and Zeuthen, Germany

[43] Institut für Experimentelle Physik IV, Technische Universität Dortmund, Dortmund, Germany

[44] Institut für Kern- und Teilchenphysik, Technische Universität Dresden, Dresden, Germany

[45] Department of Physics, Duke University, Durham NC, United States of America

[46] SUPA - School of Physics and Astronomy, University of Edinburgh, Edinburgh, United Kingdom

[47] INFN Laboratori Nazionali di Frascati, Frascati, Italy

[48] Fakultät für Mathematik und Physik, Albert-Ludwigs-Universität, Freiburg, Germany

[49] Section de Physique, Université de Genève, Geneva, Switzerland

[50] (a) INFN Sezione di Genova; (b) Dipartimento di Fisica, Università di Genova, Genova, Italy

[51] (a) E. Andronikashvili Institute of Physics, Iv. Javakhishvili Tbilisi State University, Tbilisi; (b) High Energy Physics Institute, Tbilisi State University, Tbilisi, Georgia

[52] II Physikalisches Institut, Justus-Liebig-Universität Giessen, Giessen, Germany

[53] SUPA - School of Physics and Astronomy, University of Glasgow, Glasgow, United Kingdom

[54] II Physikalisches Institut, Georg-August-Universität, Göttingen, Germany

[55] Laboratoire de Physique Subatomique et de Cosmologie, Université Joseph Fourier and CNRS/IN2P3 and Institut National Polytechnique de Grenoble, Grenoble, France

[56] Department of Physics, Hampton University, Hampton VA, United States of America

[57] Laboratory for Particle Physics and Cosmology, Harvard University, Cambridge MA, United States of America

[58] (a) Kirchhoff-Institut für Physik, Ruprecht-Karls-Universität Heidelberg, Heidelberg; (b) Physikalisches Institut, Ruprecht-Karls-Universität Heidelberg, Heidelberg; (c) ZITI Institut für technische Informatik, Ruprecht-Karls-Universität Heidelberg, Mannheim, Germany

[59] Faculty of Applied Information Science, Hiroshima Institute of Technology, Hiroshima, Japan

[60] Department of Physics, Indiana University, Bloomington IN, United States of America

[61] Institut für Astro- und Teilchenphysik, Leopold-Franzens-Universität, Innsbruck, Austria

[62] University of Iowa, Iowa City IA, United States of America

[63] Department of Physics and Astronomy, Iowa State University, Ames IA, United States of America

[64] Joint Institute for Nuclear Research, JINR Dubna, Dubna, Russia

[65] KEK, High Energy Accelerator Research Organization, Tsukuba, Japan

[66] Graduate School of Science, Kobe University, Kobe, Japan

[67] Faculty of Science, Kyoto University, Kyoto, Japan

[68] Kyoto University of Education, Kyoto, Japan

[69] Department of Physics, Kyushu University, Fukuoka, Japan

[70] Instituto de Física La Plata, Universidad Nacional de La Plata and CONICET, La Plata, Argentina

[71] Physics Department, Lancaster University, Lancaster, United Kingdom

[72] [a] INFN Sezione di Lecce; [b] Dipartimento di Matematica e Fisica, Università del Salento, Lecce, Italy

[73] Oliver Lodge Laboratory, University of Liverpool, Liverpool, United Kingdom

[74] Department of Physics, Jožef Stefan Institute and University of Ljubljana, Ljubljana, Slovenia

[75] School of Physics and Astronomy, Queen Mary University of London, London, United Kingdom

[76] Department of Physics, Royal Holloway University of London, Surrey, United Kingdom

[77] Department of Physics and Astronomy, University College London, London, United Kingdom

[78] Louisiana Tech University, Ruston LA, United States of America

[79] Laboratoire de Physique Nucléaire et de Hautes Energies, UPMC and Université Paris-Diderot and CNRS/IN2P3, Paris, France

[80] Fysiska institutionen, Lunds universitet, Lund, Sweden

[81] Departamento de Fisica Teorica C-15, Universidad Autonoma de Madrid, Madrid, Spain

[82] Institut für Physik, Universität Mainz, Mainz, Germany

[83] School of Physics and Astronomy, University of Manchester, Manchester, United Kingdom

[84] CPPM, Aix-Marseille Université and CNRS/IN2P3, Marseille, France

[85] Department of Physics, University of Massachusetts, Amherst MA, United States of America

[86] Department of Physics, McGill University, Montreal QC, Canada

[87] School of Physics, University of Melbourne, Victoria, Australia

[88] Department of Physics, The University of Michigan, Ann Arbor MI, United States of America

[89] Department of Physics and Astronomy, Michigan State University, East Lansing MI, United States of America

[90] [a] INFN Sezione di Milano; [b] Dipartimento di Fisica, Università di Milano, Milano, Italy

[91] B.I. Stepanov Institute of Physics, National Academy of Sciences of Belarus, Minsk, Republic of Belarus

[92] National Scientific and Educational Centre for Particle and High Energy Physics, Minsk, Republic of Belarus

[93] Department of Physics, Massachusetts Institute of Technology, Cambridge MA, United States of America

[94] Group of Particle Physics, University of Montreal, Montreal QC, Canada

[95] P.N. Lebedev Institute of Physics, Academy of Sciences, Moscow, Russia

[96] Institute for Theoretical and Experimental Physics (ITEP), Moscow, Russia

[97] Moscow Engineering and Physics Institute (MEPhI), Moscow, Russia

[98] D.V.Skobeltsyn Institute of Nuclear Physics, M.V.Lomonosov Moscow State University, Moscow, Russia

[99] Fakultät für Physik, Ludwig-Maximilians-Universität München, München, Germany

[100] Max-Planck-Institut für Physik (Werner-Heisenberg-Institut), München, Germany

[101] Nagasaki Institute of Applied Science, Nagasaki, Japan

[102] Graduate School of Science and Kobayashi-Maskawa Institute, Nagoya University, Nagoya, Japan

[103] [a] INFN Sezione di Napoli; [b] Dipartimento di Fisica, Università di Napoli, Napoli, Italy

[104] Department of Physics and Astronomy, University of New Mexico, Albuquerque NM, United States of America

[105] Institute for Mathematics, Astrophysics and Particle Physics, Radboud University Nijmegen/Nikhef, Nijmegen, Netherlands

[106] Nikhef National Institute for Subatomic Physics and University of Amsterdam, Amsterdam, Netherlands

[107] Department of Physics, Northern Illinois University, DeKalb IL, United States of America

[108] Budker Institute of Nuclear Physics, SB RAS, Novosibirsk, Russia

[109] Department of Physics, New York University, New York NY, United States of America

[110] Ohio State University, Columbus OH, United States of America

[111] Faculty of Science, Okayama University, Okayama, Japan

[112] Homer L. Dodge Department of Physics and Astronomy, University of Oklahoma, Norman OK, United States of America

[113] Department of Physics, Oklahoma State University, Stillwater OK, United States of America

[114] Palacký University, RCPTM, Olomouc, Czech Republic

[115] Center for High Energy Physics, University of Oregon, Eugene OR, United States of America

[116] LAL, Université Paris-Sud and CNRS/IN2P3, Orsay, France

[117] Graduate School of Science, Osaka University, Osaka, Japan

[118] Department of Physics, University of Oslo, Oslo, Norway

[119] Department of Physics, Oxford University, Oxford, United Kingdom

[120] [a] INFN Sezione di Pavia; [b] Dipartimento di Fisica, Università di Pavia, Pavia, Italy

[121] Department of Physics, University of Pennsylvania, Philadelphia PA, United States of America

[122] Petersburg Nuclear Physics Institute, Gatchina, Russia

[123] [a] INFN Sezione di Pisa; [b] Dipartimento di Fisica E. Fermi, Università di Pisa, Pisa, Italy

[124] Department of Physics and Astronomy, University of Pittsburgh, Pittsburgh PA, United States of America

[125] [a] Laboratorio de Instrumentacao e Fisica Experimental de Particulas - LIP, Lisboa; [b] Faculdade de Ciências, Universidade de

Lisboa, Lisboa; [c] Department of Physics, University of Coimbra, Coimbra; [d] Centro de Física Nuclear da Universidade de Lisboa, Lisboa; [e] Departamento de Fisica, Universidade do Minho, Braga; [f] Departamento de Fisica Teorica y del Cosmos and CAFPE, Universidad de Granada, Granada (Spain); [g] Dep Fisica and CEFITEC of Faculdade de Ciencias e Tecnologia, Universidade Nova de Lisboa, Caparica, Portugal

[126] Institute of Physics, Academy of Sciences of the Czech Republic, Praha, Czech Republic

[127] Czech Technical University in Prague, Praha, Czech Republic

[128] Faculty of Mathematics and Physics, Charles University in Prague, Praha, Czech Republic

[129] State Research Center Institute for High Energy Physics, Protvino, Russia

[130] Particle Physics Department, Rutherford Appleton Laboratory, Didcot, United Kingdom

[131] Physics Department, University of Regina, Regina SK, Canada

[132] Ritsumeikan University, Kusatsu, Shiga, Japan

[133] [a] INFN Sezione di Roma; [b] Dipartimento di Fisica, Sapienza Università di Roma, Roma, Italy

[134] [a] INFN Sezione di Roma Tor Vergata; [b] Dipartimento di Fisica, Università di Roma Tor Vergata, Roma, Italy

[135] [a] INFN Sezione di Roma Tre; [b] Dipartimento di Matematica e Fisica, Università Roma Tre, Roma, Italy

[136] [a] Faculté des Sciences Ain Chock, Réseau Universitaire de Physique des Hautes Energies - Université Hassan II, Casablanca; [b] Centre National de l'Energie des Sciences Techniques Nucleaires, Rabat; [c] Faculté des Sciences Semlalia, Université Cadi Ayyad, LPHEA-Marrakech; [d] Faculté des Sciences, Université Mohamed Premier and LPTPM, Oujda; [e] Faculté des sciences, Université Mohammed V-Agdal, Rabat, Morocco

[137] DSM/IRFU (Institut de Recherches sur les Lois Fondamentales de l'Univers), CEA Saclay (Commissariat à l'Energie Atomique et aux Energies Alternatives), Gif-sur-Yvette, France

[138] Santa Cruz Institute for Particle Physics, University of California Santa Cruz, Santa Cruz CA, United States of America

[139] Department of Physics, University of Washington, Seattle WA, United States of America

[140] Department of Physics and Astronomy, University of Sheffield, Sheffield, United Kingdom

[141] Department of Physics, Shinshu University, Nagano, Japan

[142] Fachbereich Physik, Universität Siegen, Siegen, Germany

[143] Department of Physics, Simon Fraser University, Burnaby BC, Canada

[144] SLAC National Accelerator Laboratory, Stanford CA, United States of America

[145] [a] Faculty of Mathematics, Physics & Informatics, Comenius University, Bratislava; [b] Department of Subnuclear Physics, Institute of Experimental Physics of the Slovak Academy of Sciences, Kosice, Slovak Republic

[146] [a] Department of Physics, University of Cape Town, Cape Town; [b] Department of Physics, University of Johannesburg, Johannesburg; [c] School of Physics, University of the Witwatersrand, Johannesburg, South Africa

[147] [a] Department of Physics, Stockholm University; [b] The Oskar Klein Centre, Stockholm, Sweden

[148] Physics Department, Royal Institute of Technology, Stockholm, Sweden

[149] Departments of Physics & Astronomy and Chemistry, Stony Brook University, Stony Brook NY, United States of America

[150] Department of Physics and Astronomy, University of Sussex, Brighton, United Kingdom

[151] School of Physics, University of Sydney, Sydney, Australia

[152] Institute of Physics, Academia Sinica, Taipei, Taiwan

[153] Department of Physics, Technion: Israel Institute of Technology, Haifa, Israel

[154] Raymond and Beverly Sackler School of Physics and Astronomy, Tel Aviv University, Tel Aviv, Israel

[155] Department of Physics, Aristotle University of Thessaloniki, Thessaloniki, Greece

[156] International Center for Elementary Particle Physics and Department of Physics, The University of Tokyo, Tokyo, Japan

[157] Graduate School of Science and Technology, Tokyo Metropolitan University, Tokyo, Japan

[158] Department of Physics, Tokyo Institute of Technology, Tokyo, Japan

[159] Department of Physics, University of Toronto, Toronto ON, Canada

[160] [a] TRIUMF, Vancouver BC; [b] Department of Physics and Astronomy, York University, Toronto ON, Canada

[161] Faculty of Pure and Applied Sciences, University of Tsukuba, Tsukuba, Japan

[162] Department of Physics and Astronomy, Tufts University, Medford MA, United States of America

[163] Centro de Investigaciones, Universidad Antonio Narino, Bogota, Colombia

[164] Department of Physics and Astronomy, University of California Irvine, Irvine CA, United States of America

[165] [a] INFN Gruppo Collegato di Udine, Sezione di Trieste, Udine; [b] ICTP, Trieste; [c] Dipartimento di Chimica, Fisica e Ambiente, Università di Udine, Udine, Italy

[166] Department of Physics, University of Illinois, Urbana IL, United States of America

[167] Department of Physics and Astronomy, University of Uppsala, Uppsala, Sweden

[168] Instituto de Física Corpuscular (IFIC) and Departamento de Física Atómica, Molecular y Nuclear and Departamento de Ingeniería Electrónica and Instituto de Microelectrónica de Barcelona (IMB-CNM), University of Valencia and CSIC, Valencia, Spain

[169] Department of Physics, University of British Columbia, Vancouver BC, Canada

[170] Department of Physics and Astronomy, University of Victoria, Victoria BC, Canada

[171] Department of Physics, University of Warwick, Coventry, United Kingdom

[172] Waseda University, Tokyo, Japan

[173] Department of Particle Physics, The Weizmann Institute of Science, Rehovot, Israel

[174] Department of Physics, University of Wisconsin, Madison WI, United States of America

[175] Fakultät für Physik und Astronomie, Julius-Maximilians-Universität, Würzburg, Germany

[176] Fachbereich C Physik, Bergische Universität Wuppertal, Wuppertal, Germany

[177] Department of Physics, Yale University, New Haven CT, United States of America

[178] Yerevan Physics Institute, Yerevan, Armenia

[179] Centre de Calcul de l'Institut National de Physique Nucléaire et de Physique des Particules (IN2P3), Villeurbanne, France

[a] Also at Department of Physics, King's College London, London, United Kingdom

[b] Also at Institute of Physics, Azerbaijan Academy of Sciences, Baku, Azerbaijan

[c] Also at Particle Physics Department, Rutherford Appleton Laboratory, Didcot, United Kingdom

[d] Also at TRIUMF, Vancouver BC, Canada

[e] Also at Department of Physics, California State University, Fresno CA, United States of America

[f] Also at Novosibirsk State University, Novosibirsk, Russia

[g] Also at CPPM, Aix-Marseille Université and CNRS/IN2P3, Marseille, France

[h] Also at Università di Napoli Parthenope, Napoli, Italy

[i] Also at Institute of Particle Physics (IPP), Canada

[j] Also at Department of Physics and Astronomy, Michigan State University, East Lansing MI, United States of America

[k] Also at Department of Financial and Management Engineering, University of the Aegean, Chios, Greece

[l] Also at Louisiana Tech University, Ruston LA, United States of America

[m] Also at Institucio Catalana de Recerca i Estudis Avancats, ICREA, Barcelona, Spain

[n] Also at CERN, Geneva, Switzerland

[o] Also at Ochadai Academic Production, Ochanomizu University, Tokyo, Japan

[p] Also at Manhattan College, New York NY, United States of America

[q] Also at Institute of Physics, Academia Sinica, Taipei, Taiwan

[r] Also at Department of Physics, Nanjing University, Jiangsu, China

[s] Also at School of Physics and Engineering, Sun Yat-sen University, Guanzhou, China

[t] Also at Academia Sinica Grid Computing, Institute of Physics, Academia Sinica, Taipei, Taiwan

[u] Also at Laboratoire de Physique Nucléaire et de Hautes Energies, UPMC and Université Paris-Diderot and CNRS/IN2P3, Paris, France

[v] Also at School of Physical Sciences, National Institute of Science Education and Research, Bhubaneswar, India

[w] Also at Dipartimento di Fisica, Sapienza Università di Roma, Roma, Italy

[x] Also at Moscow Institute of Physics and Technology State University, Dolgoprudny, Russia

[y] Also at Section de Physique, Université de Genève, Geneva, Switzerland

[z] Also at Department of Physics, The University of Texas at Austin, Austin TX, United States of America

[aa] Also at Institute for Particle and Nuclear Physics, Wigner Research Centre for Physics, Budapest, Hungary

[ab] Also at International School for Advanced Studies (SISSA), Trieste, Italy

[ac] Also at Department of Physics and Astronomy, University of South Carolina, Columbia SC, United States of America

[ad] Also at Faculty of Physics, M.V.Lomonosov Moscow State University, Moscow, Russia

[ae] Also at Physics Department, Brookhaven National Laboratory, Upton NY, United States of America

[af] Also at Moscow Engineering and Physics Institute (MEPhI), Moscow, Russia

[ag] Also at Department of Physics, Oxford University, Oxford, United Kingdom

[ah] Also at Institut für Experimentalphysik, Universität Hamburg, Hamburg, Germany

[ai] Also at Department of Physics, The University of Michigan, Ann Arbor MI, United States of America

[aj] Also at Discipline of Physics, University of KwaZulu-Natal, Durban, South Africa

[*] Deceased

Internal Note

Report number	
Title	**Preliminary results on the muon reconstruction efficiency, momentum resolution, and momentum scale in ATLAS 2012 pp collision data**
Author(s)	Goblirsch, M ; Vanadia, M ; Salvucci, A ; Sforza, F ; Kortner, O ; Dimitrievska, A ; Vranjes, N
Imprint	17 Jul 2013. - 16 p.
Subject category	Detectors and Experimental Techniques
Accelerator/Facility, Experiment	CERN LHC ; ATLAS
Free keywords	MCP ; Muon Performance ; Combined Performance ; Resolution ; Efficiency
Abstract	The ATLAS experiment identifies and reconstructs muons with two high precision tracking systems, the Inner Detector and the Muon Spectrometer, which provide independent measurements of the muon momentum. This note summarizes the performance of the muon reconstruction algorithms and the data-driven techniques used for the measurements as derived from a dataset corresponding to an integrated luminosity of 20.4~fb^{-1} of 8~TeV pp collisions recorded in 2012. We also describe the corrections to be applied to simulation to reproduce the efficiency, momentum resolution and scale observed in experimental data. Finally, we introduce a method to determine the momentum uncertainty using the muon track fit uncertainty.

Email contact: edward.moyse@cern.ch ; kortner@mppmu.mpg.de ; Maximilian.Goblirsch-Kolb@cern.ch ; Federico.Sforza@cern.ch

[Check status]

Record created 2013-07-17, last modified 2013-09-09

Similar records

ATLAS NOTE

ATLAS-CONF-2013-088

Preliminary results on the muon reconstruction efficiency, momentum resolution, and momentum scale in ATLAS 2012 pp collision data

The ATLAS collaboration

Abstract

The ATLAS experiment identifies and reconstructs muons with two high precision tracking systems, the Inner Detector and the Muon Spectrometer which provide independent measurements of the muon momentum. This note summarizes the performance of the muon reconstruction algorithms and the data-driven techniques used for the measurements as derived from a dataset corresponding to an integrated luminosity of 20.4 fb^{-1} of 8 TeV pp collisions recorded in 2012. We also describe the corrections to be applied to simulation to reproduce the efficiency, momentum resolution and scale observed in experimental data. Finally, we introduce a method to determine the momentum uncertainty using the muon track fit uncertainty.

Corrected typo in the legend of Figure 10 with respect to the version of August 15, 2013

1 Introduction

Efficient and accurate muon identification and reconstruction is of primary importance for the physics program of the ATLAS experiment [1]. This note describes preliminary results on the muon reconstruction efficiency, momentum resolution, and momentum scale derived from the dataset corresponding to an integrated luminosity of 20.4 fb^{-1} of 8 TeV pp collisions delivered by the Large Hadron Collider (LHC) during the 2012 run.

Section 2 briefly describes the algorithms used for muon identification and reconstruction in the AT-LAS experiment. They use the independent track reconstruction provided by two sub-detector systems: the Inner Detector [2] (ID) and the Muon Spectrometer [3] (MS). The combination of the ID and MS information increases the purity of the muon sample and ensures good momentum resolution over three orders of magnitude of muon energy: from a few GeV up to a few TeV.

Section 3 summarizes the characteristics of the selected datasets and of the Monte Carlo samples (MC) used for data-simulation comparisons.

Sections 4 and 5 report the measurements of the muon reconstruction efficiency and momentum resolution. The methodologies used in these measurements, documented in detail in previous publications [4, 5], are based on the reconstruction of $Z \rightarrow \mu\mu$ decays in simulated events and in experimental data. The decays of $J/\psi \rightarrow \mu\mu$ and $\Upsilon \rightarrow \mu\mu$ are also used for validation and for the study of systematic uncertainties.

Finally, Section 6 describes a method that uses the muon track fit uncertainty to evaluate the momentum uncertainties in an independent way.

2 Muon identification and reconstruction

The ATLAS experiment uses the information of the MS and ID sub-detectors, and to a lesser extent, of the calorimeter, to identify and precisely reconstruct muons produced in the pp collisions.

The MS is the largest of all ATLAS sub-detectors: it is designed to detect charged particles in the pseudorapidity[1] region up to $|\eta| = 2.7$ and to provide momentum measurement with a relative resolution better than 3% over a wide p_T range and up to 10% at $p_T \approx 1$ TeV. The MS consists of one barrel part (for $|\eta| < 1.05$) and two end-cap sections. A system of magnet coils provides a toroidal magnetic field with a bending integral of about 2.5 Tm in the barrel and up to 6 Tm in the end-caps. Triggering and η, ϕ position measurements, with typical resolution of $5 - 10$ mm, are provided by the Resistive Plate Chambers (RPC, three layers for $|\eta| < 1.05$) and by the Thin Gap Chambers (TGC, three layers for $1.0 < |\eta| < 2.4$). Precision muon momentum measurement in the plane transverse to the beam-pipe is possible up to $|\eta| = 2.7$ and it is provided by three layers of Monitored Drift Tube Chambers (MDT) everywhere except for $|\eta| > 2$ where the innermost MDT layer is replaced by one layer of Catode Strip Chambers (CSC). The single hit resolution in the bending plane for the MDT and the CSC is about 80 μm and 60 μm, respectively.

An independent determination of the muon momentum is provided by the ID. It consists of three sub-detectors: the inner Silicon Pixels and the Semi-Conductor Tracker (SCT) detectors for $|\eta| < 2.5$, and the outer Transition Radiation Tracker (TRT) covering $|\eta| < 2.0$. They provide high-resolution coordinate measurements for track reconstruction inside a solenoidal magnetic field of 2 T.

---

[1]ATLAS uses a right-handed coordinate system with its origin at the nominal interaction point (IP) in the centre of the detector and the z-axis along the beam pipe. The x-axis points from the IP to the centre of the LHC ring, and the y-axis points upward. Cylindrical coordinates (r, ϕ) are used in the transverse plane, ϕ being the azimuthal angle around the beam pipe. The pseudorapidity and the transverse momentum are defined in terms of the polar angle θ as $\eta = -\ln\tan(\theta/2)$ and $p_T = p\sin\theta$, respectively. The $\eta - \phi$ distance between two particles is defined as $\Delta R = \sqrt{\Delta\eta^2 + \Delta\phi^2}$.

Muon identification is performed according to several reconstruction criteria (leading to different muon "types"), according to the available information from the ID, the MS, and the calorimeter sub-detector systems. The different types are:

- Stand-alone (SA) muons: the muon trajectory is reconstructed only in the MS. The direction of flight and the impact parameter of the muon at the interaction point are determined by extrapolating the MS track back to the point of closest approach to the beam line, taking into account the energy loss of the muon in the calorimeters;

- Combined (CB) muon: track reconstruction is performed independently in the ID and MS, and a combined track is formed from the successful combination of a SA track with an ID track;

- Segment-tagged (ST) muons: a track in the ID is identified as a muon if the track extrapolated to the MS is associated with at least one track segment in the MDT or CSC.

- Calorimeter-tagged (CaloTag) muons: a track in the ID is identified as a muon if the track can be associated to an energy deposit in the calorimeter as expected from a minimum ionizing particle. This type has the lowest purity of all the muon types but it recovers acceptance in the uninstrumented region of the MS. The identification criteria of this muon type are optimized for a region of $|\eta| < 0.1$ and a momentum range of $25 \lesssim p_{\mathrm{T}} \lesssim 100$ GeV.

CB candidates have the highest muon purity. The CB muon reconstruction efficiency is strongly affected by acceptance losses in the MS, mainly in two regions:

- at $\eta \approx 0$, the MS is only partially equipped with muon chambers in order to provide space for services for the ID and the calorimeters;

- in the region ($1.1 < \eta < 1.3$) between the barrel and the end-caps, there are regions in ϕ where only one layer of chambers is traversed by muons in the MS, due to the fact that some of the chambers of that region were not yet installed[2]. Therefore, no SA momentum measurement is available and the CB muon efficiency is decreased.

The reconstruction of the first three muon types (all using the MS information) is performed using two independent and complementary strategies [6] (named "Chains"): the first chain (or "Chain 1") performs a statistical combination of the track parameters of the SA and ID muon tracks using the covariance matrices of both track parameter measurements. The second chain (or "Chain 2") performs a global refit of the muon track using the hits from both the ID and MS sub-detectors. All the figures presented in Sections 4, 5 of this note refer to the Chain 1 reconstruction while the corresponding figures for Chain 2 are shown in Appendix A.

3 Data and Monte Carlo Samples

The results presented in this note are obtained from the analysis of $\sqrt{s} = 8$ TeV pp collision events corresponding to an integrated luminosity of 20.4 fb^{-1} and collected by the ATLAS detector in 2012. Online event selection is performed by a three-level trigger system described in Ref. [7]. Events are accepted for the analyses documented in this note only if the ID and MS detectors were in good data-taking conditions and both solenoidal and toroidal magnet systems were on. The $Z \rightarrow \mu\mu$ candidates are selected online by requiring at least one muon candidate with $p_{\mathrm{T}} > 24$ GeV and isolated from other activity in the tracker, while lower di-muon mass candidates are selected online by requiring at least two

---

[2]The installation of all the muon chambers in this region has been completed during the 2013-2014 LHC shutdown.

muon candidates with $p_T > 6$ GeV and with a reconstructed di-muon invariant mass in a window around the J/ψ or the Υ resonance mass.

In the following, experimental data are compared to MC simulations of signal and background processes. The $J/\psi \rightarrow \mu\mu$ and $\Upsilon \rightarrow \mu\mu$ signal MCs are generated with PYTHIA [8], while the $Z \rightarrow \mu\mu$ signal MC is generated with POWHEG [9]. The generated signal events are passed through the full Geant4 [10] simulation of the ATLAS detector, the trigger simulation and the same reconstruction chain used for data. The samples used for background simulation are described in detail in Refs. [4, 5], they include, depending on the case, $Z \rightarrow \tau\tau$, $W \rightarrow \mu\nu$, $W \rightarrow \tau\nu$, $b\bar{b}$, $c\bar{c}$, and $t\bar{t}$ production and decays.

The simulation includes a realistic evaluation of the MS detector misalignment obtained by studying straight muon tracks from cosmic ray events [11] and from special runs performed with the toroidal magnetic field off [12]. When the effect of the realistic misalignment is taken into account the momentum resolution for muons of 1 TeV of energy reaches approximately 13% in the barrel region of the MS, 17% in the end-cap region of the MS, and 15% in the region covered by the CSC sub-detector.

4 Muon reconstruction efficiency

As the track reconstruction in the ID and MS are performed independently, the reconstruction efficiency of the different muon types can be decomposed in the product of the reconstruction efficiency in the ID, the reconstruction efficiency in the MS, and the matching efficiency between the ID and MS measurements (which includes the refit efficiency in the case of Chain 2).

A tag-and-probe method, described in detail in Ref. [4], is employed to measure the reconstruction efficiencies[3] of all muon types within the acceptance of the ID ($|\eta| < 2.5$). As discussed below, the method is sensitive to the quantities of interest, i.e. the ID reconstruction efficiency, and the MS reconstruction efficiency together with the matching efficiency. For $Z \rightarrow \mu\mu$ decays, events are selected by requiring two oppositely charged isolated muons[4] with $p_T > 20$ GeV and a di-muon invariant mass within 10 GeV from the Z-boson mass. One of the muons is required to be a CB muon, and to have triggered the readout of the event. This muon is called the "tag". The other muon, the so-called "probe", is required to be a "MS track" (i.e. a SA or a CB muon) when the ID or CaloTag muon efficiencies are to be measured. CaloTag muons are used as probes when the MS reconstruction efficiency together with the matching efficiency is to be measured. The use of CaloTag muons instead of ID track probes as done in Ref. [4] reduces the background in the $Z \rightarrow \mu\mu$ sample by an order of magnitude without biasing the efficiency measurement. A total of more than 10^7 data events are selected for the tag-and-probe studies.

After selecting all tag-and-probe pairs an attempt is made to match the probe to the reconstructed muons in the event: a match is successful when the muon and the probe have the same measured charge and they are close in the $\eta - \phi$ plane ($\Delta R < 0.01$ for ID probes, $\Delta R < 0.05$ for MS probes). For each muon reconstruction type the equation of the reconstruction efficiency is:

$$\varepsilon(\text{Type}) = \varepsilon(\text{Type}|\text{ID}) \cdot \varepsilon(\text{ID}) \quad \text{with Type} = \text{CB, ST,} \tag{1}$$

where $\varepsilon(\text{Type}|\text{ID})$ is the MS reconstruction and the matching efficiency for a specific muon type measured with CaloTag probes, and $\varepsilon(\text{ID})$ is the ID reconstruction efficiency which is the fraction of MS track probes associated to an ID track.

The level of agreement of the measured muon efficiencies ε^{Data} with the efficiencies ε^{MC} predicted by the MC simulation is expressed as the ratio between these two numbers, further on called "efficiency

---

[3]Efficiencies determined with the tag-and-probe method, and with an alternate method based on MC truth, were found to agree within statistical uncertainty [6, p.221]. This also shows that any possible correlations between the tag and the probe muons are negligible.

[4]In the rest of this note a muon is considered to be isolated when the sum of the momenta of the tracks with $p_T > 1$ GeV detected in a cone of $\Delta R = 0.4$ around the muon track is less than 0.1 times the muon momentum itself.

scale factor" or SF:

$$SF = \frac{\varepsilon^{Data}}{\varepsilon^{MC}} \ . \tag{2}$$

The sample of selected tag-and-probe pairs has a very high purity and consists of $Z \rightarrow \mu\mu$ decays to a level of more than 99.9%. Previous studies [13, 4] showed that a systematic uncertainty of 0.2% on the efficiency SF value is associated to the uncertainty on the evaluation of the residual background contamination and to the comparison of the SF extraction using CaloTag or ID track probes. Another source of systematic uncertainty derives from the measurement of the muon reconstruction efficiency for muons with lower momenta. This was studied in 2010 with $J/\psi \rightarrow \mu\mu$ decays [14]. The efficiency measurements of muons with $p_T > 10$ GeV from J/ψ decays were found to agree (within uncertainties) with the efficiency measurements of muons from $Z \rightarrow \mu\mu$ decays. A deviation of the SFs up to 2% was found for lower momenta. Hence, as done in Ref. [4], the SF derived from $Z \rightarrow \mu\mu$ decays is used also for lower momenta but a systematic uncertainty of 1% is used for $7 < p_T < 10$ GeV whereas 2% uncertainty is assigned for $p_T < 7$ GeV.

The third source of systematic uncertainty is related to the use of the SFs for muons with transverse momenta beyond the range covered by this efficiency measurement. As shown in the rest of the section, the measured SFs do not depend on the transverse momentum of the muons in the range considered. An upper limit on the SF variation for muon momentum of 1 TeV has been extracted by using a MC simulation with built-in imperfections, like a realistic residual misalignment of the detector components or a 10% variation of the muon energy loss. On the basis of this analysis a systematic uncertainty of $1\% \times p$, with p in TeV, is added for $p_T > 100$ GeV.

The very large sample of $Z \rightarrow \mu\mu$ decays recorded in the 2012 data taking period allows also the study of the reconstruction efficiency with very fine binning in several variables of interest in order to derive corrections for small discrepancies between data and simulation.
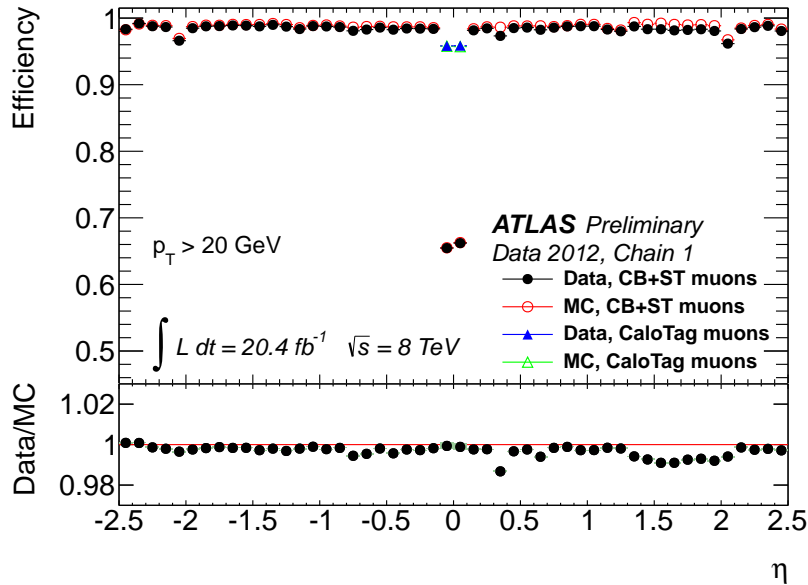

Figure 1: Muon reconstruction efficiency as a function of η for muons with $p_T > 20$ GeV and different muon reconstruction types. CB and ST muon types are reconstructed using the Chain 1 reconstruction algorithm. CaloTag muons are used only in the region $|\eta| < 0.1$. The panel at the bottom shows the ratio between the measured and predicted efficiencies.

Figure 1 shows the muon reconstruction efficiency as a function of η. The combination of all the muon reconstruction types (for CB, ST, and CaloTag muons) gives a uniform muon reconstruction efficiency of about 0.98 over all the detector regions. The inefficiency of the CB+ST muons at $\eta \approx 0$ is almost fully recovered by the use of CaloTag muons. The efficiencies measured in experimental and simulated data are in good agreement (within 0.5%) apart from the region at $1.5 \lesssim \eta \lesssim 2.2$. This behaviour originates from a mis-modeling of the ID reconstruction efficiency that will be discussed below.

The ID muon reconstruction efficiency for $p_T > 20$ GeV as a function of η is analysed in Figure 2: the left part of the figure shows an efficiency greater than 0.99, apart from the regions around $\eta = 0$ and $|\eta| = 1.7$. Figure 2, on the right, shows the ID muon reconstruction efficiency when only minimal ID track identification requirements (described in Ref. [15]) are applied on the muon track. The additional requirement of one hit in the innermost pixel detector layer is applied to muons passing through a sensitive area of this detector in order to ensure an accurate impact parameter measurement. The fact that not all non-operating pixel modules were treated as insensitive regions at the time of the muon reconstruction causes an inefficiency in experimental data at $1.5 \lesssim \eta \lesssim 2.2$ not modeled in simulation.
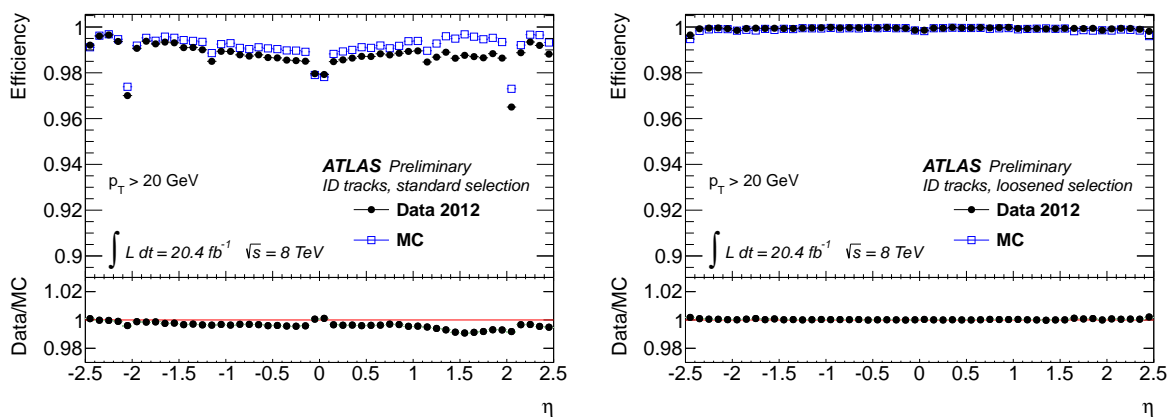
Figure 2: Measured ID muon reconstruction efficiency as a function of η for muons with $p_T > 20$ GeV. On the left plot the efficiency is calculated with the standard selection requirements on the hit multiplicity in the ID while the requirements are relaxed on the right plot. The panel at the bottom shows the ratio between the measured and predicted efficiencies.

A further break down of the results into the CB and CB+ST categories is shown in Figure 3. The CB efficiencies are significantly lower than 0.95 in the partially instrumented regions of the MS at $\eta \approx 0$ and in the poorly instrumented MS region at $\eta \approx 1.2$. The origin of the deviation of the SFs from 1 at $|\eta| \approx 1.2$ and $|\eta| \approx 1.0$ is under investigation. A higher efficiency is achieved when ST muons are added to CB muons.

The CB and CB+ST reconstruction efficiencies are predicted to be independent of the transverse momentum of the muon in the p_T range under consideration which is confirmed by the experimental results as shown in Figure 4. The CaloTag muon efficiency is also well predicted by the MC simulation reaching a plateau efficiency of approximately 0.97 for $p_T \gtrsim 30$ GeV.

Figure 5 shows the reconstruction efficiency for CB+ST muons as a function of the average number of inelastic pp interactions per bunch crossing (the $\langle\mu\rangle$ parameter) displaying a high value (on average above 0.97) and remarkable stability. A small efficiency drop of about 2% is only observed for $\langle\mu\rangle \gtrsim 35$ mainly caused by a decrease in the ID reconstruction efficiency. The discrepancy in the data/MC ratio is due to the additional requirement of one hit in the innermost pixel detector layer (for muons passing through a sensitive area of this detector) as discussed above.

5
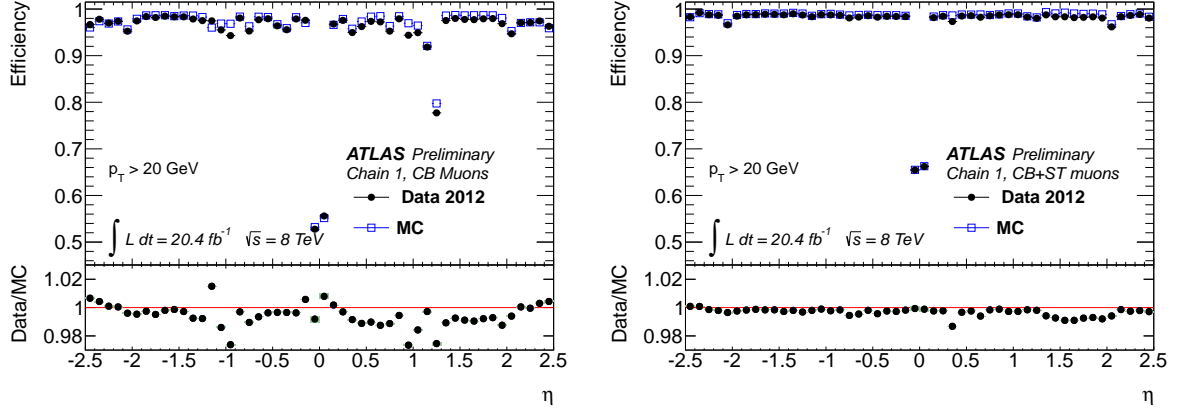
Figure 3: Reconstruction efficiency for Chain 1 CB only muons (left) and CB+ST muons (right) as a function of η for muons with $p_T > 20$ GeV. The panel at the bottom shows the ratio between the measured and predicted efficiencies.

Figure 4: Reconstruction efficiency for Chain 1 CB only muons (top left) and CB+ST muons (top right) as well as CaloTag muons (bottom) as a function of the p_T of the muon for muons with $0.1 < |\eta| < 2.5$ for Chain 1 and $0 < |\eta| < 0.1$ for CaloTag muons. The panel at the bottom shows the ratio between the measured and predicted efficiencies.

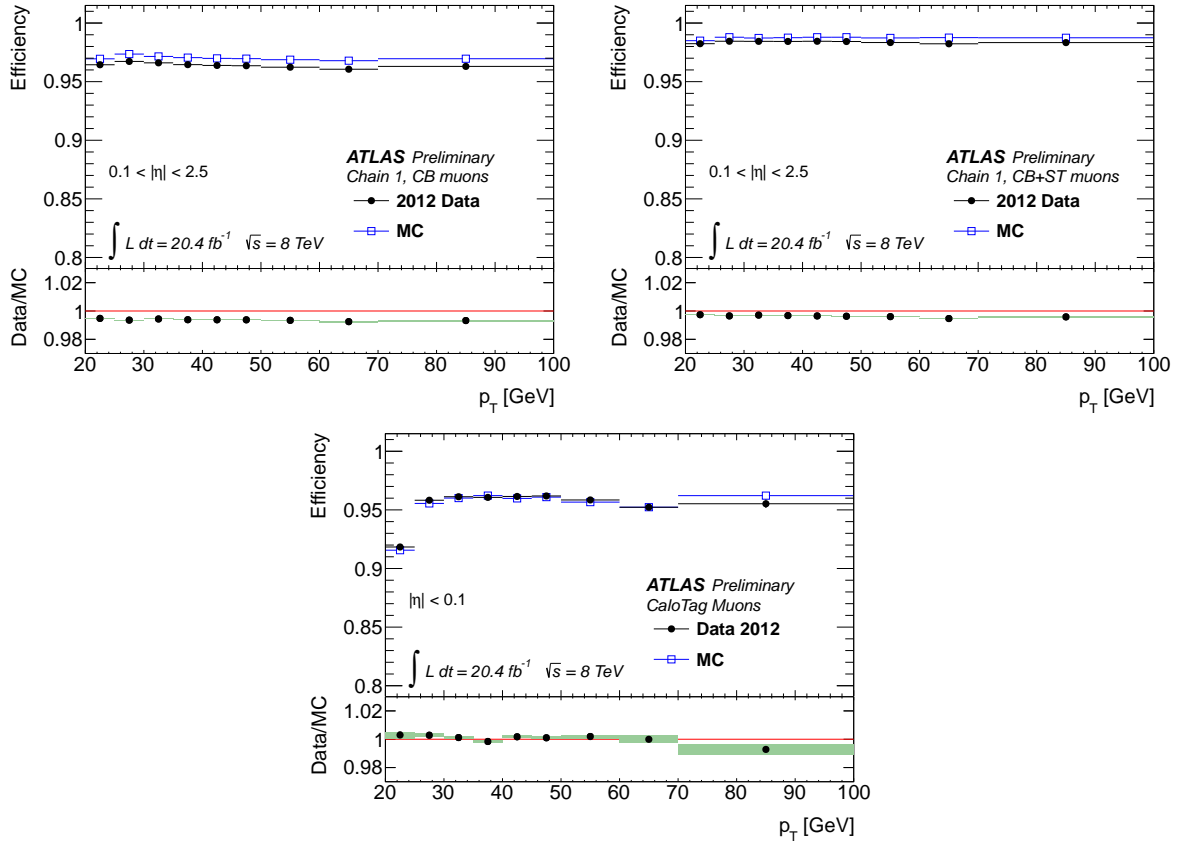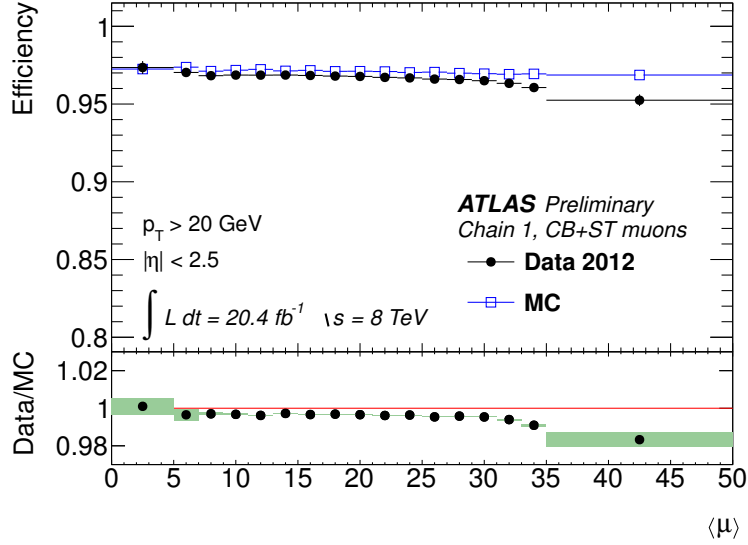Figure 5: Measured CB+ST (Chain 1) muon reconstruction efficiency for muons with $p_T > 20$ GeV as a function of the average number of inelastic pp collisions per bunch crossing (the $\langle \mu \rangle$ parameter). The panel at the bottom shows the ratio between the measured and predicted efficiencies.

5 Muon momentum scale and resolution

The momentum resolution and scale are additional important parameters used in the evaluation of the muon reconstruction performance. Di-muon decays of the Z, J/ψ, and Υ resonances are used to determine the muon momentum resolution and scale. This allows a validation of the MC prediction for these quantities.

The basic algorithm used in this measurement is described in detail in Ref. [5]. Due to the very large data sample collected in 2012, several improvements of the original method have been made during the analysis of this dataset. A $Z \rightarrow \mu\mu$ sample of more than $5 \cdot 10^6$ data events is selected by requiring two isolated CB muons of opposite charge, $p_T > 25$ GeV, and with a reconstructed invariant mass in a window of ± 15 GeV around the Z-boson mass. This gives a very pure sample where the background fraction, estimated using MC simulation, is of the order of 0.1%. The left part of Figure 6 shows that the measured $Z \rightarrow \mu\mu$ mass spectrum for the experimental data has a slight shift and a larger spread with respect to the simulated one, obtained with $Z \rightarrow \mu\mu$ POWHEG [9] event simulation plus MC background for non-$Z \rightarrow \mu\mu$ events.

As reported in Ref. [5], the muon fractional momentum resolution $\frac{\sigma(p_T)}{p_T}$, for $p_T > 20$ GeV, can be parametrized to good approximation by the quadratic sum of two terms:

$$\frac{\sigma(p_T)}{p_T} = a \oplus b \cdot p_T, \tag{3}$$

where the first term, constant in p_T, describes the multiple scattering contribution whilst the second term, proportional to p_T, describes the intrinsic resolution caused by the spatial resolution of the detector components, and any residual misalignment. Consequently, the correction to the simulated resolution can also be parametrized by two terms: the first, constant in p_T, corrects the multiple scattering contribution while the second, linear in p_T, corrects the intrinsic resolution. Finally, if also a momentum scale correction, s, is considered, one arrives to an equation[5] that can be used to derive a corrected momentum

---

[5]Equation 4 is an approximation, valid in the typical p_T range of muons originating from $Z \rightarrow \mu\mu$ decays, of the momentum
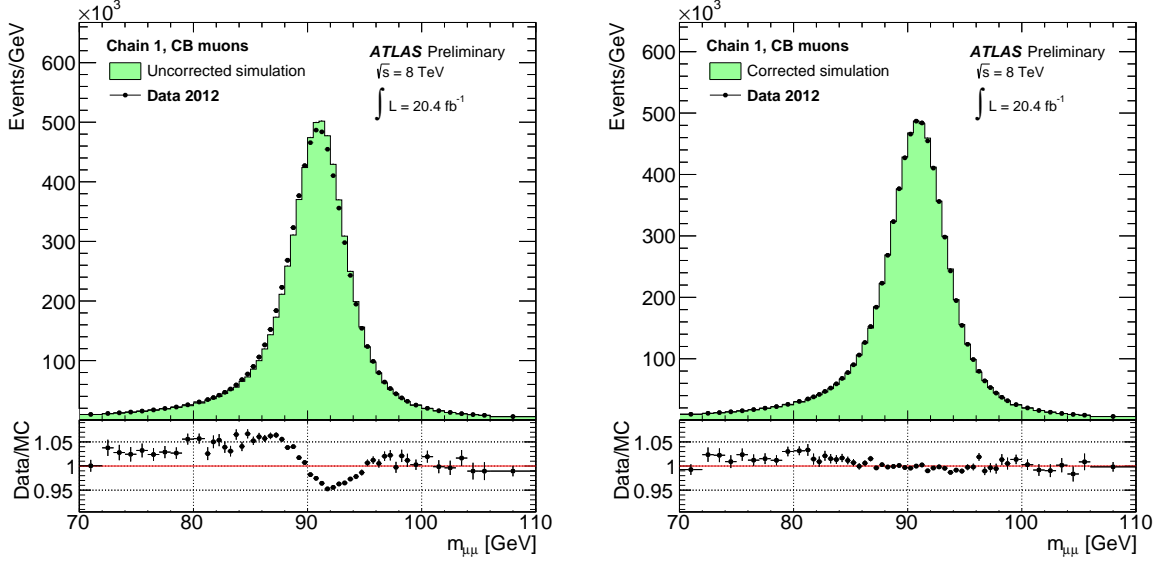
7

Figure 6: Di-muon invariant mass for Chain 1, CB muons, isolated and with $p_T > 25$ GeV. The plot shows the invariant mass for 2012 data and for the POWHEG [9] simulation of $Z \rightarrow \mu\mu$ plus background events. No corrections are applied on the left plot while smearing and scale corrections are applied to the plot on the right. The corrections have been derived from the full 2012 dataset.

measurement, p_T^{Cor}, from the simulated momentum measurement, p_T^{MC}, with an improved agreement with the one measured in data in the ID and in the MS sub-detectors:

$$p_T^{Cor,det} = p_T^{MC,det} \cdot s^{det}(\eta) \left(1 + \Delta a^{det}(\eta) \, G(0,1) + \Delta b^{det} \, G(0,1) \, p_T^{MC,det}\right) \quad \text{with} \quad det = \text{MS, ID,} \quad (4)$$

$G(0,1)$ is a normally distributed random variable with mean 0 and width 1, and the correction factors $s^{det}(\eta)$, $\Delta a^{det}(\eta)$ and $\Delta b^{det}(\eta)$ are derived in 16 different η regions of the detector. The correction of the CB muon momentum is computed as the average of the ID and MS momentum correction weighted by the inverse square of the ID and MS muon momentum resolutions.

The correction parameters are obtained using a MC template fitting technique: a series of mass spectrum distributions is derived from the $Z \rightarrow \mu\mu$ simulation by applying Equation 4 with varied correction parameters. Then a binned likelihood fit is used to match the best template to the data mass spectrum. The procedure is iterated across 16 η bins of the detector: the first fit is performed with $Z \rightarrow \mu\mu$ events reconstructed with both muons in the same η bin, while the following fits allow also one of the muons in a previously analysed η bin. After all the detector η bins have been analysed, the fit is iterated twice in order to improve the stability of the results.

Figure 7 shows the derived Δa^{MS} and Δb^{ID} resolution correction terms. The main systematic uncertainty derives from the extraction of the corrections from a template fit with a varied window around the Z-boson mass. The two remaining resolution correction terms, i.e. Δa^{ID} and Δb^{MS}, are not extracted from the fit but they are set to zero and varied within the range allowed by systematic uncertainties, as described in Ref. [5]. This procedure is possible because independent measurements constrain Δa^{ID} and Δb^{MS} to be small. The measurement of the material budget in the ID, studied in Ref. [16, 17], is used to predict precisely the contribution of the multiple scattering of muons in the ID, therefore a small Δa^{ID}

---

resolution correction to be applied to Equation 3. The correction available for physics analyses, which can also probe higher momentum ranges, allows the direct correction of the $1/p_T$ quantity.

8

term is expected. The effect of the residual misalignment of MS detector components, giving an effective Δb^{MS} term, has been included in the simulation thanks to the studies reported in Section 3.
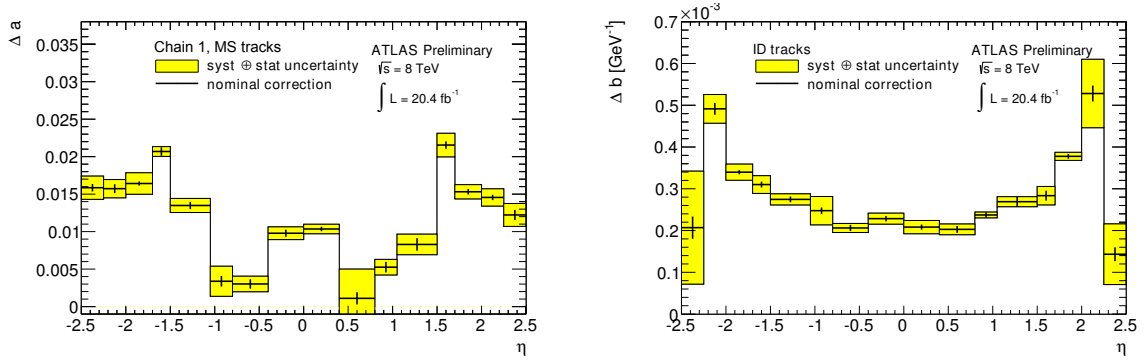
Figure 7: Δa resolution correction term for the MS (left plot), and Δb resolution correction term for the ID (right plot) for MC, derived from $Z \to \mu\mu$ data for the Chain 1 reconstruction. The systematic uncertainty on the correction is shown in yellow.
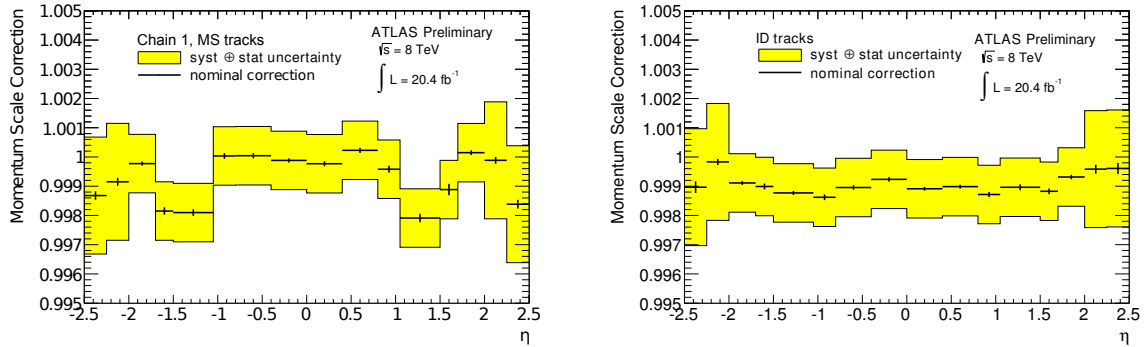
Figure 8: MS (left plot) and ID (right plot) momentum scale correction, for MC, derived from $Z \to \mu\mu$ data for the Chain 1 reconstruction. The systematic uncertainty on the correction is shown in yellow.

Figure 8 shows the derived scale corrections s^{MS} and s^{ID}. Here, the main systematic uncertainties of 0.1% and 0.2% (the second in the forward region of the detector) were introduced to cover a possible momentum dependence of the correction. Figure 9 shows the comparison of the scale obtained at the Z resonance with the Data/MC ratio of the reconstructed mass for lower mass di-muon resonances, J/ψ selected with $p_T > 6$ GeV and Υ selected with $p_T > 6.5$ GeV. The data to MC mass ratio for the $Z \to \mu\mu$ events is obtained with the method described in Section 6 while for $J/\psi \to \mu\mu$ and $\Upsilon \to \mu\mu$ events the mass ratio is obtained with a Gaussian fit of the peak position in data and in MC.

The study shows that there is only a small dependence of the muon momentum scale on the muon momentum. This is caused by the residual inaccuracy of the energy loss correction applied to the MS stand-alone muon momentum measurement. The effect, visible only at small momenta, is covered by the applied systematic uncertainty. A charge dependent effect on the scale corrections has been also investigated and it was found to be covered by the present systematic uncertainty.

The right part of Figure 6 shows the improved agreement between data and MC in the $Z \to \mu\mu$ mass spectrum reconstructed with CB, Chain 1 muons, after the application of the smearing and scale
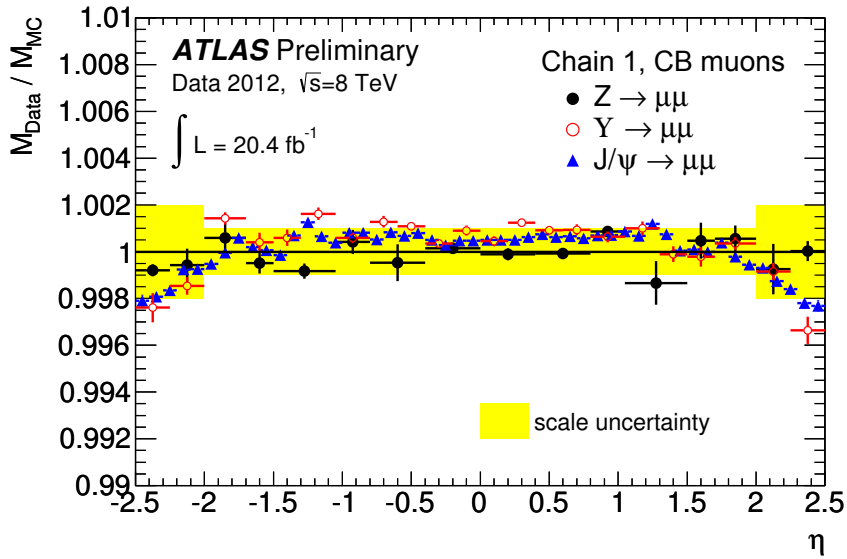
Figure 9: Comparison of the data to MC mass ratio as a function of η for the di-muon decays of Z, J/ψ, and Υ resonances. Selected Z events require two CB muons with $p_T > 25$ GeV and same η bin, selected Υ events require two CB muons of $p_T > 6.5$ GeV and same η bin, selected J/ψ events require two CB muons of $p_T > 6$ GeV and the η of the leading muon is shown. The data to MC mass ratio for the $Z \to \mu\mu$ events is obtained with the method described in Section 6 while for $J/\psi \to \mu\mu$ and $\Upsilon \to \mu\mu$ events the mass ratio is obtained with a Gaussian fit of the peak position in data and in MC.

corrections. The di-muon mass resolution for data and for the uncorrected and corrected simulation is shown in Figure 10: at the Z mass the total Chain 1 CB resolution ranges from 1.5 to 3 GeV in the different detector regions.

6 Validation of the momentum uncertainty estimate of the track fit

In this section we describe an alternative method for addressing the muon momentum resolution and scale that uses the muon track fit uncertainty, $\sigma_{q/p}$, as a per-muon momentum uncertainty function.

The muon momentum resolution can be estimated from the shape of the minimum of the χ^2 minimized by the track fit for each individual muon track. In the χ^2 of the track fit the uncertainties in the positions of the individual components of ID and MS tracking detectors are only treated in an approximate way. This approximate treatment of alignment uncertainties makes it necessary to apply uncertainty scale factors to the momentum uncertainties from the track fit to obtain the correct momentum resolution.

MC simulation studies show that the inverse of the reconstructed muon momentum $1/p_{rec}$ is Gaussian distributed around the true inverse muon momentum $1/p_{gen}$ to good approximation. In order to correct for systematic shifts of p_{rec} with respect to p_{gen} and for an underestimation of the inverse momentum resolution $\sigma_{q/p}$, a momentum scale factor $\alpha(\eta)$ and a resolution scale factor $\beta(\eta)$ are introduced. This leads to a response function of the form:

$$T\left(1/p_{rec}, 1/p_{gen}\right) \equiv \frac{1}{\sqrt{2\pi}\beta(\eta)\sigma_{q/p}} \exp\left[-\frac{\left(\frac{1}{p_{rec}} - \frac{1}{\alpha(\eta)p_{gen}}\right)^2}{2\left(\beta(\eta)\sigma_{q/p}\right)^2}\right], \tag{5}$$
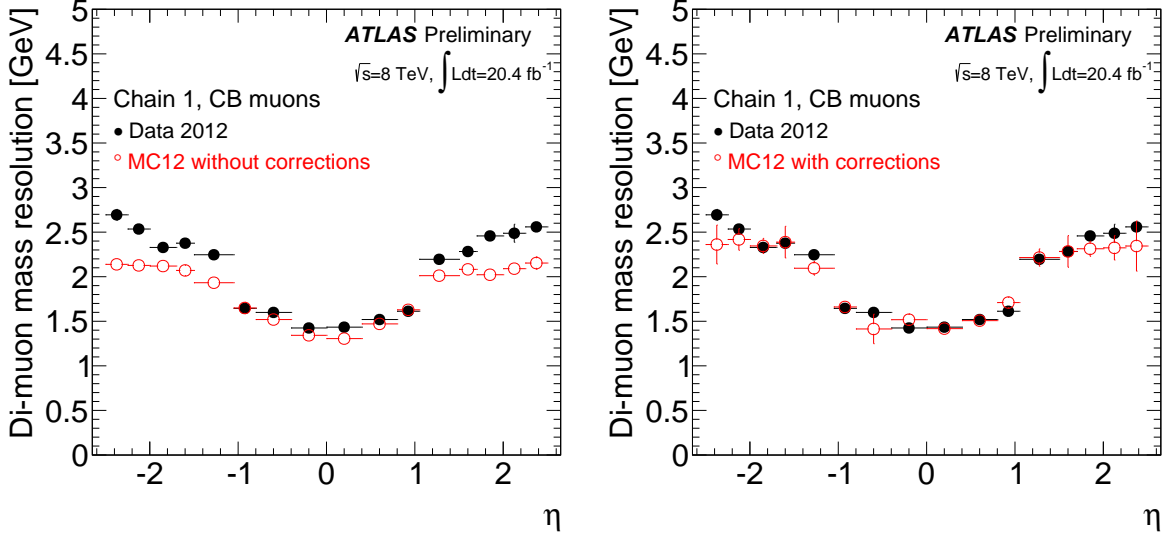
Figure 10: Di-muon mass resolution measured as described in Section 6 for data (black points) and for the uncorrected (left, red points) and corrected (right, red points) simulation for Chain 1 CB reconstructed muons at the Z mass. The two muons are required to be in the same η interval which is indicated in the plot by the horizontal error bars.

where $\alpha(\eta)$ and $\beta(\eta)$ are derived from data and parametrized in pseudorapidity bins.

Due to the good momentum resolution, also the measured mass of a given muon pair $m_{\mu\mu}$ is Gaussian distributed around its true value[6], m_{gen}, to good approximation. As the muon momentum resolution depends on η, ϕ, and p_T of a muon, the mass resolution $\sigma_{m_{\mu\mu}}$ is not a constant, but varies from event to event according to the configuration of the muons in $\eta - \phi - p_T$ space. Therefore the di-muon mass resolution is a superposition of Gaussian distributions with different variances $\sigma^2_{m_{\mu\mu}}$. Assuming the two muons to be in the same pseudorapidity interval, the mass response function can be written as

$$
T\left(m_{\mu\mu}, m_{gen}\right) \equiv \int_0^\infty f(\sigma^2_{m_{\mu\mu}}) \cdot \frac{1}{\sqrt{2\pi}\beta(\eta)\sigma_{m_{\mu\mu}}} exp\left[-\frac{\left(m_{\mu\mu} - \alpha(\eta)m_{gen}\right)^2}{2\sigma^2_{m_{\mu\mu}}\beta(\eta)^2}\right] d\sigma^2_{m_{\mu\mu}} \tag{6}
$$

where $\sigma_{m_{\mu\mu}}$ is the di-muon mass resolution computed with the track fit uncertainties and $f(\sigma^2_{m_{\mu\mu}})$ the probability density function of the mass variances.

A fit of the di-muon mass spectrum in $Z \rightarrow \mu\mu$ events with a convolution of the generated mass spectrum and the di-muon resolution of Equation 6 allows the extraction of the $\alpha(\eta)$ and $\beta(\eta)$ parameters and the calibration of the response function. The fit is performed in bins of pseudorapidity by requiring the reconstruction of two CB muons in the same η bin and with a di-muon invariant mass in a window of [85 GeV, 97 GeV]. Studies on simulated data show that the mass scale factor $\alpha(\eta)$ of Equation (6) provided by the fit agrees with the muon momentum scale factor $\alpha(\eta)$ of Equation (5) at the level of 0.05% which is significantly larger than the statistical uncertainty on $\alpha(\eta)$. According to these studies the mass resolution scale factor $\beta(\eta)$ of Equation (6) agrees with the muon momentum resolution scale factor $\beta(\eta)$ of Equation (5) at the level of 3% which is also significantly larger than the statistical error on $\beta(\eta)$. From now on a relative error of 0.05% is assigned to the fit result for $\alpha(\eta)$ and a relative error of 3% to the fit results for $\beta(\eta)$. Repeating the fits in alternative mass windows of [87 GeV, 96 GeV] and

---

[6]m_{gen} is computed from the four-momenta of the muon pair after final state radiation.

[83 GeV, 99 GeV] leads to values of $\alpha(\eta)$ and $\beta(\eta)$ matching the values from the initial fit within these errors.
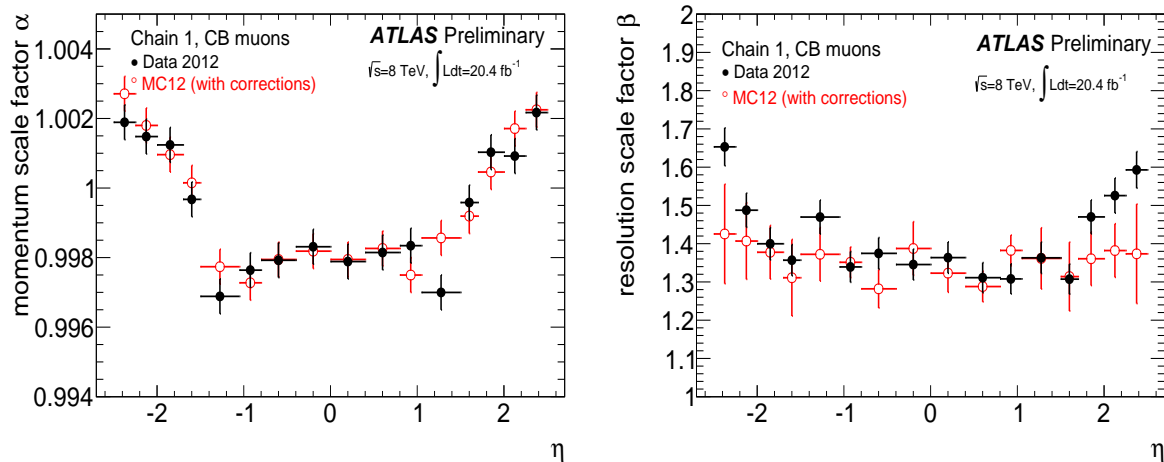

Figure 11: Dependence of the momentum scale factor α (on the left) and of the momentum resolution scale factor β (on the right) on the pseudorapidity of the muon as obtained with the fit described in Section 6. The horizontal error bars represent the size of the pseudorapidity intervals; the vertical error bars shows the total uncertainties on the scale factors. The values have been derived from experimental $Z \rightarrow \mu\mu$ data (black points) and for the $Z \rightarrow \mu\mu$ POWHEG [9] simulation (red points). The errors of the $\beta(\eta)$ values for the corrected MC sample include the uncertainties of the momentum corrections described in Section 5, they are the dominant contribution to the error bars for $|\eta| > 2.0$.

Figure 11 shows the comparison of the correction factors $\alpha(\eta)$ and $\beta(\eta)$ extracted from experimental data and from the simulation after the application of the corrections of Section 5. The errors of the $\beta(\eta)$ values for the corrected MC sample include the uncertainties of the momentum corrections described in Section 5, they are the dominant contribution to the error bars for $|\eta| > 2.0$. The experimental and simulated data agree within the quoted uncertainties providing an independent validation of both the correction parameters derived in Section 5 and the assumptions of the per-muon momentum error calibrations.

The calibration of the track fit uncertainty $\sigma_{q/p}$, due to the $\beta(\eta)$ parameter, allows the derivation of the di-muon mass resolution in a straightforward way. For each event the corrected $\sigma_{q/p}$ is used to compute a di-muon mass resolution $\sigma_{m_{\mu\mu}}$, the average di-muon mass resolution is defined as the square root of the mean of $\sigma^2_{q/p}$. Figure 10 shows the average di-muon mass resolution as a function of the η of the decay muons for experimental and simulated data. It illustrates the need for muon momentum corrections to match the simulated di-muon mass resolution with the experimentally measured resolution.

7 Summary

This note summarizes the performance of muon identification and reconstruction algorithms used in the ATLAS experiment, the reconstruction efficiency and muon momentum resolution and scale achieved in the 20.4 fb^{-1} dataset of 8 TeV pp collisions recorded during 2012.

The muon reconstruction efficiency is measured to be greater than 0.98, stable against the average number of interactions per bunch crossing and uniform across the detector. The comparison of the reconstruction efficiency in data and in simulation shows good agreement and provides the possibility to

derive efficiency corrections to the simulated muon efficiency in regions of small data/MC disagreement.

The analysis of the $Z \to \mu\mu$ decay mass spectrum is used to measure the muon momentum resolution and scale. The di-muon mass resolution ranges from 1.5 to 3 GeV at the Z mass in the different detector regions. A smearing correction is derived to match the simulated resolution to the data. The muon momentum scale measured in the ID and in the MS is corrected by approximately 0.1%.

A Appendix

This section reports the values of muon reconstruction efficiency and muon momentum corrections for the Chain 2 muon reconstruction algorithm introduced in Section 2. The techniques used in the extraction of the values have been described in Sections 4 and 5, only the noticeable differences are reported in the following.

In particular the comparison of Figure 3 (left plot) with the top right plot of Figure 12 shows that there is no efficiency loss at $\eta \approx 1.2$ for the Chain 2 CB muon reconstruction. This is caused by the fact that the CB muon reconstruction in Chain 2 also accepts MS tracks with poor momentum measurements.

The comparison of the left plot in Figure 13 shows slightly larger correction values for the Δa resolution term of the MS for the Chain 2 muons if compared to the left part of Figure 7; however no appreciable resolution difference appears. Figure 14 shows the $Z \to \mu\mu$ mass spectrum reconstructed with CB, Chain 2 muons (isolated and with $p_\mathrm{T} > 25$ GeV), for data and simulation before and after the smearing and scale corrections.

References

[1] ATLAS Collaboration, The ATLAS Experiment at the CERN Large Hadron Collider, JINST 3 (2008) S08003.

[2] ATLAS Collaboration, The ATLAS Inner Detector commissioning and calibration, Eur.Phys.J. C 70, (2010) 787.

[3] ATLAS Collaboration, Commissioning of the ATLAS Muon Spectrometer with Cosmic Rays, Eur.Phys.J. C 70, (2010) 875.

[4] ATLAS Collaboration, Muon reconstruction efficiency in reprocessed 2010 LHC proton-proton collision data recorded with the ATLAS detector, ATLAS-CONF-2011-063 (2011). `https://cds.cern.ch/record/1345743`

[5] ATLAS Collaboration, Muon Momentum Resolution in First Pass Reconstruction of pp Collision Data Recorded by ATLAS in 2010, ATLAS-CONF-2011-046 (2011). `https://cds.cern.ch/record/1338575`

[6] ATLAS Collaboration, Expected Performance of the ATLAS Experiment - Detector, Trigger and Physics, CERN-OPEN-2008-020 (2009) 165, arXiv:0901.0512 [hep-ex].

[7] ATLAS Collaboration, Performance of the ATLAS Muon Trigger in 2011, ATLAS-CONF-2012-099 (2012). `https://cds.cern.ch/record/1462601`

[8] T. Sjöstrand et al., A Brief Introduction to PYTHIA 8.1, Comput. Phys. Comm. 178 (2008) 852, arXiv:0710.3820 [hep-ph].

[9] S. Alioli et al., A general framework for implementing NLO calculations in shower Monte Carlo programs: the POWHEG BOX, JHEP 1006 (2010) 43.
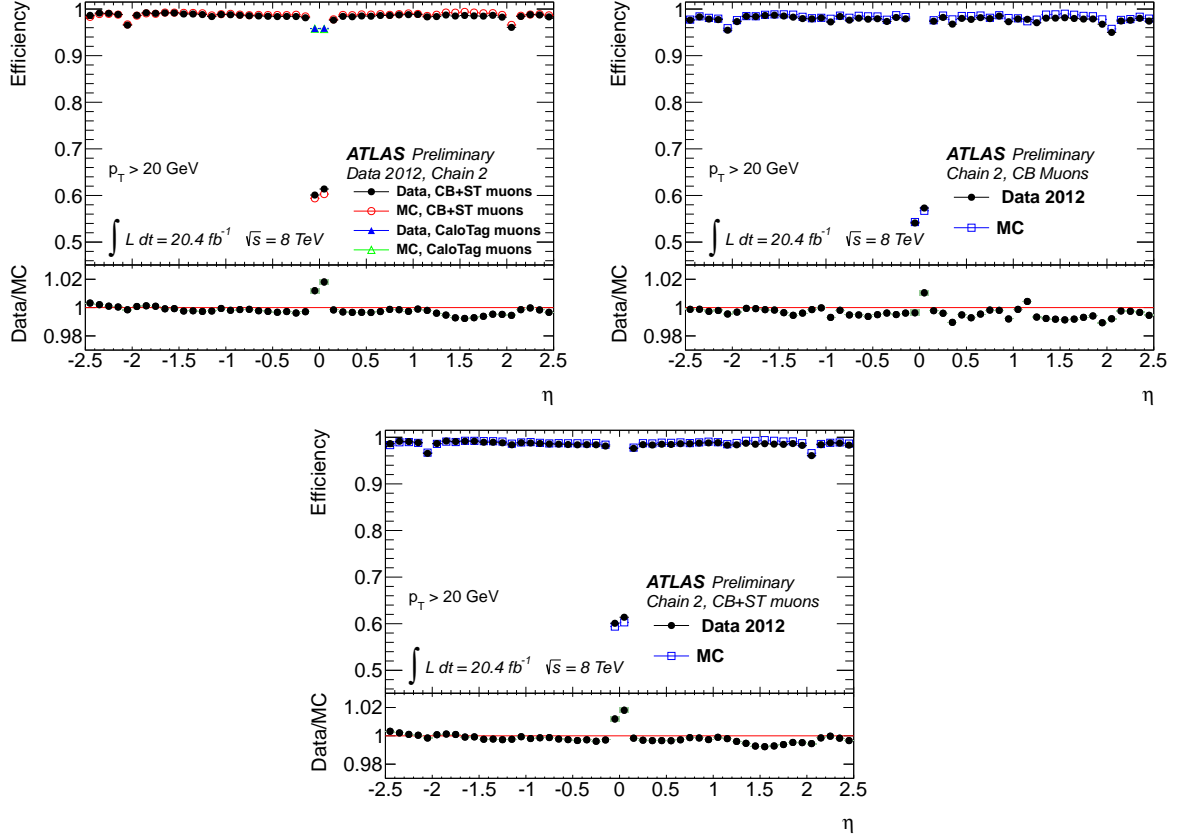
Figure 12: Muon reconstruction efficiency as a function of η for muons with $p_\mathrm{T} > 20$ GeV for various combinations of muon reconstruction types. CB and ST muon types are reconstructed using the Chain 2 reconstruction algorithm. The panel at the bottom of each insert shows the ratio between the measured and predicted efficiencies. The top left plot shows the reconstruction efficiency obtained by combining all the available muon reconstruction types (CaloTag muons are used only in the region $|\eta| < 0.1$). The top right plot shows the CB muon reconstruction efficiency. The bottom plot shows the CB+ST muon reconstruction efficiency.

[10] GEANT4 Collaboration, S. Agostinelli et al., Nucl.Instrum.Meth. A506 (2003) 250303.

[11] ATLAS Collaboration, Studies of the performance of the ATLAS detector using cosmic-ray muons, Eur. Phys. J. (2011), arXiv:1011.6665 [hep-ex].

[12] ATLAS Collaboration, Update on muon alignment for Rel 17, ATLAS-PLOT-MUON-2011-003 https://cds.cern.ch/record/1383415

[13] ATLAS Collaboration, Determination of the muon reconstruction efficiency in ATLAS at the Z resonance in proton-proton collisions at $\sqrt{s}$ = 7 TeV, ATLAS-CONF-2011-008 (2011). https://cds.cern.ch/record/1330715

[14] ATLAS Collaboration, A measurement of the muon reconstruction efficiency in 2010 ATLAS data using J/ψ decays, ATLAS-CONF-2012-125 (2012). https://cds.cern.ch/record/1474642
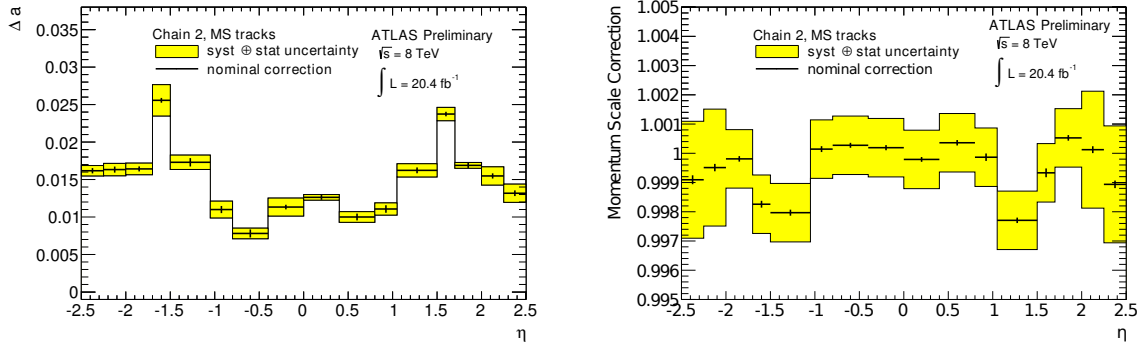
Figure 13: Resolution and scale MC correction terms for Chain 2 muon reconstruction algorithm derived from $Z \rightarrow \mu\mu$ events. The systematic uncertainty on the correction is shown in yellow. The left plot shows the Δa resolution correction term for the MS. The right plot shows the MS momentum scale correction.
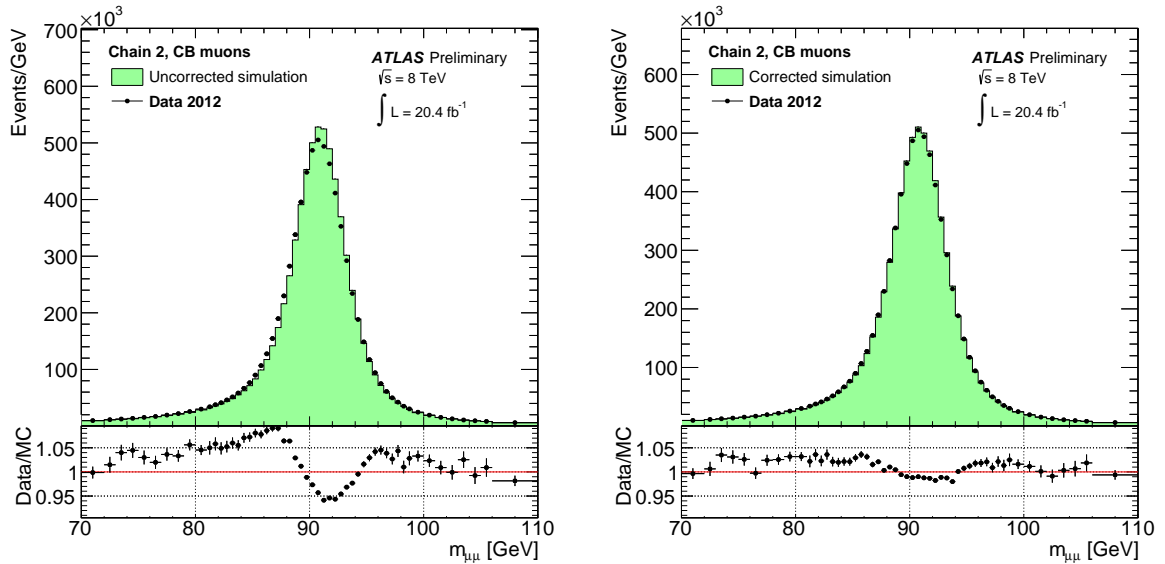

Figure 14: Di-muon invariant mass for Chain 2, CB muons, isolated and with $p_T > 25$ GeV. The plot shows the invariant mass for 2012 data and for the POWHEG [9] simulation of $Z \rightarrow \mu\mu$ plus background events. No corrections are applied on the left plot while smearing and scale corrections are applied to the plot on the right. The corrections have been derived from the full 2012 dataset.

[15] ATLAS Collaboration, Performance of the ATLAS Inner Detector Track and Vertex Reconstruction in the High Pile-Up LHC Environment, ATLAS-CONF-2012-042 (2012). `https://cds.cern.ch/record/1435196`

[16] ATLAS Collaboration, J/ψ Performance of the ATLAS Inner Detector, ATLAS-CONF-2010-078 (2010). `https://cds.cern.ch/record/1281369`

[17] ATLAS Collaboration, Alignment of the ATLAS Inner Detector Tracking System with 2010 LHC proton-proton collisions at $\sqrt{s} = 7$ TeV, ATLAS-CONF-2011-012 (2011). `https://cds.cern.ch/record/1334582`

CERN Document Server

| Information | Discussion (0) | Files |

S c i e n t i f i c   C o m m i t t e e   P a p e r

Conference title	**117th LHCC Meeting**
Date(s), location	5 - 6 Mar 2014, CERN, Geneva, Switzerland
Conference contact	European Laboratory for Particle Physics CH-1211 Geneva 23 Switzerland email: patricia.mage@cern.ch
Imprint	2014
Subject category	Detectors and Experimental Techniques

External link:

Scientific Committees

Contributions to this conference in CDS

ATLAS HL-LHC Tile Calorimeter Upgrade

by Solans, CA

Jet calibration, substructure techniques and preparation for the HL-LHC in ATLAS

by Delitzsch, C

A Search for Resonant Higgs-Pair Production in the bbbb final state

by Falla, R

Determination of spin and parity of the Higgs boson in the WW decay channel

by Mattmann, J

Search for charginos, neutralinos and sleptons in 1 or 2L final state events

by David, C

Spin Correlations in Top Events at 7 TeV

by Lemmer, B

Measurements of the Higgs boson in the WW decay channel with the ATLAS detector

by Long, J D

ATLAS Offline Beam Spot in 2012

by Yu, D

Measurement of helicity amplitudes of the decay $\Lambda_b^0 \to J/\psi + \Lambda^0$ in the ATLAS experiment

by Cheng, H

Mixing and CP violation in the B_s system with ATLAS

by Jakoubek, T

Electron Performances in ATLAS

by Benhar Noccioli, E

A general search for new phenomena with the ATLAS detector at sqrt(s) = 8 TeV

by Amoroso, S

ATLAS detector performance in Run1: Calorimeters

by Burghgrave, B

Performance of the ATLAS muon trigger in pp collisions at a centre-of-mass energy of 8 TeV

by Ninomiya, Y

Muon reconstruction efficiency, momentum scale and resolution in pp collisions at 8TeV with ATLAS

by Dimitrievska, A

Measurement of the electroweak production of dijets in association with a Z boson

by Gutschow, C

Missing transverse momentum in ATLAS: current and future performance

by Schramm, S

Show contributions in CDS

Record created 2014-02-11, last modified 2014-02-11

Similar records

External link:

Scientific Committees

➡ **Add to personal basket**

➡ **Export as** BibTeX, MARC, MARCXML, DC, EndNote, NLM, RefWorks

Muon reconstruction efficiency, momentum scale and resolution in *pp* collisions at 8TeV with ATLAS

The ATLAS experiment identifies and reconstructs muons with two high precision tracking systems, the Inner Detector and the Muon Spectrometer, which provide independent measurements of the muon momentum. This poster summarizes the performance of the combined muon reconstruction in terms of reconstruction efficiency, momentum scale and resolution. Data-driven techniques are used to derive corrections to be applied to simulation in order to reproduce the reconstruction efficiency, momentum scale and resolution as observed in experimental data, and to asses systematic uncertainties on these quantities. The analysed dataset corresponds to an integrated luminosity of 20.4 fb^{-1} from $\sqrt{s} = 8$ TeV pp collisions recorded in 2012.

MUON SPECTROMETER

The Muon Spectrometer is designed for efficient muon detection in the range $|\eta|<2.7$ using three large air core toroidal magnets with mean magnetic field of 0.5 T to measure momentum.
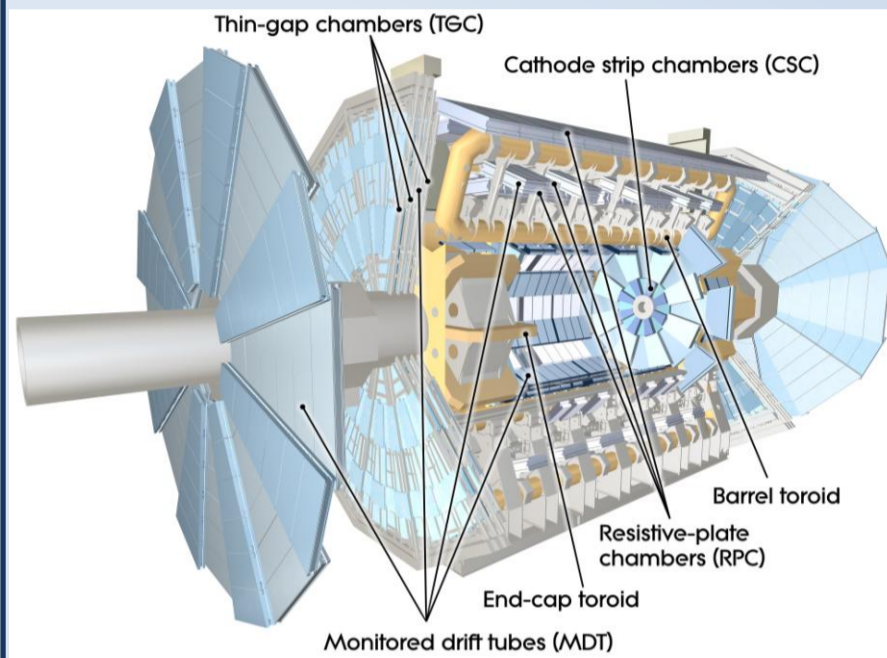

Four different detector technologies:
- **Precision chambers**
  Monitored Drift Tubes Chambers – three layers for $|\eta|<2.0$ and two layers for $2.0<|\eta|<2.7$
  Cathode Strip Chambers – one layer for $2.0<|\eta|<2.7$
- **Trigger chambers**
  Resistive Plate Chambers – three layers for $|\eta|<1.05$
  Thin Gap Chambers – three layers for $1.05<|\eta|<2.7$

Chambers are monitored by an optical alignment system.

INNER DETECTOR

The Inner Detector task is to track charged particles and determine their charge, momentum, direction and their vertex location up to $|\eta|<2.5$ in a 2 T solenoidal magnetic field.
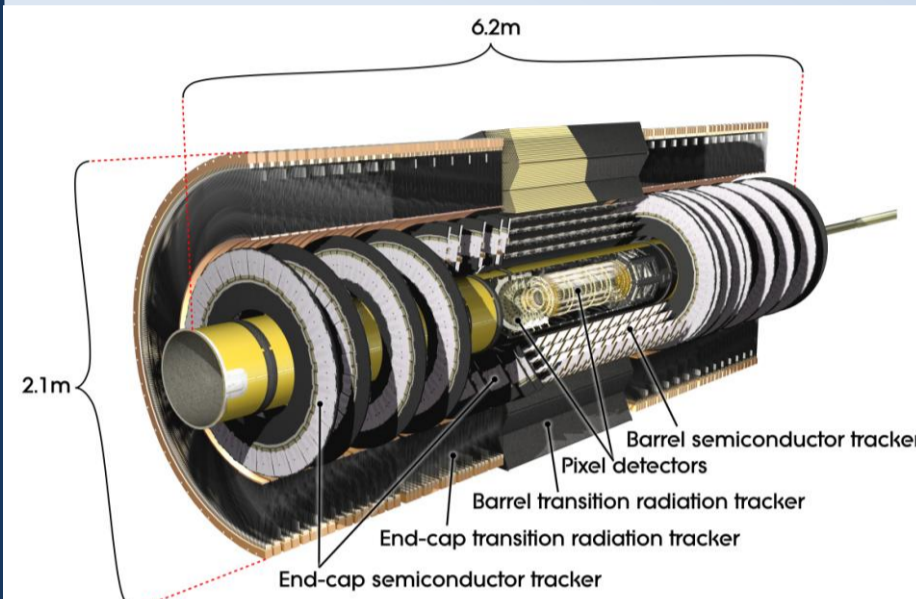
Tree complementary sub-detectors:
Silicon Pixel Detector – *three layers in barrel and three disks in each endcap provide precise vertex reconstruction*
Semi-Conductor Tracker – *four layers in barrel and nine in endcaps provide accurate momentum measurement*
Transition Radiation Tracker – *essential for pattern recognition and particle identification*

MUON RECONSTRUCTION AND IDENTIFICATION IN ATLAS

ATLAS software implements different strategies for muon reconstruction and identification, there are four different types of reconstructed muons:

STAND-ALONE (SA)
Muon tracks are reconstructed only in Muon Spectrometer. The track is extrapolated to the interaction point taking into account muon energy loss in the calorimeters. Recommended for region $2.5<|\eta|<2.7$.

COMBINED (CB)
Muon tracks are reconstructed independently in Inner Detector and Muon Spectrometer and a combined track is formed using a statistical combination or a global refit of the two tracks, for region $|\eta|<2.5$ ($|\eta|<2.65$ with ID tracklets).

SEGMENT-TAGGED (ST)
Muon track in Inner Detector whose extrapolation to Muon Spectrometer is associated with at least one track segment in the MDT or CSC, used for increasing acceptance of low p_T muons.

CALORIMETER-TAGGED
Muon track in Inner Detector which has an energy deposit in the calorimeter compatible with a minimum ionizing particle. These tracks have low purity and are used for the region $|\eta|<0.1$.
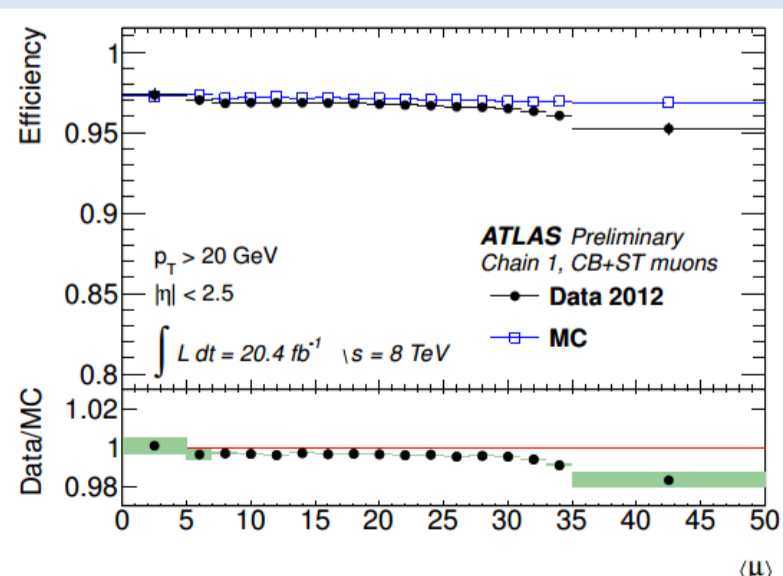
MUON RECONSTRUCTION EFFICIENCY

Reconstruction efficiency is measured using the tag-and-probe method based on Z->$\mu\mu$. Muon efficiency is measured in both, data and simulation, and a scale factor is derived as the ratio between measured efficiency in data and simulation. These scale factors are applied to the simulation in order to correct for the mis-modeling of muon reconstruction efficiency.
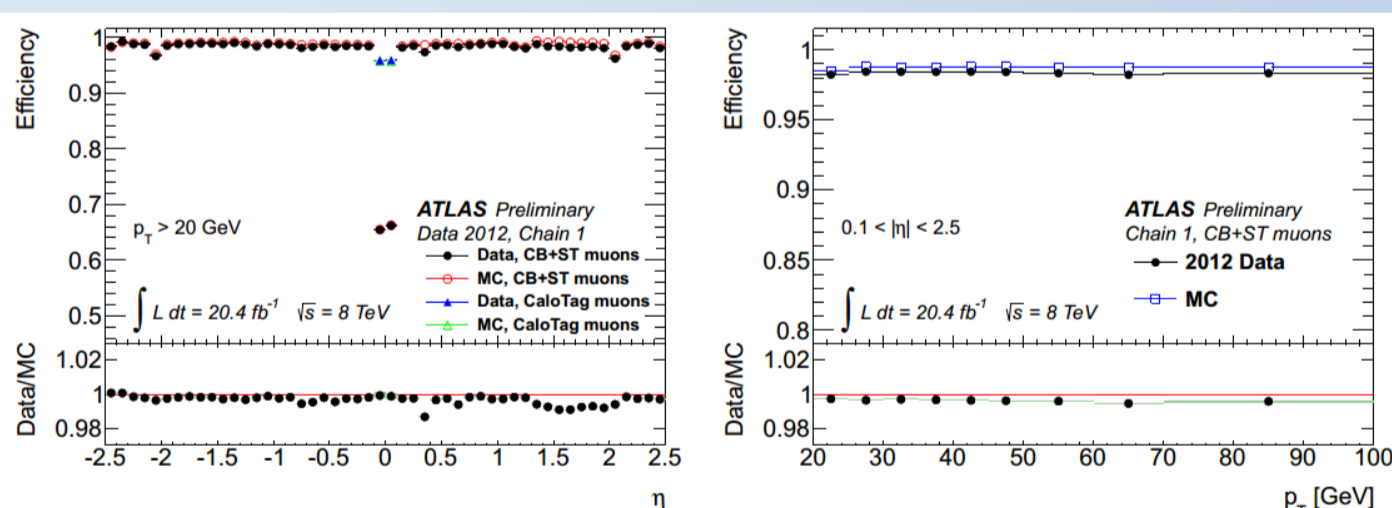
Muon reconstruction efficiency as a function of η for muons with $p_T > 20$ GeV (left) and as a function of p_T for muons with $0.1<|\eta|<2.5$ (right). Bottom panel shows the ratio between measured and predicted efficiencies.

Measured reconstruction efficiency for muons with $p_T > 20$ GeV as a function of the average number of inelastic pp collisions per bunch crossing <μ>. Bottom panel shows the ratio between measured and predicted efficiencies. The green band is statistical uncertainty.

Measured muon reconstruction efficiency is greater than 0.97, except for the region $|\eta|<0.1$. It is stable as a function of the average number of interactions per bunch crossing and uniform across the detector. Good agreement between reconstructed efficiencies in data and simulation.

ATLAS-CONF-2013-088

MUON MOMENTUM SCALE AND RESOLUTION

Muon momentum scale and resolution corrections are extracted separately for ID and MS tracks with a maximum likelihood template fit method using Z->$\mu\mu$ decays in 16 bins of η. Corrections for combined muons are computed as the average of the ID and MS momentum correction weighted by the inverse square of the ID and MS muon momentum resolution. Systematic uncertainties on the corrections are estimated by varying the extraction procedure and comparing the results with the scale from Z invariant mass distribution.
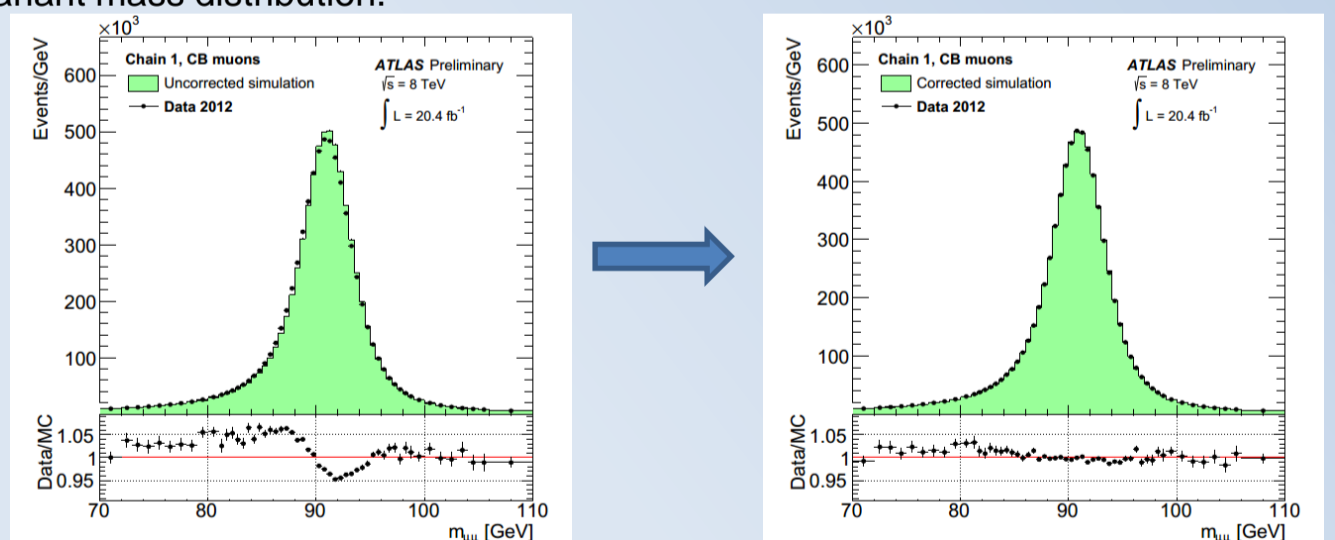
Invariant mass distribution for data and simulation of Z→$\mu\mu$, before (left) and after (right) correction. Uncorrected simulation has a slight shift and a smaller width with respect to experimental data.
Validation of these corrections is done for J/ψ, ϒ and Z resonance.
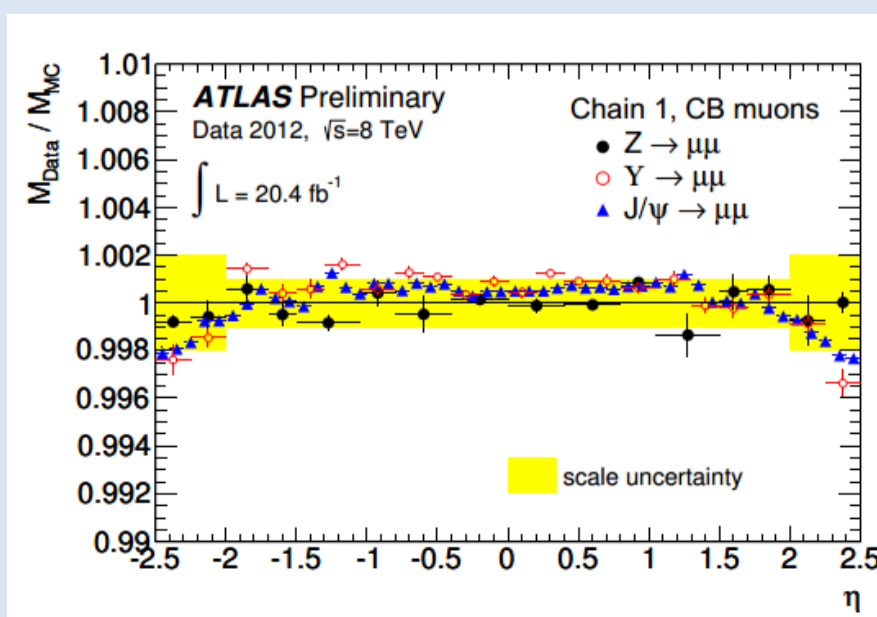
Ratio of reconstructed mean mass of data and corrected simulation for J/ψ, ϒ and Z resonance as a function of η for combined muons. J/ψ events are selected requiring two muons with p_T>6 GeV and are shown as a function of the highest-pt muon; ϒ and Z events are selected requiring two muons in the same η bin with p_T>6.5 GeV and p_T>20 GeV, respectively.

ATLAS-CONF-2013-088

КАРАКТЕРИСТИКЕ РЕКОНСТРУКЦИЈЕ МИОНА НИСКОГ ИМПУЛСА НА АТЛАС ДЕТЕКТОРУ

А. Димитриевска[1] и Н. Врањеш[2]

1) Универзитет у Београду – Институт за физику, Прегревица 118, 11000 Београд
2) CEA-Saclay
e-mail: adimitrievska@ipb.ac.rs

Апстракт. Испитиване су карактеристике реконструкције миона ниског импулса на АТЛАС детектору коришћењем миона из распада J/ψ мезона. Како је маса J/ψ мезона веома прецизно измерена на претходним експериментима, и како је природна ширина занемарива према инструменталној ширини, те како се J/ψ мезони обилно производе на Великом хадронском сударачу, они представљају одлично оруђе за калибрацију импулса миона у опсегу компатибилном са опсегом импулса миона из распада Z бозона.

1. УВОД

АТЛАС детектор [1] је један од четири експеримената који су постављени на LHC[1]-у. Он је, по димензијама, највећи конструисани детектор, има цилиндричну симетрију дужине 44 m, са пречником 25 m и масом око 7000 t.

АТЛАС детектор има слојевиту структуру и састоји се од четири система, унутрашњег детектора, калориметарског система, мионског спектрометра и магнетног система. Унутрашњи детектор се налази најближе вакуумској цеви кроз коју пролазе протони. Основна функција унутрашњег детектора је одређивање трајекторија наелектрисаних честица, мерење импулса честица, као и за реконструкцију вертекса. Калориметерски систем се састоји од електромагнетног и хадронскиг калориметра. Електромагнетни калориметар је постављен око соленоида који окружује унутрашњи детектор. Основни циљ калориметара је мерење енергије електрона, фотона и хадронских џетова. Мионски спектрометар [2] окружује хадронски калориметар и омогућава тригеровање и веома прецизно мерење импулса миона. Магнетни систем АТЛАС детектора се састоји од суперпроводног соленоидног магнета који се налази у средини детектора, да би се створило константно магнетно поље, и три суперпроводна магнета у облику торуса који стварају магнетно поље у мионском спектрометру.

---

[1] Велики хадронски сударач

2. РЕКОНСТРУКЦИЈА МИОНА

У зависности од начина реконструкције разликујемо неколико типова миона на АТЛАС детектору [3]:

- *combined* су миони који су реконструисани на основу статистичке комбинације импулса и пложаја из мионског спектрометра и унутрашњег детектора. Енергетски губици миона приликом проласка кроз калориметре су урачунати коришћењем параметризоване функције која узима у обзир расподелу материјала испред мионског система;
- *stand-alone* су миони који су реконструисани само у мионском спектрометру, уз пропагацију положаја миона до тачке интеракције и урачунавање енертегских губитака кроз калориметар;
- *segment-tagged* су миони чији је импулс потпуно реконструисан у унутрашњенем детектору. Идентификација миона извршена је поклапањем трага у унутрашњем детектору и сегемента реконструисаног у мионској комори најближој калориметру;
- *calo-tagged* су попут *segment-tagged* потпуно реконструисани у унутрашњем детектору. али се за њихову идентификацију користи депонована енергија у калориметру.

На реконструкцију миона утичу непрецизно познавање мапе магнетног поља у детектору, губитак енергије миона при проласку кроз калориметре, недовољно познавање поравнање мионских комора, као и неодређености у моделовању вишеструког расејања миона при проласку кроз детектор.

3. РЕЗУЛТАТИ И ДИСКУСИЈА

На основу реконструкције миона који су настали распадом J/ψ мезона, одређена је инваријантна маса ова два миона у зависности од рапидитета. Услов који ови миони треба да испуне је да се налазе у малом просторном углу у детектору и да имају трансверзални импулс већи од 6 GeV. Селектовани су само *combined* миони. На основу података прикупљених током 2012. године на енергији од 8 TeV реконструисано је око 30 милиона кандидата J/ψ мезона. Велики број прикупљених J/ψ мезона омогућава прецизно испитивање карактеристика Мионског спектрометра.

Сл. 1. приказује инваријантну масу два миона реконструисана на три начина у зависности од рапидитета. Инваријантна маса је израуната користећи измерене импулсе миона и угао између њих:

$$M_{\mu\mu} = \sqrt{p_1^\mu p_2^\mu (1 - \cos_{12})}.$$

Инваријантна маса је израчуната на три начина: користећи импулс измерен у унутрашњем детектору, користећи импулс измерен у мионском спектрометру са урачунатим енертегтским губицима, као и комбиновани импулс. У сва три случаја угао је измерен у унутрашњем детекору.

Са Сл.1. се види да је инваријантна маса добиејена коришћењем импулса измереног у унутрашњем детектору веома блиска табличној вредности 3096.916±0.011 MeV, што указује на добру калибрацију имулса у унутрашњем детектору. Инваријантна маса израчуната коришћењем импулса из мионског спектрометра одступа од табличне вредности у централној области ($|\eta|<1$) у средњем за око 20 MeV, односно ~0.6%. Вредност масе добијене из комбинованог импулса је ближа табличној вредности, пошто у статистичкој комбинацији за мионе ниског импулса доминира информација из унутрашњег детектора. Ипак одступање од табличне вредности износи око ~0.1% под утицајем спектрометра.

Како је проверено да одступање не зависи од импулса миона, узето је да енергијски губици миона у калориметрима већи од параметризованих вредности које се урачунавају при реконструкцији миона у мионском спектрометру. Корекција за појединачне мионе је добијена фитовањем разлике импулса миона у спектрометру и унутрашњем детектору у функцији рапидитета. После примене оваквих корекција на импулс миона у спектрометру добијено је много боље слагање са табличном вредношћу масе J/ψ користећи спектрометраски и последично комбиновани импулса миона.
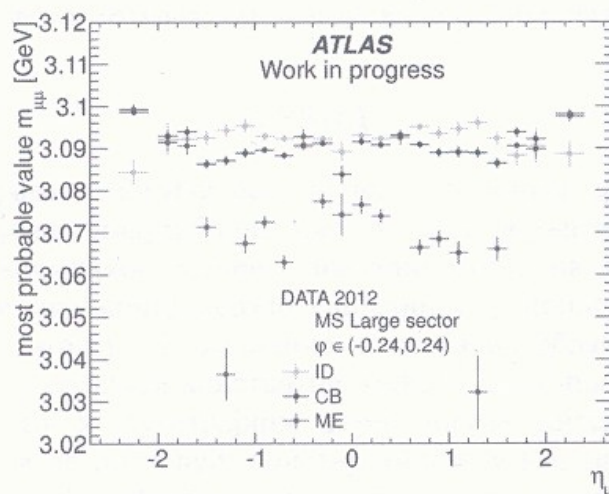
СЛИКА 1. Инваријантна маса два миона у зависности од рапидитета. Инваријантна маса је израчуната н три начина: користећи импулс измерен у унутрашњем детектору, користећи импулс измерен у мионском спектрометру са урачунатим емертегтским губицима, као и комбиновани импулс. У сва тру случаја угао је измерен у унутрашњем детекору

ЗАХВАЛНИЦА

ЛИТЕРАТУРА

[1] ATLAS Collaboration, JINST 3 , S08003 (2008).
[2] ATLAS Collaboration, *ATLAS muon spectrometer: Technical Design Report*, Genava, CERN, 1997.
[3] https://twiki.cern.ch/twiki/bin/view/AtlasPublic/MuonPerformancePublicPlots

РЕПУБЛИКА СРБИЈА

Физички факултет
(назив факултета - више школе)

Београд
(седиште)

БРОЈ 31 II / 2011

31. 10. 2013 _____ године

ДОКТОРСКЕ СТУДИЈЕ

УВЕРЕЊЕ

Димитриевска (Радован) Александра _____ рођен-а 5. 10. 1984.
(презиме, име једног од родитеља и име)

у Бору _____ Република, односно држава Србија _____, уписао-ла је III (Трећу
(словима)

годину студија, школске 2013/ 14 године, као редован студент Физичког _____
(редован-ванредан)

факултета - више школе у Београду _____ Физика језгара и честица
(одсек, смер, група)

Према статуту факултета - више школе студије трају 3 / 6
(година-семестара)

Ово се уверење може употребити за регулисање војне обавезе, права на дечији додатак, породичне пензије, инвалидског додатка, добијања здравствене књижице и легитимације за повлашћену вожњу.

Уверење је ослобођено таксе према чл. 18 ставу 1. тач. 6, 7, и 8 Закона о административним таксама ("Службени гласник РС", бр. 49/92, 70/92, 37/93, 44/93, 67/93, 28/94, 30/94, 53/95, 39/96, 42/98).

Овлашћено лице
факултета - више школе

_____

Ознака поруџбине: 10634

Назив производа:
UVERENJE O STUDIRANJU
A5/OFSET

Proizvođač: OPTIMUM d.o.o.
10 oktobra 6, Smed. Palanka
Srbija

8606003 422775